TECHNICAL REPORTS

GROUP TRAINING COURSE IN OFFSHORE PROSPECTING

1978

JAPAN INTERNATIONAL
COOPERATION AGENCY
March, 1979

GROUP TRAINING COURSE IN OFFSHORE PROSPECTING 1978

Sponsored by

GOVERNMENT OF JAPAN

In Collaboration with

GEOLOGICAL SURVEY OF JAPAN

AGENCY OF INDUSTRIAL SCIENCE AND TECHNOLOGY

TECHNICAL REPORTS BY PARTICIPANTS

Printed by

JAPAN INTERNATINAL COOPERATION AGENCY

March, 1979

PREFACE

The 1978 Group Training Course in Offshore Prospecting was held in Tokyo, Japan from 11 May to 11 December 1978 as part of the Technical Cooperation Scheme of the Government of Japan. Nine participants were received from seven countries, namely Bangladesh (1), Burma (1), Indonesia (2), Peru (1), The Philippines (2), Tanzania (1) and Thailand (1).

The course is being conducted annually since 1967, when it was inaugulated in accordance with recommendations made at the first session of the Committee for Co-ordination of Joint Prospecting for Mineral Resources in Asian Offshore Areas (CCOP). Arrangements for conducting the course were administrated by the Japan International Cooperation Agency (JICA), a semi-governmental body commissioned by the Government of Japan to execute its technical cooperation programmes, in collaboration with the Geological Survey of Japan (GSJ), Agency of Industrial Science and Technology, Ministry of International Trade and Industry. Besides financial arrangements made by JICA, the Office of the International Research and Development Cooperation (known as ITIT Office), Agency of Industrial Science and Technology provided an additional fund for practices of the participants.

The aim of the training course is to provide the participants with a fundamental understanding of offshore prospecting for mineral resources and to train them in basic techniques with emphasis on geophysical surveys. In view of increasing capability of the participants in the past few years, the curriculum gradually elevates its standard year by year. Since the 1975 course, the participants were separated into two groups toward the end of the course: one group is mainly trained in petroleum geology and interpretation of multichannel seismic profiling, whereas the other in interpretation of satellite remote sensing imagery. The latter group was organized for those who were not much involved in offshore prospecting, but much in mineral exploration on land.

Individual technical reports were voluntarily prepared by the participants of the 1971 course and then, were regularly submitted to the Course Leader since the 1974 course. These reports mostly were summaries of existing knowledge and information with some exercises on the topics

selected by the participants, while a few of them the results of original research works. Although the technical reports were thus drawn up for their own memoranda, the reports submitted by the participants of the 1977 course were printed and distributed among the authorities and the organizations concerned, so as to encourage the participants and, on the other hand, to show the standard and the achievement of the training course. It is very fortunate that JICA agreed to support printing of the technical reports of the 1978 course.

It was hoped by some participants that the course would emphasize individual work on specific items and would allocate more period of time to preparation of individual reports. The financial and institutional circumstances should, however, be improved before such arrangements for individual type training could be realized. The present course is still of basic nature, although raising standard of the participants and pursuance of rapidly advancing techniques should be important function of this training course. Active debate should be invited on this matter.

Taking this opportunity, I wish to express my sincere thanks to the competent authorities of our Government, JICA, the Steering Committee of the course chaired by the Director of GSJ, the lecturers, particularly those who instructed in preparation of the reports and the officers of the course. It should be again noted with thanks that JICA agreed to support financially printing of the technical reports. Finally, I should like to extend my many thanks to Dr. Hiroshi Hasegawa who gave guidance to the participants as the Course Leader in preparation of the reports, as well as Mr. Tomasaburo Saito who made great efforts to process the manuscripts for the printing.

February 1979

Shun-ichi Sano

Chief,
Overseas Geology Office

CONTENTS

1. Seismic Reflection Survey and Processing

Md.Abdur Razzaque*

Summary: This technical report is written on partial fulfilment of the Group Training Course in offshore prospecting held in Japan during May to December, 1978. To say something on the topics the author is to mention that all of his previous experience was based on single fold analog system. The idea of seismic survey on digital field system has little bit acquired during this group training. So this paper is merely a short compilation of the lecture notes and some published articles. Due to the limited of time available a more comprehensive and detailed literature research was not possible.

1. Introduction

The Seismic reflection survey has come to be increasingly important for the exploration of hydrocarbon. It does not find directly oil, but it searches for geological conditions which are commonly associated with the accumulation of hydrocarbon. During last twenty years this survey procedure and its processing have been repidly developed. Nowadays common depth point method is widely used and several new energy sources have come into use as alternatives to dynamite and new arrangements of source and receiving elements have been introduced to improve data quality by minimizing noise.

2. Seismic Theory

Seismic waves are generally referred to as elastic waves because they cause deformation of the material in which they propagate. So it follows all the elastic properties.

2.1 Elasticity

Elasticity is the property of a body to resist the changes in size or

* Bangladesh Oil and Gas Corporation (Petrobangla) Ministry of Petroleum & Mineral Resources, Bangladesh

shape and to return into the deformed condition. In relates the forces applied and deformation which are expressed in terms of stress and strain. The elastic properties of matter are also described by elastic constant.

Stress and Strain

Stress is the force per unit area which strain can be defined as the change in size or shape caused by stress.

Hooke's Law

Below the elastic limit in perfectly elastic substance, the ratio of stress and strain is a constant. This constant is called the modulus the elasticity and the relation between stress and strain is known as Hooks'l Low.

For change in length,

$$\frac{\delta}{\epsilon} = \frac{\frac{F}{A}}{\frac{\Delta \ell}{\ell}} = E$$

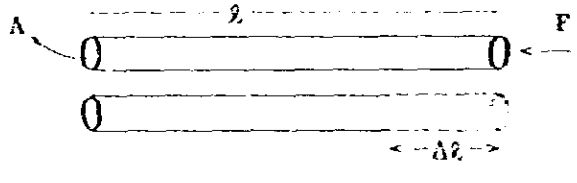

Fig. 1 (a)

where δ= Stress, ϵ = Strain, F = Force, A = Area,
l= Length, Δl= change in length, E = Young's Modulus

For change in volume,

$$\frac{\delta}{\epsilon} = \frac{P}{\frac{\Delta v}{V}} = K$$

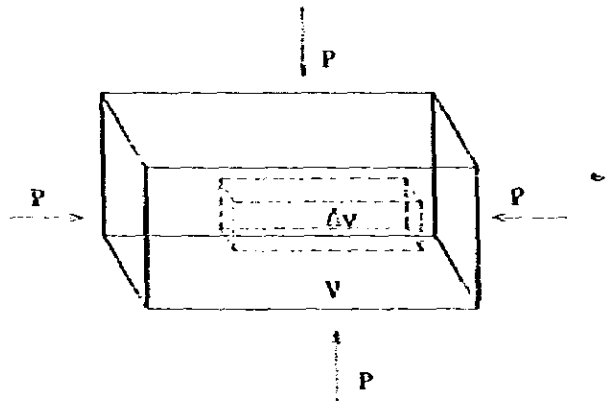

Fig. 1 (b)

where P = Force, V = Original volume,
Δv = Change in volume, K = Bulk modulus

For angular Distortion,

$$\frac{\delta}{\nu} = \frac{\frac{F}{A}}{\frac{\Delta X}{X}} = \frac{\frac{F}{A}}{\tan\theta} = \frac{\frac{F}{A}}{\theta} = G$$

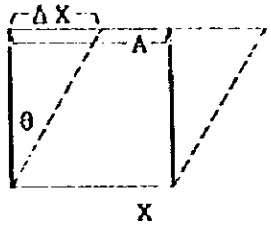

Fig. 1 (c)

where F = Force, A = Area,

G = Shear modulus as modulus of rigidity

In a perfectly elastic solid the ratio of change in diameter to change in length is also constant, and their constant is known as Poisson's ratio.

$$\nu = \frac{\frac{\Delta d}{d}}{\frac{\Delta \ell}{\ell}}$$

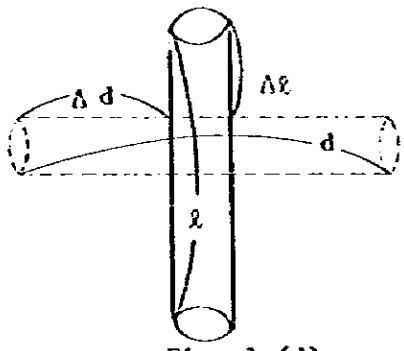

Fig. 1 (d)

From the theory of elasticity, the relation among these constants are

$$G = \frac{E}{2(1+\nu)} \qquad K = \frac{E}{3(1-2\nu)}$$

2.2 Types of Seismic Wave

Seismic waves are of two types

(a) Body wave

(b) Surface

Body wave is also two types,

(1) P wave

(2) S wave

4.

P wave is known by various waves such as, primary wave, compressional wave, longitudinal wave, dilatational wave or irrotational wave. It always propagates along the direction of propagation.

S wave is also recognized by secondary wave, shear wave, transverse wave or rotational wave. It propagates at right angle to direction of propagation.

The velocity of P and S wave are as follows,

$$Vp = \sqrt{\frac{K + G}{D}}$$

$$Vs = \sqrt{\frac{G}{D}}$$

where D = density

Surface Wave;

The wave which is constituted at boundary is called "surface wave". This wave is mostly Rayleigh wave and Love wave

Rayleigh Wave (R)

Rayleigh wave are waves at the free surface of a semi-infinite elastic solid. The motion is a sort of combination of longitudinal and transverse vibration giving rise to an ellipsoidal motion of the particle.

Love Wave (L)

Love wave are transverse waves propagated in a surface layer having elastic properties differing from those of an underlying semi-infinite elastic solid. The velocity of Love wave which are propagated along the surface depends on the wave length and varies between that of transverse waves in the surface layer and that of transverse waves in the lower medium.

2.3 Reflection

Seismic wave follows the laws of reflection and refraction. Since the topic is seismic reflection survey this technical report emphasizes on the subject only.

From Fig. 2(a), 2(b), 2(c) and 2(d) let us calculate travel time and velocity at four different cases of reflection.

(a) Reflection at Horizontal Two layer:

According to Pathagoroux Theorem, from Fig. 2(a)

$$(VT)^2 = (2H)^2 + X^2$$

$$T = \left(\frac{2H}{V}\right)^2 + \left(\frac{X}{V}\right)^2$$

$$\text{But } To = \frac{2H}{V}$$

$$T = To^2 + \frac{X^2}{V} \quad \ldots\ldots\ldots\ldots\ldots (1)$$

Where T = Travel Time, V = Velocity, H = Depth
X = Shot-receiver distance, To = Normal Time

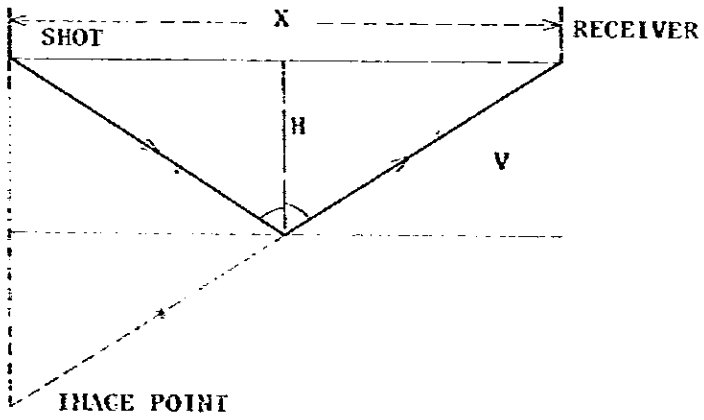

Fig. 2 (a)

6.

(b) Reflection at Oblique Layer:

Let

α = Dip angle

To = Normal time

$$= \frac{2H}{V}$$

or $2H = VTo$

So from Fig. 2(b)

$$(VT)^2 = X^2 + (VTo + X\sin\alpha)^2 - 2 \times (VTo + X \sin\alpha)\cos\left(\frac{\pi}{2} - \alpha\right)$$

$$= X^2 \cos^2\alpha + (VTo)^2$$

$$T = \sqrt{To^2 + \frac{X^2}{\left(\frac{V}{\cos\alpha}\right)^2}} \quad \ldots\ldots\ldots\ldots\ldots\ldots (2)$$

But apparant velocity $Va = \frac{V}{\cos\alpha} \gg V$

$$T = \sqrt{To^2 + \left(\frac{X}{Va}\right)^2}$$

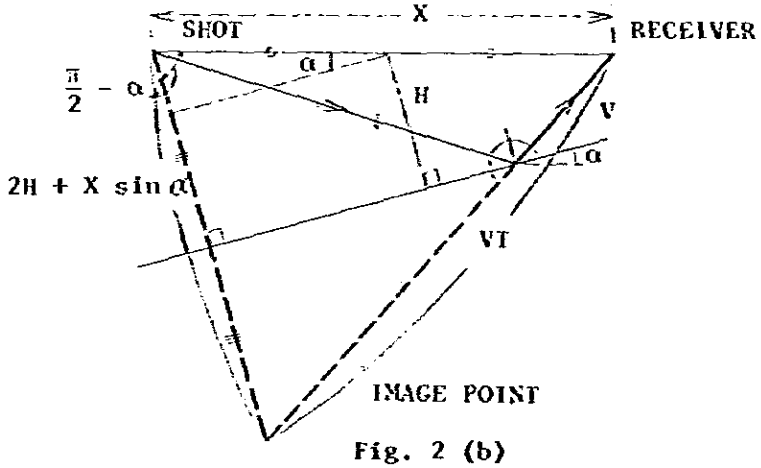

Fig. 2 (b)

(c) Reflection at Horizontal Multilayer:

$$\text{Sin}\ \frac{\Theta_1}{\Theta_2} = \frac{V_1}{V_2}, \quad \frac{\sin\Theta_2}{\sin\Theta_3} = \frac{V_2}{V_3}, \quad \frac{\sin\Theta i - 1}{\sin\Theta i} = \frac{Vi - 1}{Vi}$$

$$\text{and} \quad \frac{\sin\Theta i}{\sin\Theta i} = \frac{V_1}{Vi} \qquad \ldots\ldots\ldots\ldots\ldots\ldots (3)$$

but ray parameter

$$P = \frac{\sin\Theta_1}{V_1}$$

putting this value in (3) we get

$$\text{Sin}\ \Theta i = PVi \qquad \ldots\ldots\ldots\ldots\ldots\ldots (4)$$

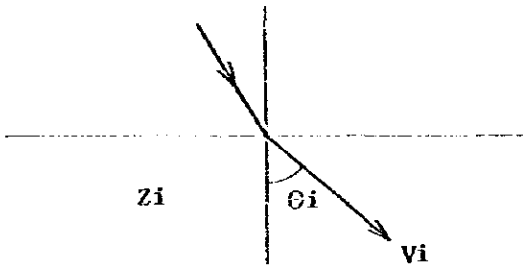

Vi cosΘ i = vertical compornent of ΘVi

Vertical component of Vi

$$Vi \cos\Theta i = Vi\sqrt{1 - P_2 Vi_2}$$

$$\text{or} \quad \cos\Theta i = \sqrt{1 - P_2 Vi_2}$$

$$T(n,p) = 2\sum_{i=1}^{n} \frac{Zi}{Vi\sqrt{1 - P_2 Vi_2}} \qquad \ldots\ldots\ldots\ldots\ldots\ldots (5)$$

$$X(n,p) = 2\sum_{i=1}^{n} Zi \tan\Theta i = 2\sum_{i=1}^{n} \frac{PVi\,Zi}{\sqrt{1 - P_2 Vi_2}} \ldots\ldots\ldots (6)$$

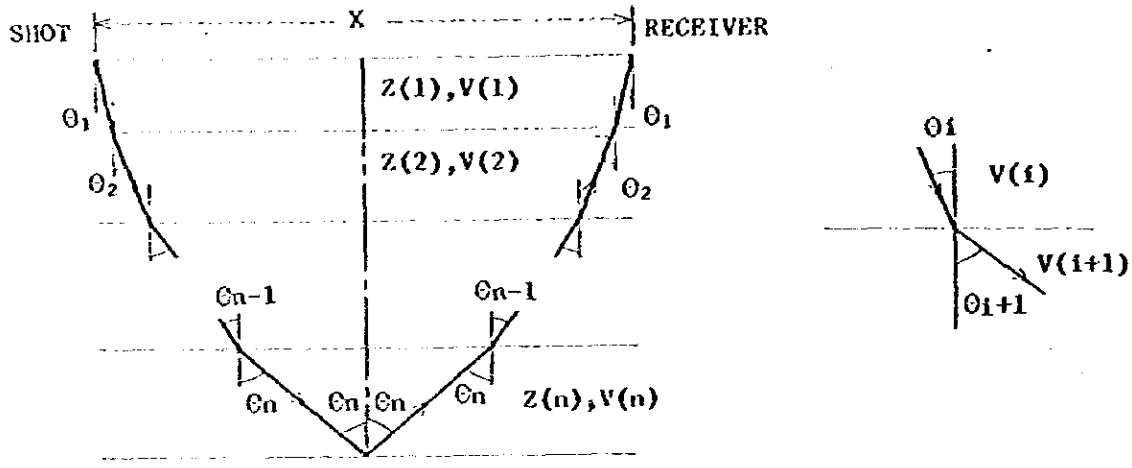

Fig. 2 (c)

$$To(n) = \sum_{i=1}^{n} \Delta Ti = 2\Sigma Zi/Vi \qquad \text{where} \quad \Delta Ti = 2\frac{Zi}{Vi} \quad \ldots\ldots (7)$$

$$Vm(n) = \frac{1}{To(n)} \sum_{i=1}^{n} Vi^2 \Delta Ti \quad \ldots\ldots (8)$$

Taylor Expansion of $(1 - P^2 Vi^2)^{-\frac{1}{2}}$ is

$$(1 - P^2 Vi^2)^{-\frac{1}{2}} = 1 + \frac{1}{2} P^2 Vi^2 + \frac{3}{8} P^4 Vi^4 + \ldots\ldots (9)$$

Putting eq. (9) in eq. (5), we get

$$T(n,p) = \Delta Ti + \frac{1}{2} P^2 \Sigma \Delta Ti Vi^2 + \frac{3}{8} P^4 \Sigma \Delta Ti Vi^4 + \ldots\ldots$$

and $Vm(n)\, To(n) = \Sigma Vi\, Ti \quad \ldots\ldots (9a)$

using the above expression we get

$$T(n,p) = To(n) + \frac{1}{2} P^2 To(n), V_2(n) + \frac{3}{8} P^4 To(n) V_4(n) + \ldots\ldots (10)$$

and $$X(n,p) = P \Sigma \Delta Ti Vi^2 + \frac{1}{2} P^3 \Sigma \Delta Ti Vi^4 + \ldots\ldots$$

again using (9a) we get

$$X(n,p) = P To(n) V_2(n) + \frac{1}{2} P^3 To(n) V_4(n) + \ldots\ldots (11)$$

From (11)

$$T^2(n,p) = To(n)^2 + P^2 V_2^2(n) \cdot To^2(n)^2 \quad \ldots\ldots\ldots\ldots\ldots\ldots \quad (12)$$

$$X(n,p) = P^2 To(n)^2 V_2^2(n) + \ldots\ldots\ldots\ldots\ldots$$

$$T^2(n,p) = To(n)^2 + \frac{X^2(n,p)}{V^2(n)}$$

$$= To(n)^2 + X(n,p)^2 / V^2 RMS(n)$$

$$T(n,p) = \sqrt{To(n)^2 + X^2(n,p)/V^2 RMS(n)} \quad \ldots\ldots\ldots\ldots \quad (13)$$

$$To(n)V^2 RMS(n) = \sum_{i=1}^{n} Vi^2 \Delta Ti$$

$$To(n-1)V^2 RMS(n-1) = \sum_{i=1}^{n-1} Vi^2 \Delta Ti$$

Subtracting these two expressions we get

$$To(n)VRMS(n)^2 - To(n-1)VRMS(n-1)^2 = V^2(n)\, Ti$$

$$V(n) = \sqrt{\frac{To(n)V^2 RMS(n) - To(n-1)V^2 RMS(n-1)}{\Delta Ti}} \quad \ldots\ldots\ldots \quad (14)$$

where $\Delta Ti = To(n) - To(n-1)$

This is called Dix Formula.

Case(d) Reflcetion at Oblique Dipping Multilayer.

From Snell's Law Fig. 2(d)

$$\frac{\sin(\theta i - \alpha i)}{\sin(\theta i - 1 - \alpha i)} = \frac{\sin(\bar{\theta} i - \alpha i)}{\sin(\bar{\theta} i + 1 - \alpha i)} = \frac{Vl}{Vi + 1} \quad \ldots\ldots \quad (15)$$

for reflection $\theta n - \alpha n = -\bar{\theta} n + \alpha n$

$$\bar{\theta} n = 2\alpha n - \theta n \quad \ldots\ldots\ldots\ldots \quad (16)$$

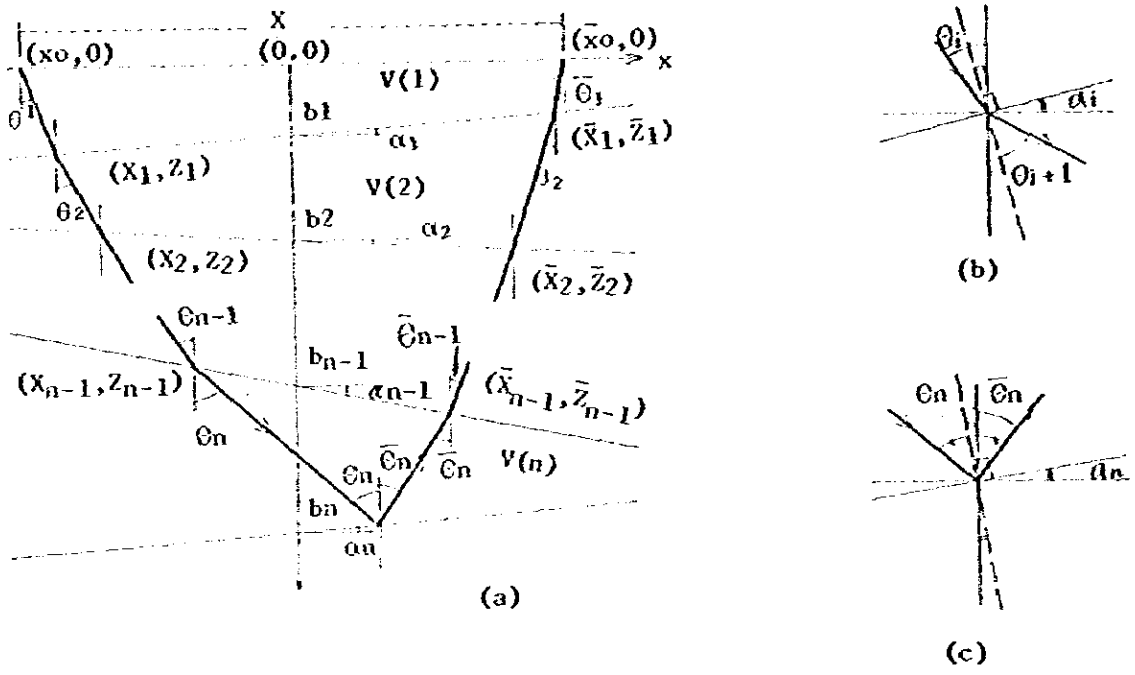

Fig. 2 (d)

In this case, it is very difficult to derive the equation for T - X relationship. However, after the computer simulation worked by some authors (Taner et.al.) it is suggested that we can use the same eq.

$T = \sqrt{To^2 = \frac{X}{Vs^2}}$ for dipping multilayer, where Vs - Best hyperbolic velocity or stacking velocity.

2.4. Multiple Reflections

Multiple reflections are of many types, some of which are shown in Fig. 3. Most common is the surface multiple which arrives at twice the time of the primary reflection from the bed.

Multiple reflection is one of the most important type of interference. It almost looks like primary reflection and the interpreters fall into the trouble to identify it. It is greatly reduced by common depth point shooting both by the velocity contrast and increase of signal to noise ratio.

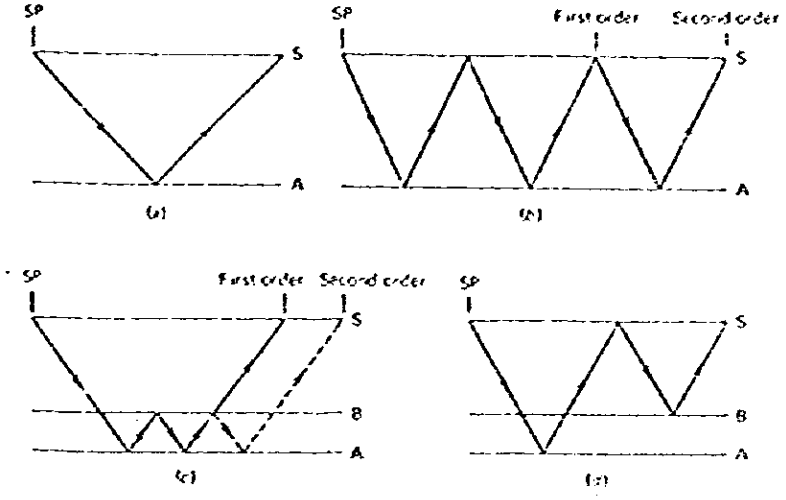

Fig. 3 Several types of multiple reflections: (a) primary; (b) surface multiple; (c) interbed multiple; (d) combination multiple. S is earth's surface. A and B are reflecting interfaces. (Amoco Production Co.)

2.5 Diffraction

When seismic wave strikes the corner or a point of a surface where there is a sudden change of curvature, the striking point acts as a point source for radiating wave in all directions. Such radiation is known as diffraction and is shown in Fig. 4.

The amplitude of the diffracted waves fall rapidly with distance from the nearest point to the source. This events are frequently observed on seismic records.

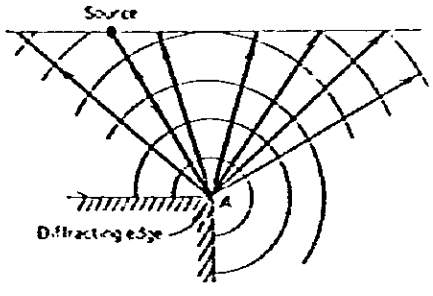

Fig. 4 Diffraction from an edge. The source A of diffracted radiation has been set into oscillation by waves generated on surface. Radial lines with arrows are ray paths; circular arcs are wave-fronts.

3. Field Operation on Land

To generate Seismic impulse external energy is used. Nowadays worldwide energy source used are as follows.

(a) Dinamite, (b) Airgun, (c) Sparker, (d) Hammer dropping and (e) Vibrosis etc.

Dinamite and Vibrosis are widely used in land seismic, on the other hand airgun and sparker are used mostly in marine seismic.

In a survey area the surveyors layout profile according to project. It is essential for noise test in almost all areas to select optimum spacing of geophone.

3.1. Noise Test

From noise test nature of the noise such as wave length, frequency, velocity are encountered. To do this a series of record is made with geophone spaced generally around 5m apart and single geophone is used per-trace. In the shooting system the spread is moved and the shot is held fixed which is shown in the Fig. 5.

After studying the wave length of the noise the optimum geophone spacing can be found by the formula.

$$l < \frac{nD}{\lambda}$$

where n = No of geophone

D = Distance between geophone

λ = Wave length of noise

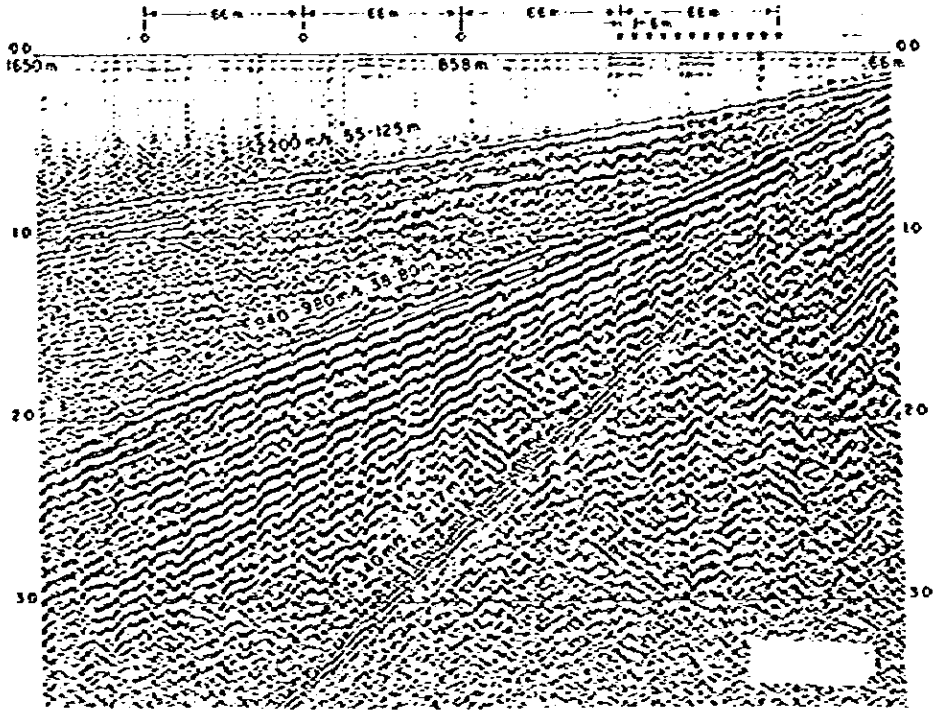

Fig 5 Traveling waves recorded over spread about 1600m long from surface source. Velocities of waves range from 2200 m/s (probably first arrivals) to 340 m/s (air waves). 940-980 m/s events are probably Rayleigh waves. (Petty-Ray Geophysical Division, Geosource Inc.)

3.2. Spread

Following sorts of spread are use in field operation.

(a) Split dip, (b) Offset split dep, (c) End-on,
(d) In line offset, (e) Broad side T, (f) Cross

These spreads are arranged as follows.

3.3. Up-hole Survey

Up-hole survey is done to know the near-surface weathering velocity. It is very much essential to select the change and shot-depth parameters for good quality record.

3.4. Detector

The detector or geophone of moving coil type is used in land seismic.

14.

Its function is to convert energy of mechanical vibration into electric voltage.

3.5. Recorder

The oldest type of recording unit was oscillographic analog equipment. Nowadays latest developed multichannel digital field system (DFS) equipment are utilized. Also somewhere magnetic analog unit are being utilizing. Both in the DFS and magnetic analog equipment the output voltage of amplifier is converted to magnetic intensity which is recorded in a magnetic tape.

3.6. Common Depth Point Shooting

Common depth point shooting involves a greater number of shots per unit distance along the line. The reflection coming from a common point. Hence it is sometimes called common reflection point (CRP) shooting. The main purpose of this type of shooting is to improve signal to noise ratio by stacking. The rate of improvement of signal to noise ratio is given by the formula.

$$\frac{S}{N} = \frac{n}{\sqrt{n}} = \sqrt{n}$$

where S = Signal (reflected wave)

N = Noise (Random noise)

n = Number of stack (fold)

The shooting procedure is described in the Fig. 6.

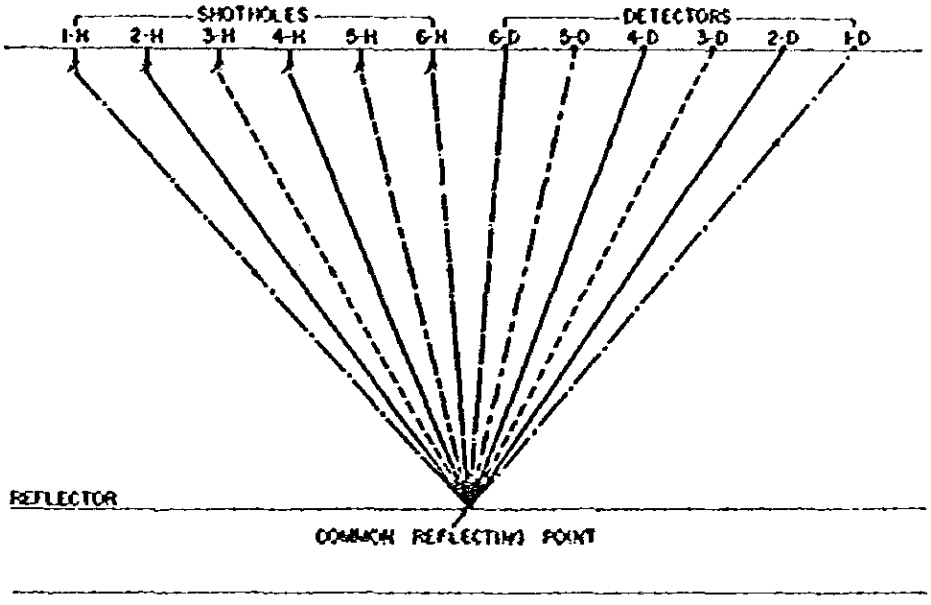

Fig. 6 Ray paths for reflections from a single point in sixfold common-depth-point shooting.

With 24 recording station 3 fold coverage will be obtained if the shots are separated by four grophone-group intervals, 4 fold if by three intervals and 6 fold if by two intervals. If the shooting is twelve fold there is a shot for every geophone group centre. Fig. 7 shows 6 fold multiple coverage.

For 24 fold coverage, shot is also at every trace of 48 channel. This is described in Fig. 8.

4. Data Processing

Most of the processing operations carried out on digital computers. The basic flow diagram of processing is shown in Fig. 9. As previously said this report is a partial fullfilment of the course, it is not possible here to explain the block diagram.

16.

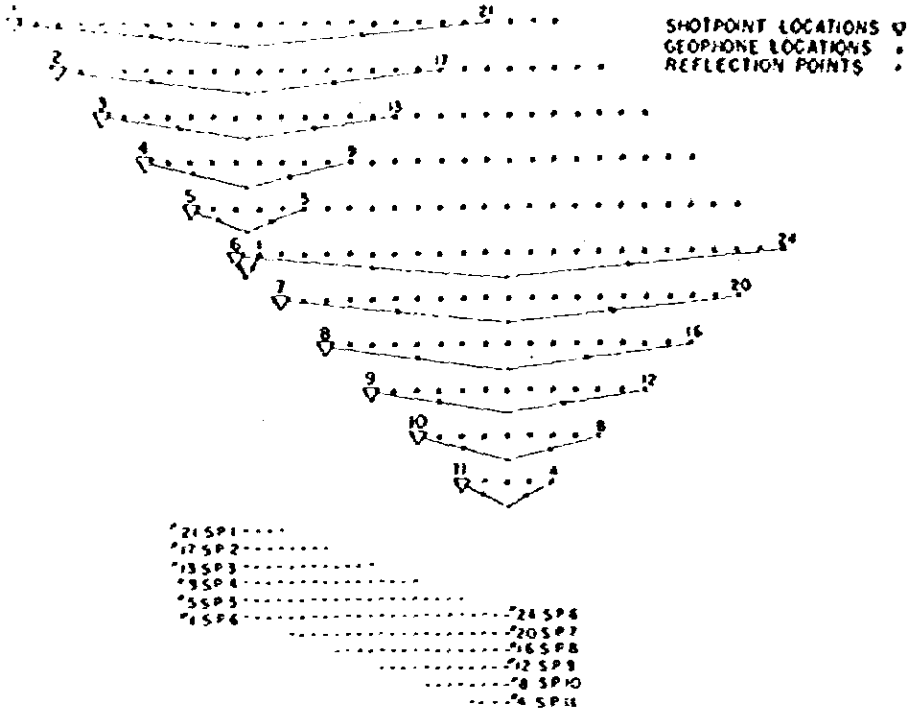

Fig. 7 Shot and geophone combinations giving sixfold multiplicity for two subsurface reflecting points. Pattern at bottom shows reflecting points for successive spreads. (Mayne.[14])

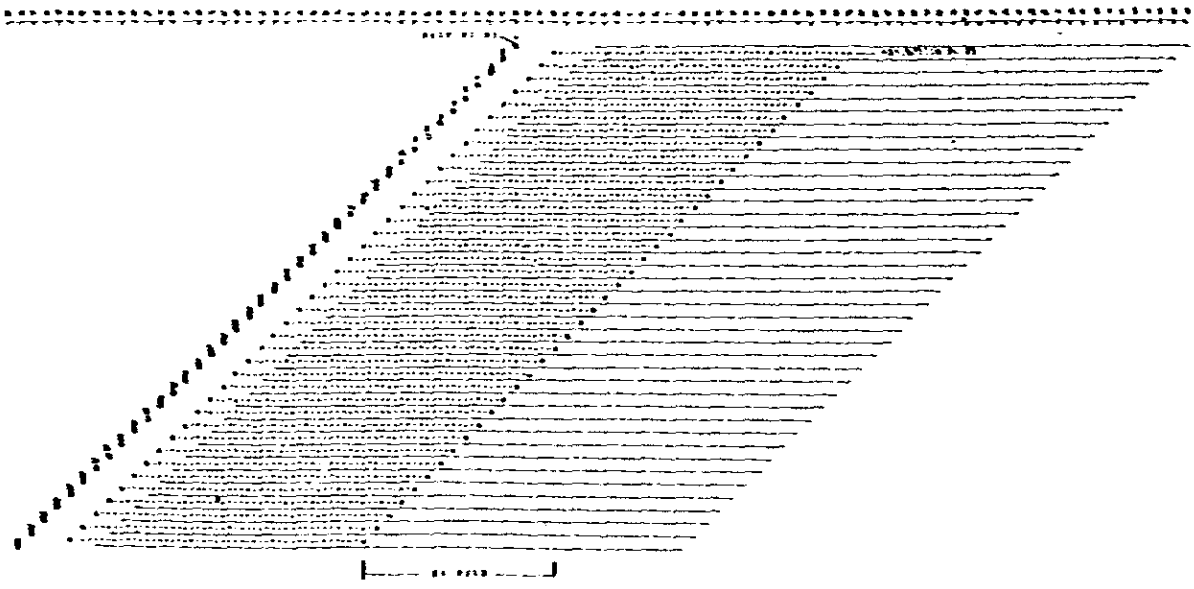

Fig. 8

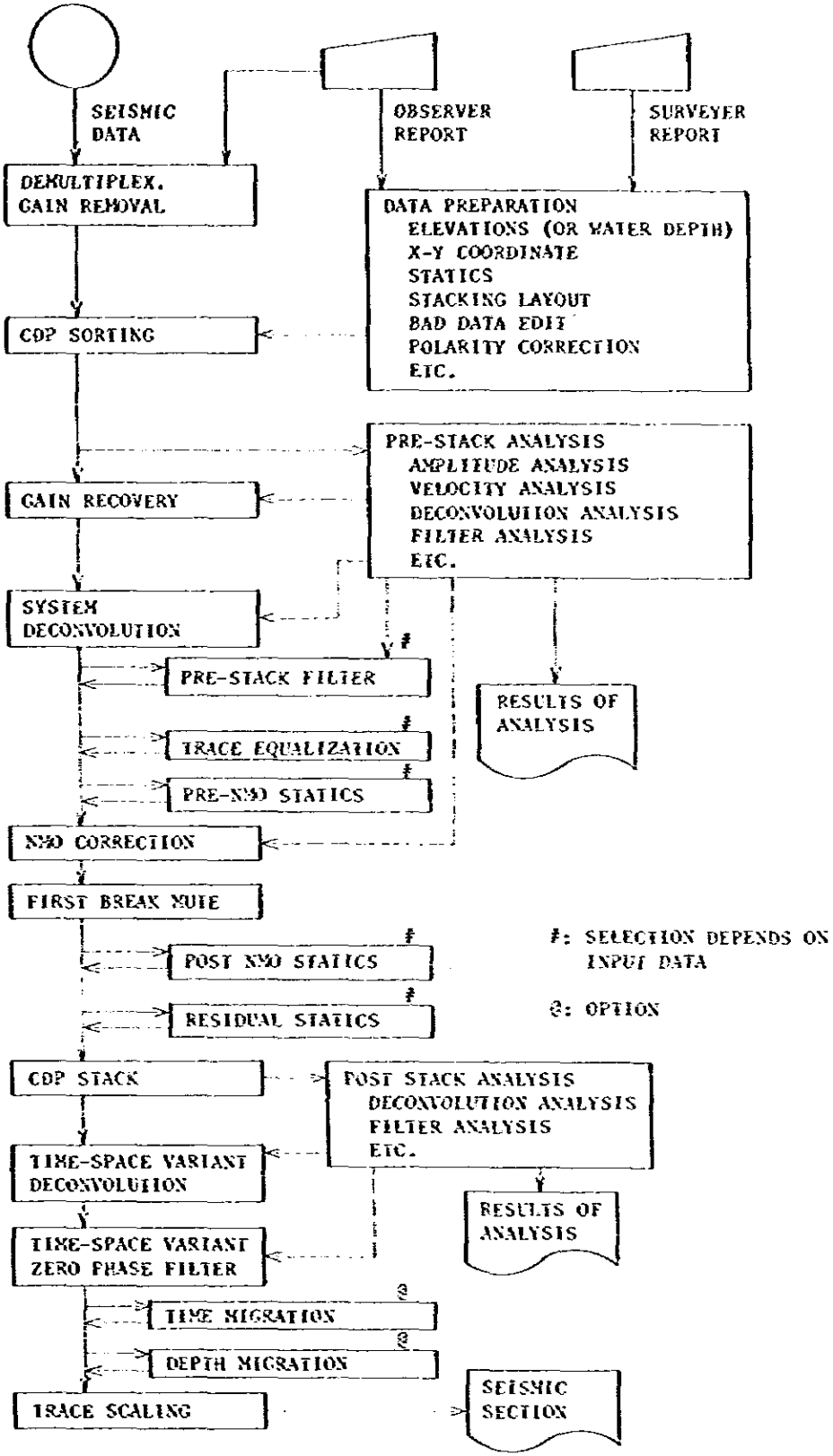

Fig. 9 Flow diagram of basic seismic processing

18.

The basic object of all seismic processing is to convert the information recorded in the field into a form that most greatly facilitates geological interpretation. The data initially recorded on magnetic tape are transformed in the processing centre into a corrected record section comparable in many ways to a geological structure section. The main object of the processing is to eliminate or at least suppress all noise and to present the reflections on the record section with the greatest possible resolution. Data processing covers filtering trace correction, stacking compositing velocity analysis, true amplitude registraction migration and plotting.

4.1. Normal Moveout Correction (N.M.O.)

In C.D.P. shooting number of records taken as many as the folds programmed which correspond to the same subsurface reflection point but which are from different shot. The reflected signals have different arrival time. Therefore, it is required to make the apparent arrival time same for all the reflection since those are from common reflection point which is referred as normal move-out correction. This is shown in Fig. 10. The main object of NMO correction is to intensity the reflected phase by stacking.

4.2. Digital Filtering

This filter provides a means of filtering data numerically in the time domain by summing weighted samples at successive time increment (convolution). Its main object is to remove undesired signals from the record leaving only useful signals. In the time domain the action of a filter can be described by impulse response while in frequency domain it can be described by frequency-response couve. Both the expression are functions of each other. If one is known the other can be derived. Fourier transformation provides the physical basis for such conversions from one domain to the other.

4.3. Fourier Transform

Fourier transform expresses here that any function of frequency

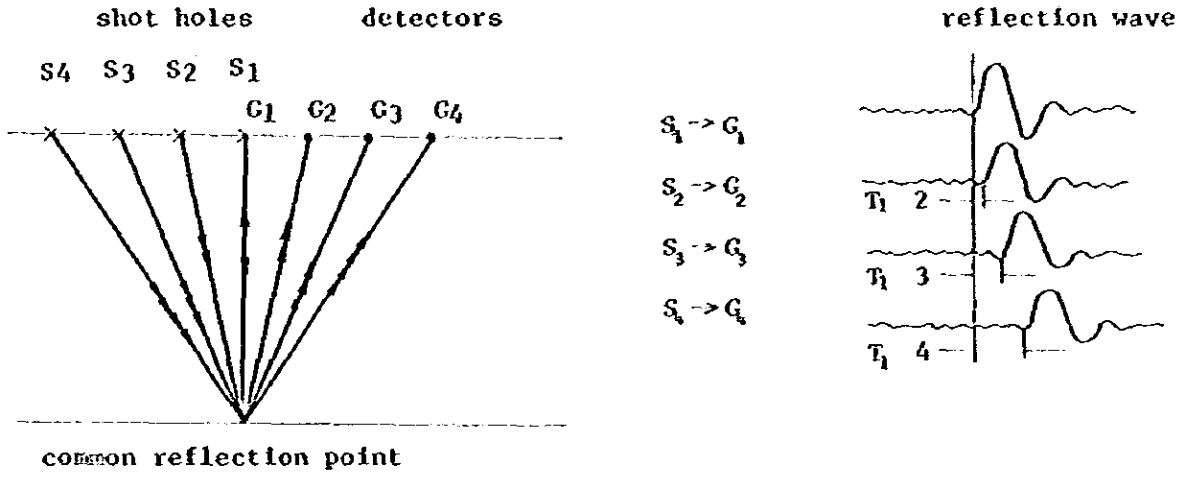

a) Common Depth Point

b) Before NMO

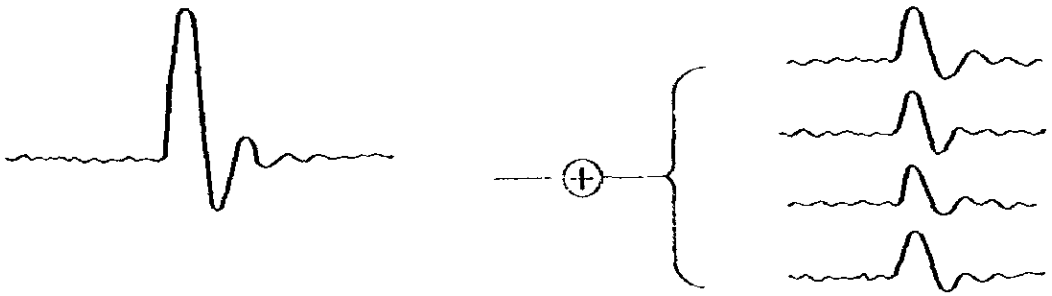

d) CDP Shooting

c) After NMO

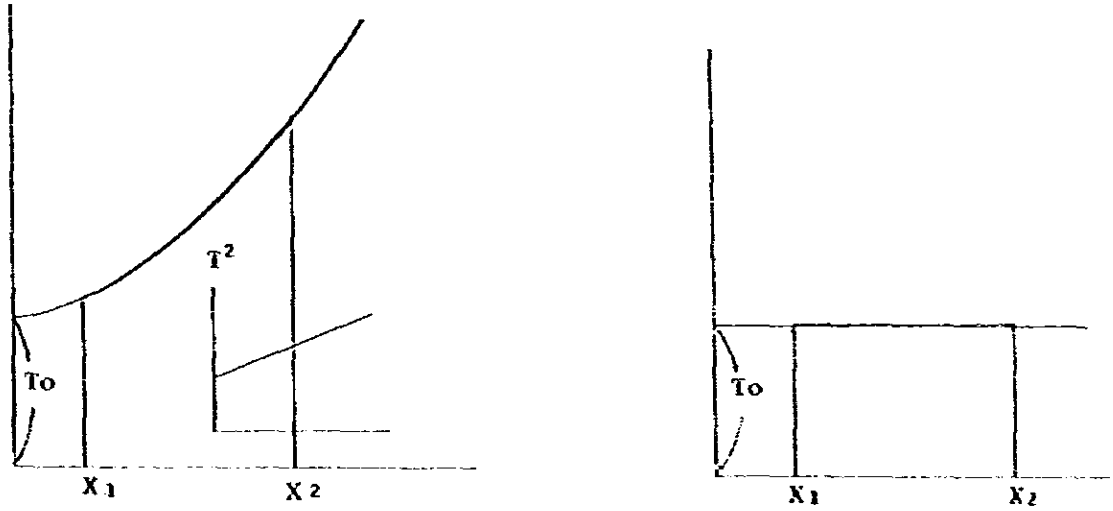

Fig. 10

can be transformed into the function of time and vice-versa. The frequency function F(n) can be obtained from the time function f(t) by the expression.

$$F(n) = \int_{-\infty}^{\infty} (t) \cos 2\pi ntdt - i \int_{-\infty}^{\infty} f(t) \sin 2\pi ntdt$$

Similarly the time function f(t) can be expressed as the frequency function F(n) by

$$f(t) = \int_{-\infty}^{\infty} F(n) \cos 2\pi ntdn + i \int_{-\infty}^{\infty} F(n) \sin 2\pi ntdn$$

It is shown in Fig. 11.

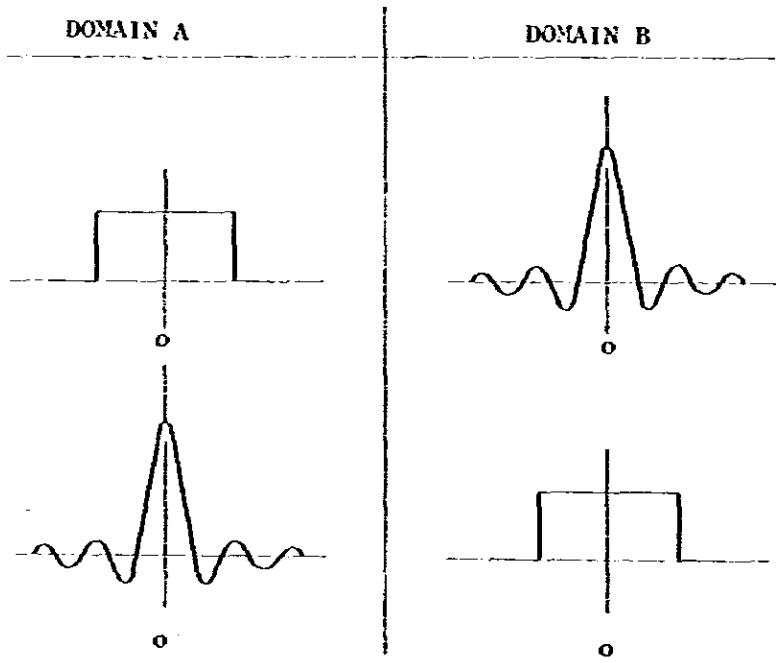

Fig. 11 Reciprocity of Fourier-transform pairs. The transformation is the same regardless of the domain of the signal to be transformed. (From Peterson and Dobrin.)

4.4. Convolution

The convolution of two functions is result obtained by scanning one function with each element of the other and summing the products at each position of the scan. It is expressed by

$$h(t) = \int_{-\infty}^{\infty} f(\mathcal{T})g(t-\mathcal{T})d\mathcal{T}$$

$$\text{or } h(t) = f(t).g(t)$$

For the sampled data it will be written as

$$h(n\Delta t) = \Delta t \sum_{K=-\infty}^{\infty} f(K\Delta t) \cdot g(n-K)\,\Delta t$$

or neglecting Δt, we get

$$hn = \sum_{k=-\infty}^{\infty} f(n)\cdot g(n-k)$$

If we have a linear time invariant system whose impulse response is g(t)

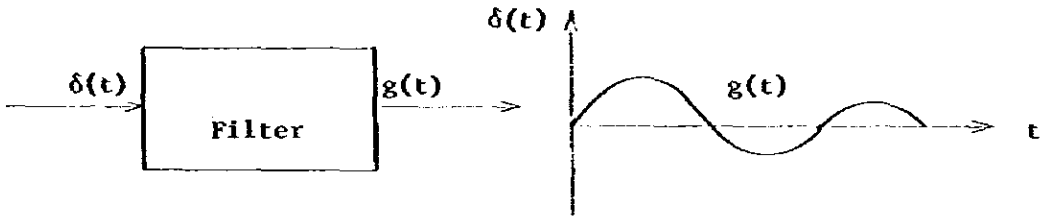

The total output h(t) of input function f(t) will be expressed

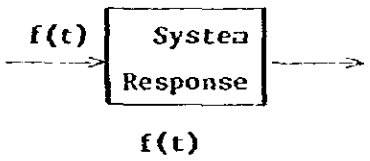

$$\text{output } h(t) = \int_{-\infty}^{\infty} f(\rho) \cdot g(t-\rho)d\rho$$

4.5. Deconvolution

Deconvolution is the inverse filtering which converts impulse response of a filter to impulse.

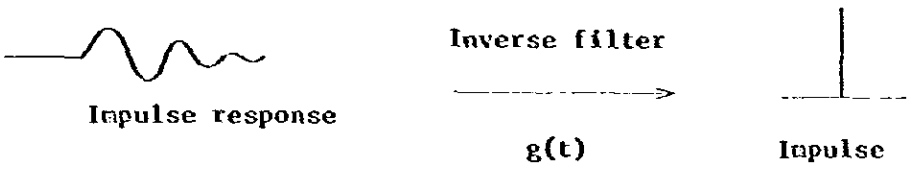

The process of cancelling the effect of a filter with a second filter designed to its inverse is called deconvolution.

The equation for the deconvolution operation in time domain is

$$f(t) = h(t) \quad * \frac{1}{g(t)} = h(t) \quad * \quad e(t)$$

where e(t) is the inverse filter with respect to g(t).

For frequency domain is

$$F(n) = \frac{H(n)}{G(n)} = H(n)E(n)$$

where F(n), H(n), G(n) and E(n) are frequency spectra or Fourier transforms of the respective time functions f(t), h(t), g(t) and e(t).

5. Conclusion

Seismic reflection survey for hydrocarbon searching is developing day by day. Multicoverage recording unit of 96 or more channels helps more noise cancellation for good data quality. The introduction of digital field system equipment brought the new capabilities in the recording and processing. We hope the technical revolution will bring more improvement in sophisticated data acquisition and processing techniques which are so far developed.

Acknowledgement

The author would like to thank Dr. H. Hasagawa, the course leader of Geoup Training Couse in Offshore Prospecting for valuable guidance and supervision during the course and also wish to thank Mr. T. Saito, Mr. H. Sato and Miss M. Kobayashi of Geological Survey of Japan for their valuable assistance in providing data and literatures. He expresses his great appreciation to Mr. I. Hirano, training co-ordinator of Japan International Cooperation Agency for his cordial sympathy and assistance. The author will never forget Mr. I. Hirano who visited and consoled him during his illness.

In preparing this report the author is specially grateful to Dr. Y.

Aoki of JAPEX who helped a lot and going through the report with great patient. He also expresses his best regards and thanks to Dr. T. Ikawa, Dr. H. Fujiura and Miss Wada of JAPEX for their assistance.

References

1) Dobrin, M.B. (1976), Introduction to Geophysical Prospecting, McGraw Hill, New York

2) Nettleton, L.L. (1940), Geophysical Prospecting for Oil, McGraw Hill, New York

3) Kawamura, T. (1978), Lecture Notes on Basic Seismic Processing.

4) Kobayashi, N. (1978), Lecture Note on Seismic Prospecting.

5) Hoshino, K. (1978), Lecture Note on Rock Mechanics.

6) Fujiura H. (1978), Lecture Note on Land Seismic.

7) Ikawa, T. (1975, 1978), Lecture Note on Digital Filtering and Velocity Analysis.

2. Evaluation of Petroleum Source Rocks by Means of Organic Richness and Natural Alkane Distribution

U Hla Myint*

Summary: Origin of petroleum is discussed on the view point of kerogen theory. Kerogen starts to generate petroleum hydrocarbons gradually at first and then rapidly by thermal crocking with increasing depth of burial.

The maturity of organic matter is, therefore, very important to know in source rock evalution.

There have been proposed several kinds of detecting method of organic maturity. CPI (carbon preference indices) is discussed on several deep wells which were drilled in Japan, and also relationship between CIP and another indicator, vitrinite reflectance.

As the organic richness is one of the most important factor in evaluation of source rocks, contrast of them between in petroleum producing area and in non-producing area are discussed for the examples of Russian platform, northern America and Japan.

1. Introduction

The origin of petroleum have very long history of controversy from the early days of the study of petroleum. Is petroleum formed biochemically (organic origin) or non-biochemically (inorganic origin) ? Although at present there is no completely satisfactory explanation for the origin of petroleum, the chemical evidence is strong that petroleum has an organic origin. Both geological and chemical evidence points to animal and vegetable organic matter accumulated in clays or fine grained carbonate rocks as being principal source of material for petroleum in general. Baker (1962) and Philippi (1956) demonstrated the positive relationships between hydrocarbons and organic material in shales and mudstones. It is also found that all sediments including recent sediments contain at least traces of hydrocarbons (Bray and Evans, 1961).

The transformation of organic material to hydrocarbons has been hy-

* Myanma Oil Corporation Ministry of Industry II, Burma

pothesized by many earth scientists in considering the origin of petroleum. But chemical analyses proved that all hydrocarbons found in the biosphere are not like hydrocarbons of petroleum. Indeed, petroleum-like hydrocarbons are only found in the subsurface as the origin. However, all the world's giant petroleum provinces are intimately associated with clays or fine grained carbonates with high content of organic matter.
Permeable and porous sediments rarely contain measurable quantities of hydrocarbons near the surface: but most clay do, and the deeper clays often contain petroleum like hydrocarbons although they may still differ in some respect from those of accumulated petroleum. Analytical evidence suggests that the original matter from which petroleum was generated consisted of fundamental organic compounds, such as protein (amino acids), fats, waxes, humus, and so on.

Hood and Castaño (1974) investigated the overall process of petroleum origin into four stages:

1. The first stage is the formation of an organic-rich sediments through the photosynthesis of an abundance of organic matter, its subaqueous deposition along with fine grained clays and/or carbonates, and its preservation in a non-oxidizing environment. These sediments represent potential source rocks for petroleum. They can be recognized by their high contents of total organic carbon.

2. Throughout the geologic time, the conversion of some organic matter to hydrocarbons and other petroleum molecules occurs with the diagenesis of organic-rich sediments. This relates to the increasing temperature and lithostatic pressure. This generation can be called as a part of the "organic metamorphism".

3. The complete migration and accumulation of petroleum from source rock to porous and permeable rock takes place in the organic metamorphism stage.

4. Sometimes, alternation stage may take place comprising a variety of process-physical, thermal and microbial.

Thus, organic richness and maturity are important factor in evaluation of source rocks. Organic richness of shales between producing and non-producing areas are clearly different (Ronov, 1900; Nixon, 1900 and Asakawa, 1978). As an indicator of organic maturity CPI of heavy normal alkanes is often used in evaluation of source rocks. The heavy normal alkanes (C24 - C34) provide another striking difference between the hydrocarbons in recent

sediments and those now contained in some ancient sediments (Stevens et al, 1956; Evans et al, 1957; and Bray and Evans, 1961). The normal alkane from the recent sediment is a strong preference for molecules with odd numbers of carbon atoms. This is in contrast to the crude oil which shows very little, if any, preference for the odd-carbon numbers. Therefore, source rocks which have a similar distribution to crude oils are recognized as a matured rocks.

In this report, source rock evaluations by means of organic richness and CPI of heavy normal alkanes are discussed.

2. Identification of Petroleum Source Rocks

a) Analytical procedure

The flow sheet of analytical procedure is shown in Fig. 1.
Detailed explanation of each procedure in the flow sheet is as follows:

1. Particle size is under 8 meshes.
2. Particle size of powder is under 100 meshes.
3. Organic matters are extracted with mixed solvent of benzene and methanol (7:3) from five hundreds grams of dried powder sample on soxhlst's extractor.
4. Liquid chromatographic analyses are determined on silica gel column with following ordered elutions: (i) with n-heptane to elutriate alkane hydrocarbons, and (ii) with mixed solvent of n-hexane and benzene (1:1) to elutriate aromatic hydrocarbons.
5. N-alkane is isolated by urea adduction from saturated hydrocarbons.
6. N-alkane distributions are analized gaschromatographically, and then CPI is calculated using the followsing equations:

$$CPI = \left[\frac{1}{\sum_{n=12}^{16} C_{2n}} + \frac{1}{\sum_{n=13}^{17} C_{2n}} \right] \times \frac{\sum_{n=12}^{16} C_{2n+1}}{2}$$

28.

where,

n = number of carbon atom

C_{2n} = even carbon number

C_{2n+1} = odd carbon number

7. Carbon content is detected by automatic elemental analyzer (C-H-N) corder for powder samples which inorganic carbon previously removed with hydrochloric acid treatment.

8. Total organic carbon is calculated as follows:

Organic carbon (%) = Insoluble organic carbon (%) + Extracts (%) x 0.85

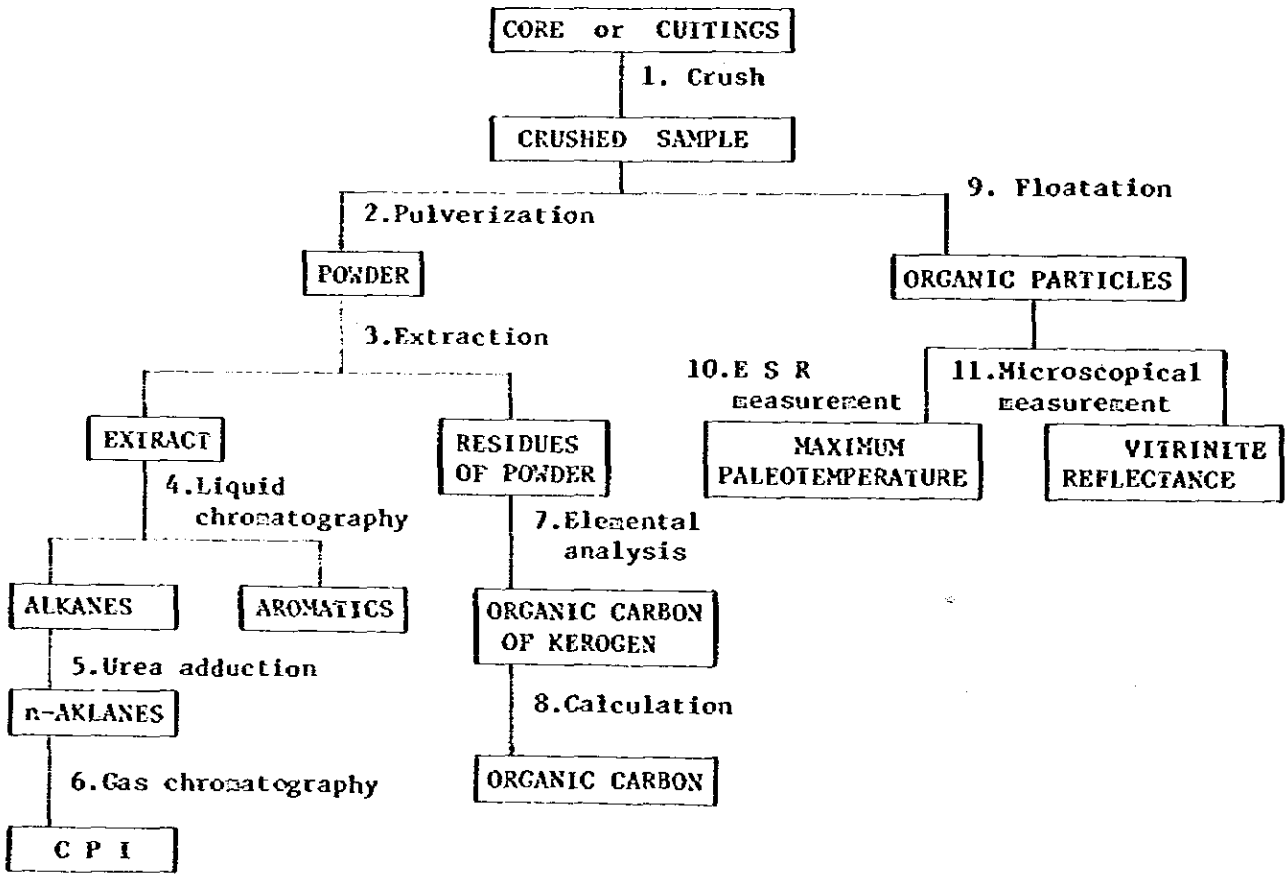

Fig. 1 Flow sheet of analytical procedure for determination of organic carbon and CPI.

9. Organic particles are collected by floatation on CCl_4.
10. ESR signals are measured with JES_{-3} x -band Spectrometer.
11. Maximum reflectivity of vitrinite is measured in oil with E. Leitz MP2 Micro Photometer.

b) Relationship between commercial oil deposits and organic rich sediments

(i) Western Russia

Ronov(1958) studied the distribution of organic carbon in 26,000 samples of rocks of different lithological composition and of different age and genesis, representing various facies and tectonic zones of the Russian platform, both in oil basins and in provinces devoid of oil.

All deposits of caustobolites (coals, petroliferous shales and oils) are closely related to stratigraphic intervals with an increased content of scattered organic carbon. The average organic carbon content in rocks of oil basins is three times as high as in rocks of areas not bearing oil (Fig. 2).

In oil basins the maximum organic carbon content is observed in sediments of marine nearshore deposits, representing epineritic environments; the minimum content — in sediments of continental and lagoonal environments are intermediate values——in sediments of open sea facies, representing infraneritic and bathyal environments (Fig. 3)

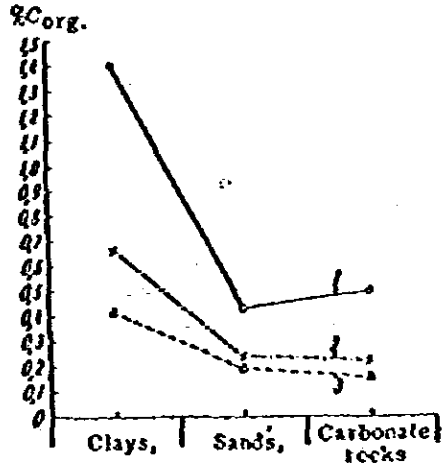

Fig. 2 Average content of organic carbon in different types of sedimentary rocks from petroliferous and non-petroliferous areas of the Russian Platform. (Based on analyses of 1105 composites (25742 samples); 1-petroliferous areas; 2-the Russian Platform as a whole; 3-non-petroliferous areas.)

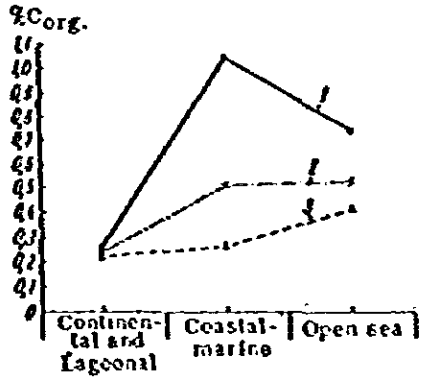

Fig.3 Average content of organic carbon in sediments of different facies zones in petroliferous and non-petroliferous areas of the Russian Platform. (Based on analyses of 1105 composites (25742 samples); 1-petroliferous areas; 2-the Russian Platform as a whole; 3-non-petroliferous areas.)

Among marine epineritic sediments of oil basins (1.77%) and of provinces not bearing oil (0.32%) clays are richest in organic carbon (Fig. 4). The organic carbon distributions in various rock types of continental and logoonal facies and of open facies are shown in Fig.5 and 6. With the aid of quantitative lighogeochemical maps most oilfields are found only in area of high organic carbon (Fig.7).

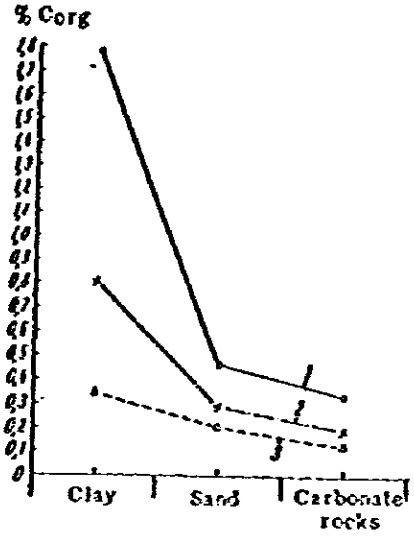

Fig. 4 Average content of organic carbon in different types of coastal-marine sediments in petroliferous and non-petroliferous areas of the Russian Platform. (Based on analyses of 455 composites (8409 samples); 1-petroliferous areas; 2-the Russian Platform as a whole; 3-non-petroliferous areas.)

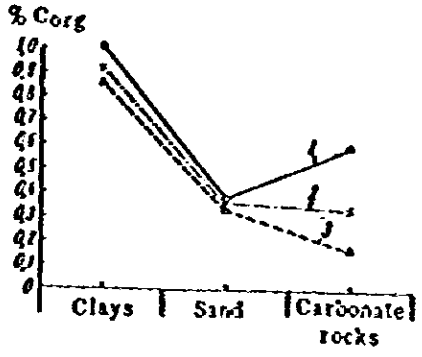

Fig. 5 Average content of organic carbon in different types of pelagic sediments in petroliferous and non-petroliferous areas of the Russian Platform. (Based on analyses of 258 composited (9039 samples); 1-petroliferous areas; 2-the Russian Platform as a whole; 3-non-petroliferous areas.)

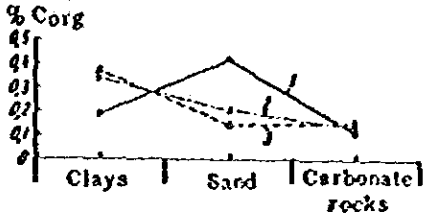

Fig. 6 Average content of organic carbon in different types of continental and lagoonal sediments in petroliferous and non-petroliferous areas of the Russian Platform. (Based on analyses of 392 composites (8294 samples); 1-petroliferous areas; 2-the Russian Platform as whole; 3-non-petroliferous areas.)

Example of oil fields found only in area of high organic carbon (After Ronov)

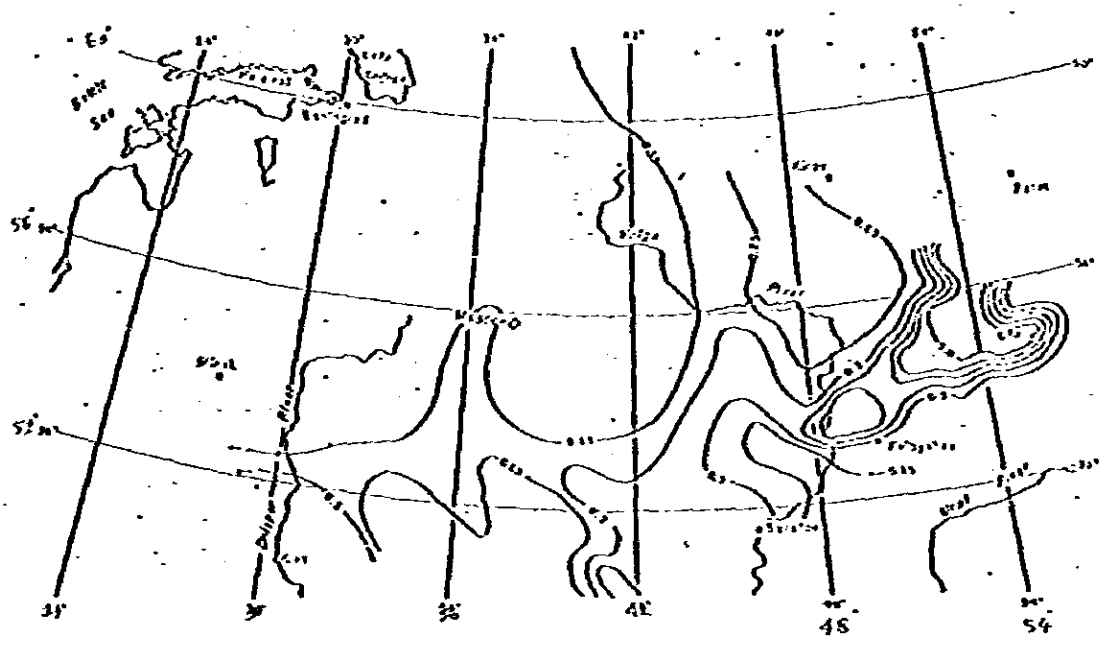

Fig.7 Oils were discovered from the Devonian in areas where organic carbon exceeds 0.5% (After Ronov, 1958)

(ii) Northern America

Nixon(1973) studied the presence of oil source beds in the Mowry shale and other marine time-equivalent rocks by organic geochemical analyses. In his study, 53 locations were sampled for source-bed character (Fig. 8).

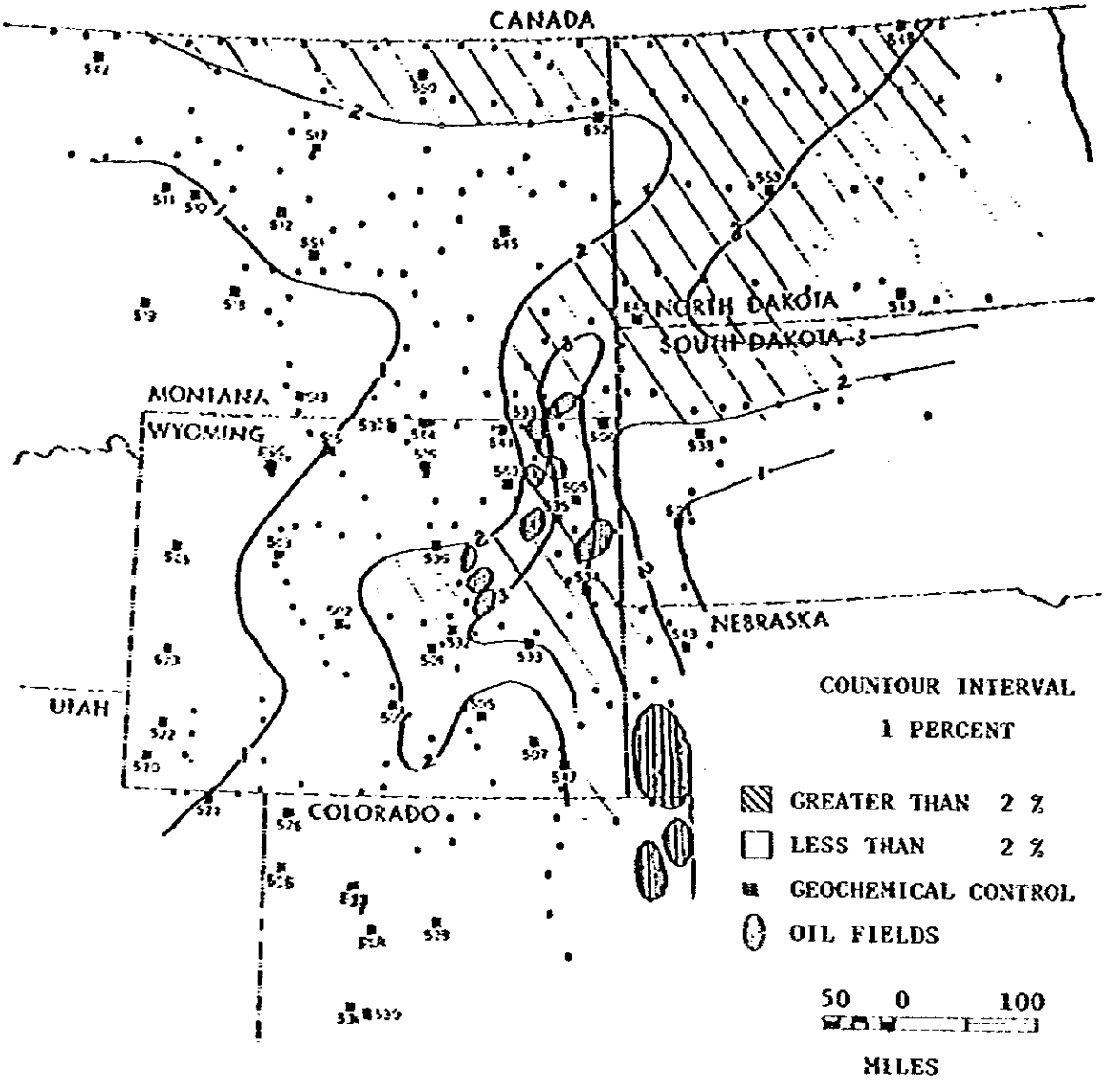

Fig. 8 Map showing regional variations in average concentration of organic carbon in Mowry interval (After Nixon)

Organic matter in the Mowry interval is widely distributed. High average concentrations of organic carbon were found at sample sites in eastern Wyoming and North Dakota. Average concentration tends to be lower in western Wyoming, Montana, and southern South Dakota.
These variations appears to be related to differences both in types of sediments and rates of deposition in various parts of the sea way.

It is found that the depositional history of the Mowry interval has influenced to the quantity and concentration of organic matter in its sediments. Mowry interval appears to have developed greatest source potential in areas where large quantity and high concentration of organic matter coincide.

It is clearly recognized that all producing oil fields fall in the place where the percentage of organic carbon is more than 2 (Fig. 8).

(iii) Japan

Asakawa et al investigated the liquid chromatographic composition of organic matter extracted by non-polar organic solvent and organic carbon content in a large number of argillaceous rocks in the petroleum provinces (backarc basin) and non-petroleum provinces (forearc basin). The analytical results were plotted in the source rock evaluation chart as shown in Fig. 9. The domain for the backarc basin (solid line) occupies positive oil source rock area while the forearc basin (broken line) occupies generally non-oil source area.
It is also conspicuous that the average of backarc basin falls in oil source area and the average of forearc basin falls in non-oil source area. It is, therefore, noted that the presence of source rock is of paramount importance to decide to drill a wildcat well in the area of interest.

(c) Differences of heavy normal alkane distribution among modern sediments, ancient sediments and crude oils.

The heavy n-alkanes (C 24 - C34) give striking difference between hydrocarbons in recent sediments and those now contained in some ancient sediments (Asakawa, 1978). These differences are illustrated in Fig. 10 where the relative abundance of the heavy n-alkanes from three samples is compared.

In the n-alkanes from recent sediment (the upper figure) there is a strong preference for molecules with old numbers of carbon atoms. This is in contract to crude oil (the lowest figure) which shows very little, if any, preference for the odd-carbon numbers. Shale sample is intermediate between

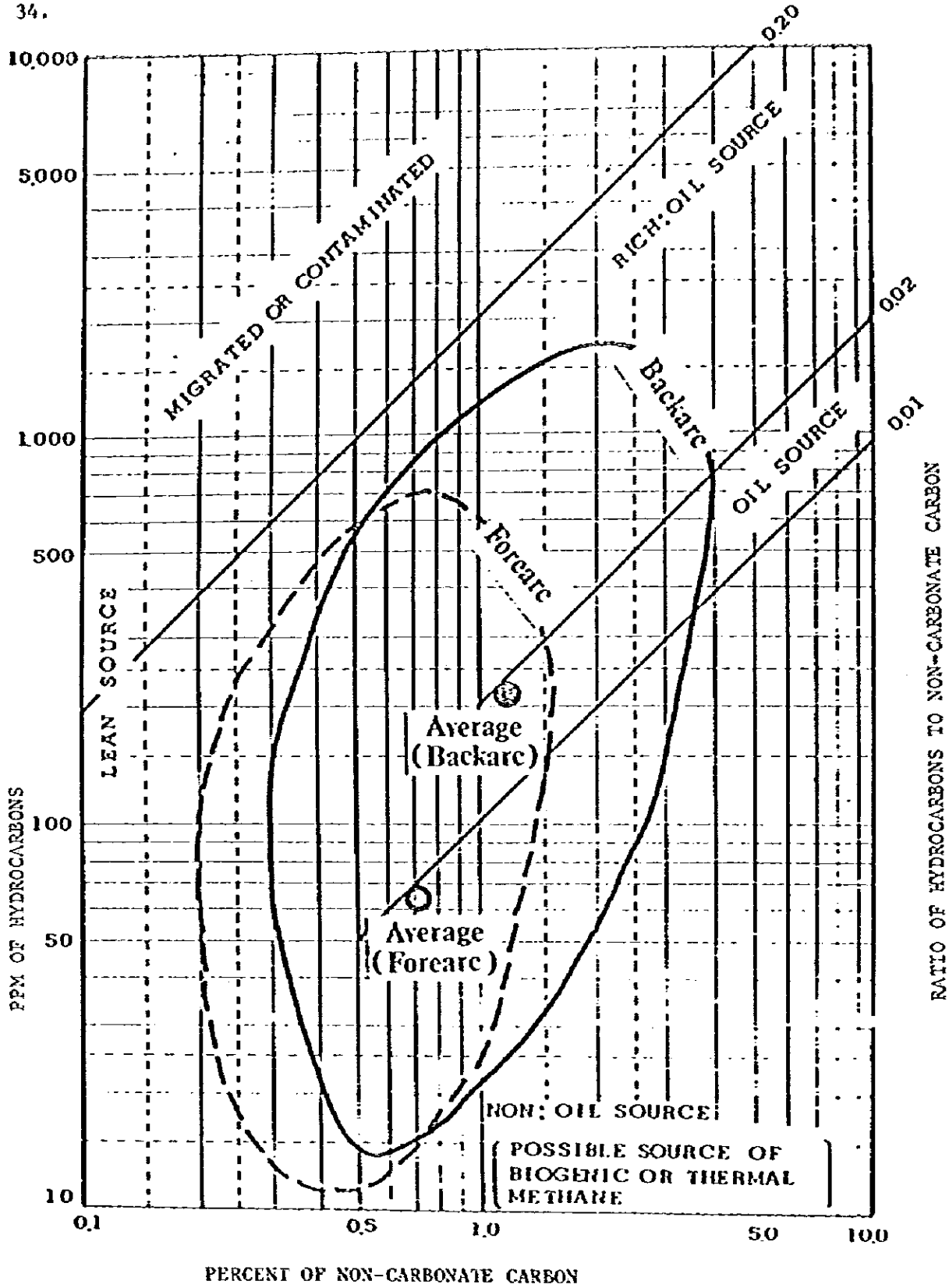

Fig. 9 Chart showing source rock comparison of petroliferous (back arc) and non-petroliferous (fore arc) provinces in Japan.

recent sediment and crude oil. CPI or carbon preference index numbers are designated in each figures that means how much more odd-carbon than even-carbon n-alkanes there are in each sample. In recent sediment there is 3 times as many odd-carbon-numbered molecules as even. In crude oil with a carbon preference index of 1.07, the odd and even-carbon-numbered molecules are practically equal in abundance.

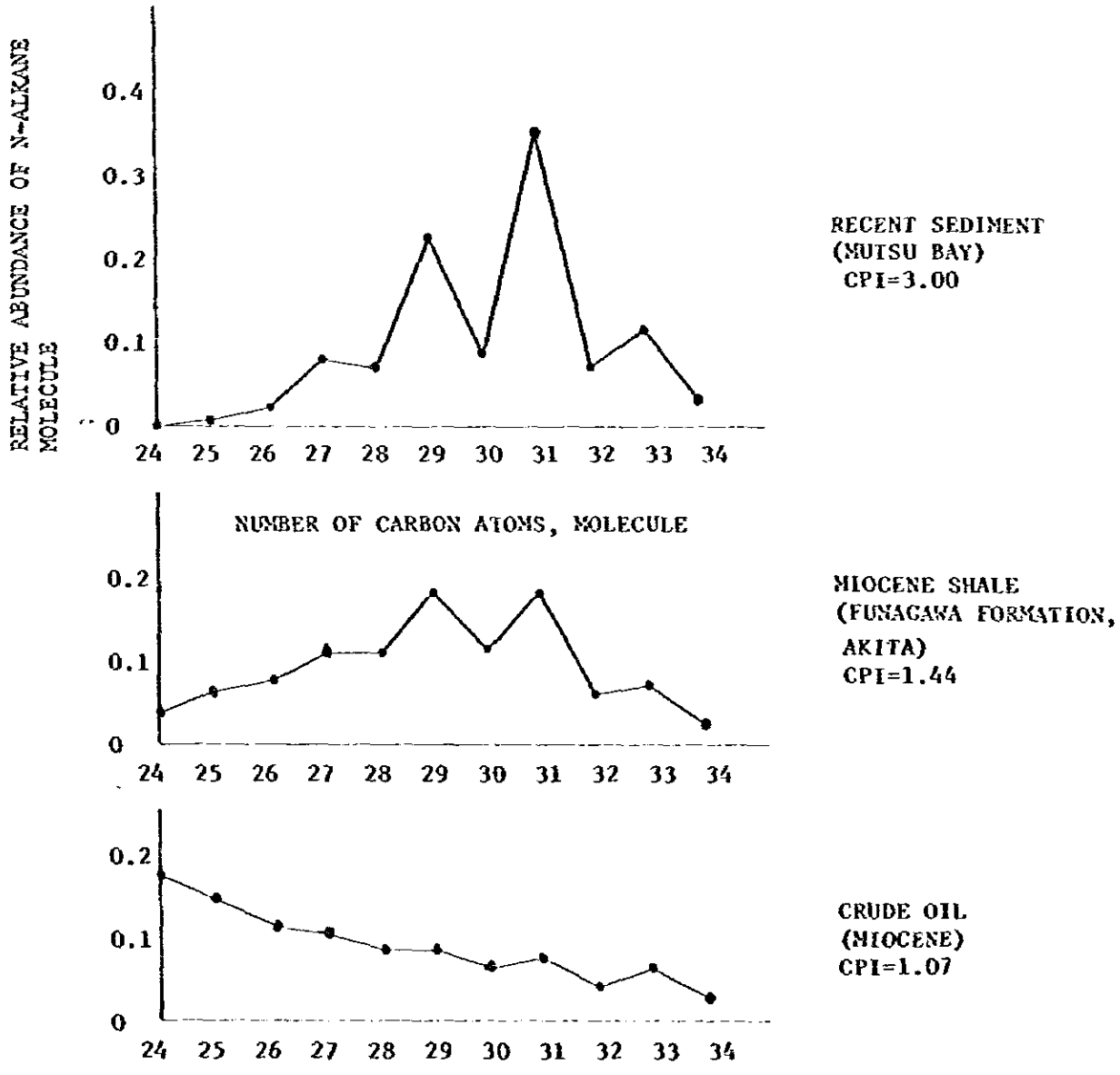

Fig. 10 Examples of n-paraffin distributions in sediments and crude oil

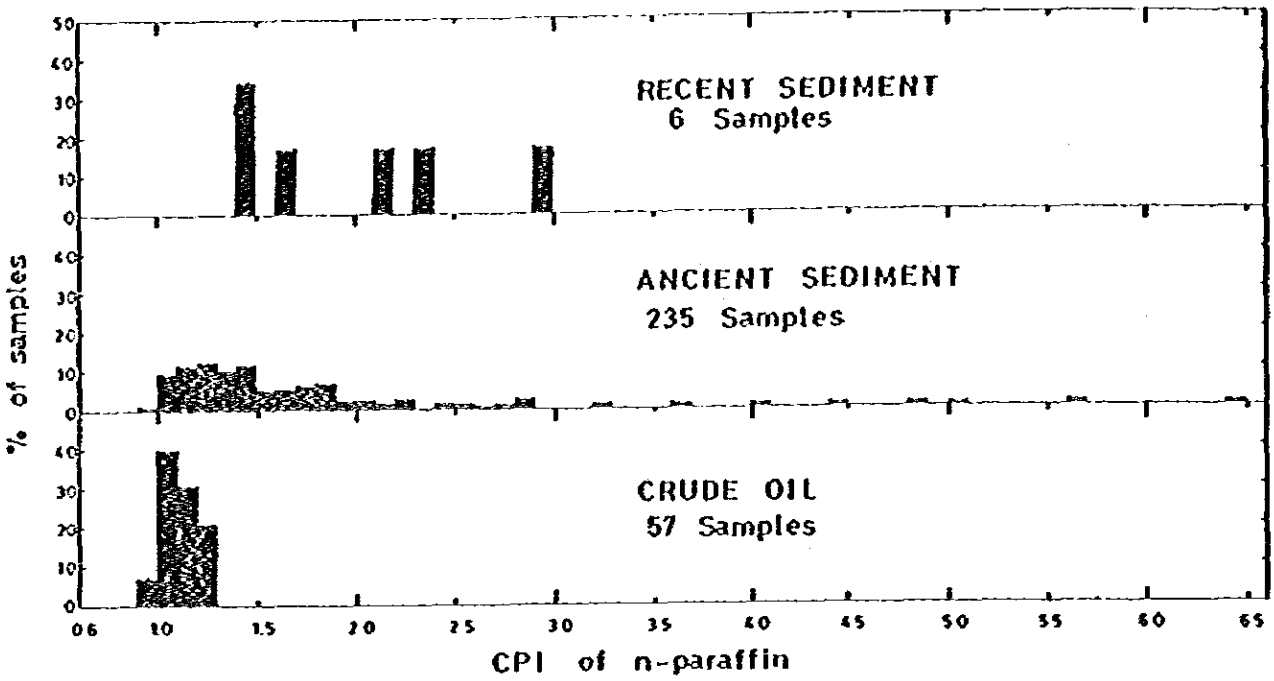

Fig. 11 Distribution of CPI in sediments and crude oils in Japan (After Asakawa, 1975)

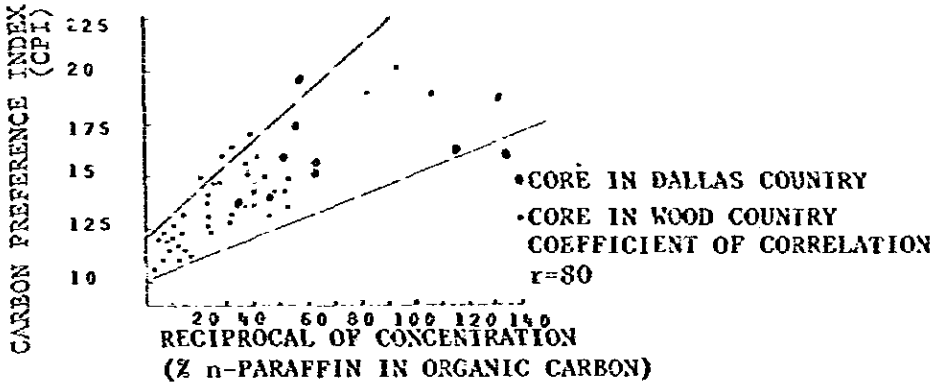

Fig. 12 Relation of carbon preference index and reciprocal n-paraffin concentration in Eagle Ford Shale.

(d) Relation of CPI of normal alkane to vitrinite reflectance of organic matter.

The n-alkane distribution depends on degree of diagenesis of organic matter. Maturity of source rock can be identified by the value of CPI of n-alkane. A source is called, therefore, mature when CPI of n-alkanes is just below 1.3 (typical crude oil).

Bray and Evans (1965) examined shales from Eagle Ford section by taking core samples. They took two coring sections, one from Dallas County, Texas and the other from Wood County. Figure 12 shows the relationship between carbon preference indix and reciprocal n-alkane concentration.

Their relation is consistent with generation of n-alkane having nearly equal proportions of odd and even carbon numbers as in petroleum. The Generally sheaking, lower CPI values and higher alkane concentrations from the section in Wood County are consistent with more transformation at depth in the basin. Robinson (1963) also examined a section of the Green River Formation and he found carbon preference indices (CPI) to decrease from 3.6 to 1.2 with increasing depth of burial. The reduction of CPI is assumed to be caused by dilution of newly formed n-alkanes with equal abundance of odd and even carbon numbered molecules.

CPI is an indicator of conversion of organic material to hydrocarbons in sediments. Sufficient dilution of newly formed n-alkanes to pre-existing n-alkanes which are not petroleum-like makes all n-alkanes to be petroleum-like characteristic.

Asakawa studied the correlation between vitrinite reflectance and CPI at various wells as shown in Fig. 13. The correlation of vitrinite reflectance to depth is relatively good, but that of CPI to depth is not very good. The smooth reduction of CPI with increasing depth of burial could not be generally expected, because it is largely influenced by the initial value at the time of deposition. The CPI values were, there on, used to the results which were projected to the smoothed trend line of each well. CPI value ranges from 1.3 to 2.0 at 0.5% of vitrinite reflectance as shown in Fig. 14. The disagreement of vitrinite reflectance which shows the initiation of hydrocarbon generation to CPI of petroleum-like, cannot be explained sufficiently. However, as an example the following explanation might be possible. The predominance of odd carbon numbered n-alkane is observed for the extracts of shallower sediments of the MITI-Hamayuchi well as shown in Fig. 15, and then it is reduced with increasing the depth of burial. Namely, at the shallower depths than 2,106m the mode is C27 or C29 in the histogram of relative number of n-alkanes, and then it shifts to C22 or C23 at the deeper depths. The change of major distribution in carbon numbers from heavy to light may show starting of generation and/or maturation of hydrocarbons. CPI of crude oil is restricted into the range from 0.95 to 1.3. Consequently at the zone in which hydrocarbon generation occurs but not reaches values of petroleum-

like, hydrocarbons generated in source rocks may be not able to migrate because of low content of hydrocarbons.

CPI values are inversely related to a proportion of hydrocarbon in organic material of shales and mudstones and, consequently, may be indicative of conversion of organic material to hydrocarbons. CPI values also give a unique clue for recognizing petroleum-like mixtures of heavy n-alkanes in non-reservoir rock. These petroleum-like mixtures occur more commonly in organic-rich and hydrocarbon-rich shales and mudstones which, from empirical observation, are inferred to be the source of oil.

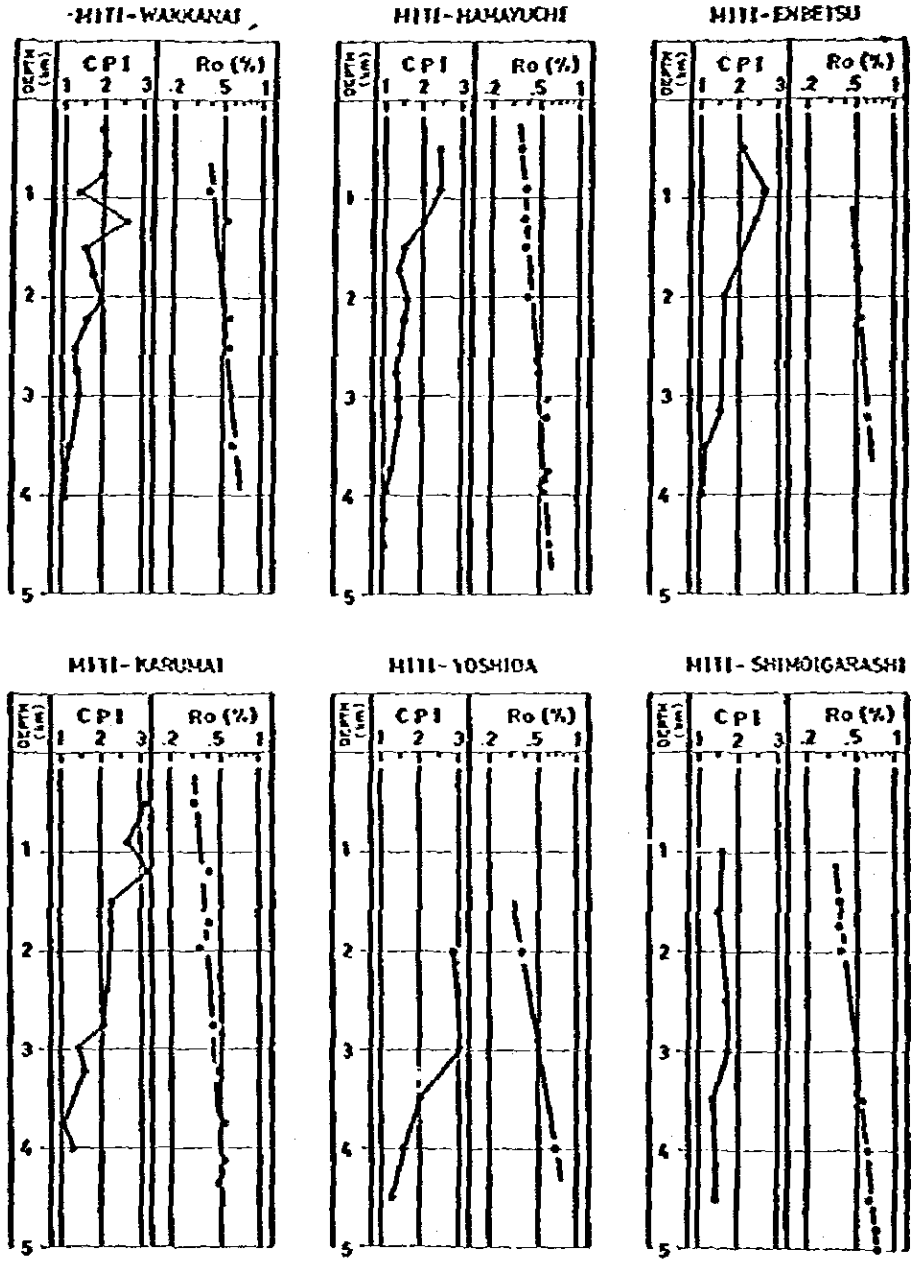

Fig. 13 Correlation between vitrinite reflectance and CPI from various wells in Japan (After Asakawa)

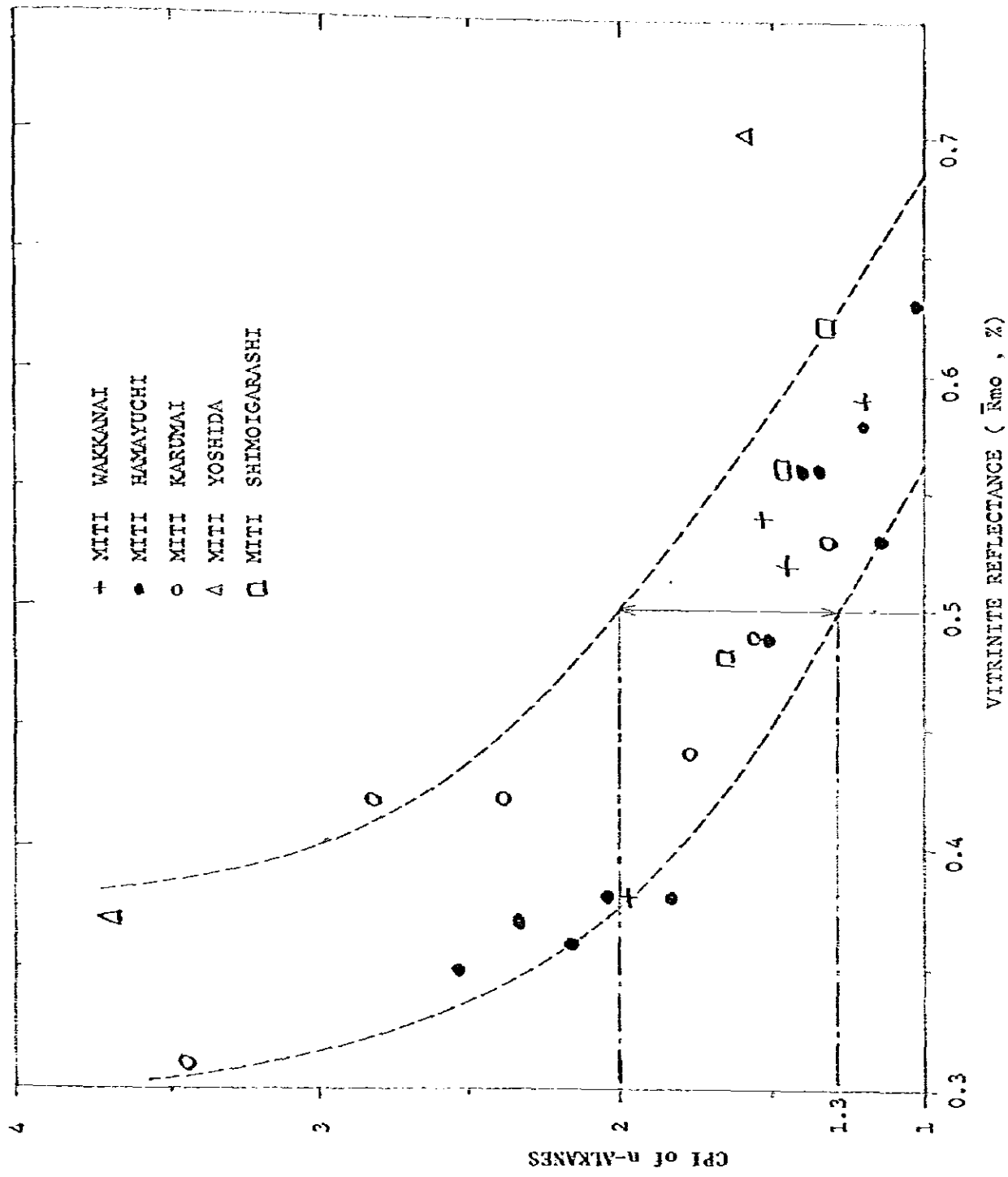

Fig. 14 Relationship between CPI of n-alkanes and vitrinite reflectance of organic matter from various wells in Japan (After Asakawa).

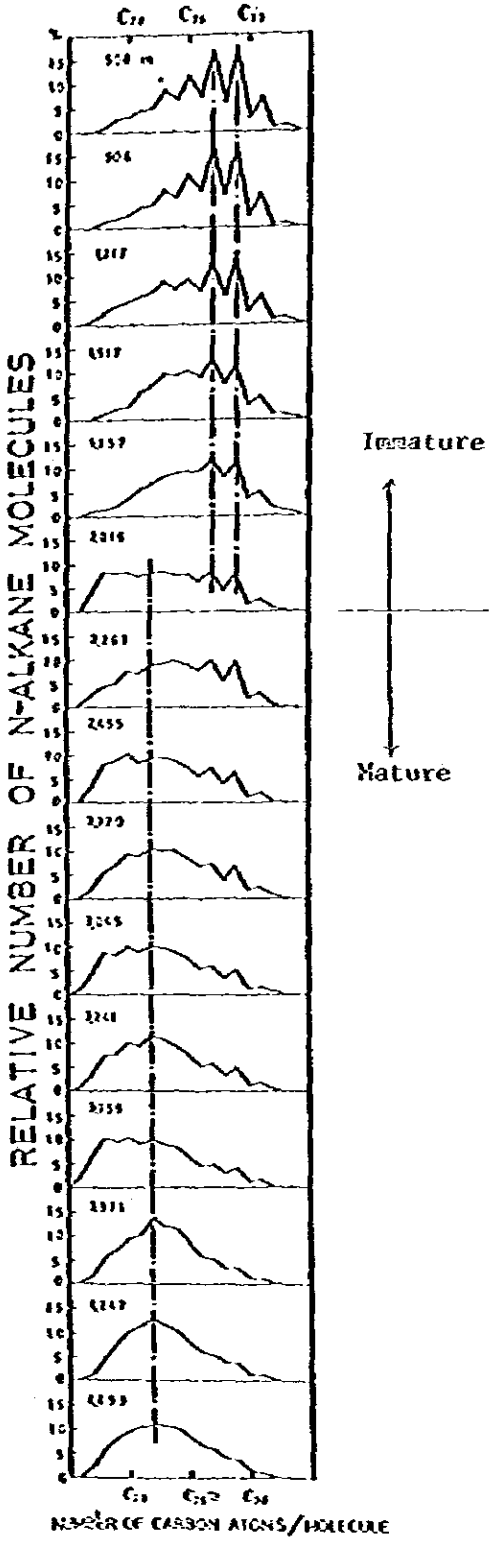

Fig. 15 Reduction of CPI with increasing depth of burial, NITI Hamayuchi, Hokkaido. (After Asakawa, 1975)

Conclusion

Determination organic richness and normal alkane distribution gives very useful clues to the identification of source rock. But we should make sure that if the samples can be representative of the stratigraphic units downdip. The variability of organic material in sediments complicates the search for 'source beds'. Systematic sampling based upon stratigraphic control is also compulsory.

The suitable relationship between the source rocks and the reservoir rock may favour the area of interest to an oil producing province. Nevertheless, the migration and accumulation phenomena must be considered - as a next step - after the identification of source rock is satisfactorily completed.

Acknowledgements

The author would like to express his best regards and thanks to Dr. T. Asakawa (JNOC) for providing references, and for the kind advice and good instruction through this study.

Thanks are also given to Mr. I. Hirano and Miss. M. Kobayashi who rendered help in preparing this report.

References

1) Asakawa, T. and Y. Fujita (1977), Organic Metamorphism and Hydrocarbon Generation in Sedimentary Basins of Japan, Paper read at CCOP/ASCOPE seminar.

2) Asakawa, T. (1978), Identification of Source Rock. Lecture Note, Offshore Prospecting Course in Japan.

3) Kudo, S., T. Asakawa and H. Yagishita (1965), Geochemical Study of Organic Matter in Petroleum Source Beds in Niigata Sedimentary Basin. Contribution from the Government of Japan to ECAFE Third Petroleum Symposium, Tokyo, Japan.

4) Bray, E.E. and E.D. Evans (1961), Distribution of n-paraffins as a Clue to Recognition of Source Beds. Geochimica et Cosmochimica Acta. vol.22,p.2-15.

5) _____ (1965), Hydrocarbons in Non-reservoir Rock Source Beds. Amer. Assoc. Petrol. Geol. Bull. 49, p.248-257.

6) Hood, A., and J.R. castaño (1974), Organic Metamorphism: Its Relationship to Petroleum Generation and Application to Studies of Authigenic Minerals. United Nations ESCAP, CCOP Technical Bullectin. vol. 8, p.85-88.

7) Nixon, R.P. (1973), Oil Source Beds in Cretaceous Mowry Shale of Northwestern Interior United States. Amer. Assoc. Petrol. Geol. Bull. 57, p.136-147.

8) Philippi, G.T. (1965), On the Depth, Time and Mechanism of Petroleum Generation. Geochimica et Cosmochimica Acta. vol. 29, p.1021.

9) Ronov, A.B (1958), Organic Carbon in Sedimentary Rocks (in Relation to the Presence of Petroleum). Geochemistry, no. 5, p.510-535.

10) Taguchi, k., and K. Sasaki (1973), Organogeochemistry and Its Relation to the Geology of Petroleum Accumulation in Japan. Biogeochemistry vol. 2, p.133-157.

3. Outline of Seismic Stratigraphy and Its Interpretation

Dadang Kadarisman*

1. Introduction

Depositional facies are predictable from seismic data through an orderly approach to the interpretation of seismic reflection termed seismic facies analysis. Seismic facies types generated by sand-shale strata vary mostly as a function of water depth at the time deposition. Therefore, a regional environmental framework of shelf, shelf margin, basin slope, and basin floor provides a useful gross subdivision for classification of clastic seismic facies units.

Shelf environment are characterized by general parallelism of reflections. The principal factors in defining seismic facies units are changes in reflection amplitude, frequency, continuity, interval velocity, and broad, low relief mound. The shelf margin and prograded-slope environment typically contains thick marine sediments and has water depth sufficient for the development of complex arrangements of sigmoid and oblique prograding reflection patterns. The basin slope and floor environment include a variety of deep basin facies as well as non prograding slope facies and facies that extend from the slope into the basin deep.

2. Seismic Facies Analysis

Seismic facies analysis is a procedure for basing interpretation of sand-shale depositional facies from seismic reflection data. This procedure involves the following:

1. interpretation and delineation of reflection geometry
2. continuity
3. amplitude
4. frequency
5. interval velocity

* Geological Research and Development Center, Ministry of Mine and Energy, Indonesia

6. external form and three-dimentional associations of groups of reflections

Description and mapping of seismic facies patterns gives a better interpretation of sedimentary processes and environmental facies leading to better lithologic prediction.

For classification and interpretation of seismic facies units, the following come in very useful :

1. Shelf environment which commonly is composed of marine and non-marine depositional sequences.
2. Shelf margin and prograded slope environment which typically contains thick marine sediments and has water depths sufficient for development of complex arrangements of sigmoid and oblique prograding reflection patterns.
3. Basin slope and floor environment which includes a variety of deep basin facies, non-prograding slope facies, and facies extending from slope to the basin deep.

2.1 Clastic Seismic Facies

Major clastic seismic facies may be classified into the following :

1. Shelf seismic facies. Sediments deposited in these environments tend to generate parallel to gently divergent reflection configurations with widespread sheet or wedge-shaped, external form

a. High-amplitude and high-continuity facies. High continuity of reflection in this facies suggest continuous strata deposit in a relatively widespread and uniform environment, and high reflection amplitudes are interpreted to indicate interbedding of shale with relatively thick sandstones, siltstones or carbonates rocks. Normally, deposit in this facies consist of neritic sediments.

HIGH AMPLITUDE AND CONTINUITY INTERPRETED

b. Low-amplitude facies (Uniform-energy depoits, high or low). Low amplitude zones on a seismic section indicate either beds too thin to be resolved by seismic methods or a zone of predominantly one lithologic type. Consequently, the low amplitude facies may be either sandprone (high-energy) or shale-prone (low energy).

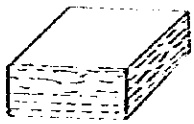

LOW AMPLITUDE
UNIFORM ENERGY

c. Low-continuity and Variable-amplitude facies (Variable energy). Low-continuity and variable-amplitude seismic facies may occur in widespread sheets or may show prominent wedging with basal onlap where sediment supply is sufficient to fill a rapidly subsiding zone (basin). Reflections are typically parallel in the sheet forms and divergent in the wedge form.

LOW CONTINUITY
VARIABLE AMPLITUDE
VARIABLE ENERGY

d. Broad, low-relief mound facies (Variable energy). This shelf facies noted at only a few location is interpreted as reflecting a complex of delta lobes formed on a subsiding shelf. The key distinguishing feature to its identification is a broad, gently mounded external form.

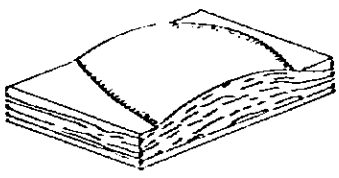

BROAD, LOW-RELIEF MOUND
VARIABLE AMPLITUDE AND
CONTINUITY (VARIABLE
ENERGY)

2. Shelf-margin and prograded-slope seismic facies. The next major class of seismic facies unit is associated with shelf-margin and prograded slope types of deposition.

a. Oblique-progradational facies (typically high-energy in up-dip portions). The distinguishing feature of this facies is a prominent oblique reflection configuration when viewed parallel with depositional dip. Reflections terminate by top-lap at or near the upper surface and by downlap at the base.

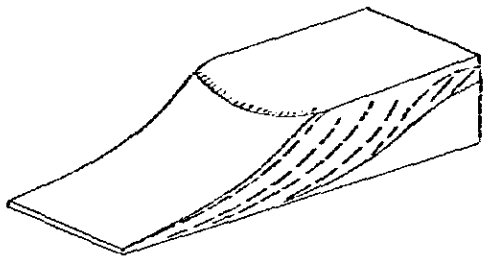

b. Sigmoid-progradational facies (low energy). These units are characterized by gentle sigmoid (S-shaped) reflections along depositional dip. The reflections down lap at the base and are concordant with the top of the unit.

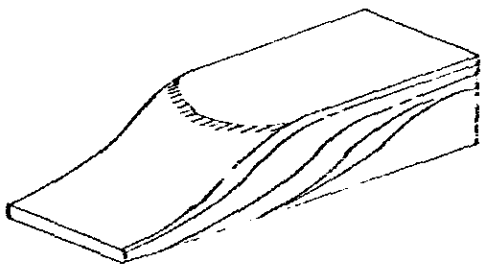

SIGMOID PROGRADATIONAL
(LOW ENERGY)

c. Basin-slope and basin floor seismic facies. The groups of seismic facies units that dominate the basin slope and floor are :

1. Parallel reflections of this seismic facies drape over contemporaneous topography with only gradual changes in thickness or reflection character and suggest uniform deposition independent of bottom relief. This pattern is strongly indicative of marine hemipelagic clays and oozes with almost no potential for sand development.

2. Slop-form fill facies (low energy). On dip sections this common deep-water facies characteristically shows parallel to sub-parallel reflections sloping seaward with pronounced up dip onlap, and down dip downlap.

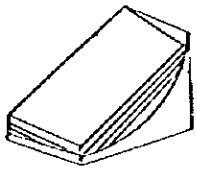

SLOPE-FRONT FILL
(LOW ENERGY)

3. Onlapping-fill seismic facies (predominantly low energy) This low energy facies does not show the mounding characteristic of mounded onlap and chaotic-fill facies and its reflections tend to have a more uniform parallel to gently divergent pattern with high continuity and variable amplitude.

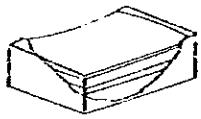

ONLAP-FILL
(USUALLY LOW ENERGY)

4. Mounded seismic facies (variable energy). The most prominent deep-water mound are fan complexes, contourite mounds and slumps.

5. Mounded onlapping-fill facies (high energy). Mounded onlapping-fill seismic facies units are characterized by a mounded form and prominent onlap away from topographic lows.

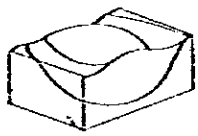

MOUNDED ONLAP-FILL
(HIGH ENERGY)

6. Chaotic-fill facies (variable energy). Chaotic-fill seismic facies units are characterized by a mounded external form by location in topographic lows, and by an internal pattern of contorted to discordant to wavy subparallel reflection.

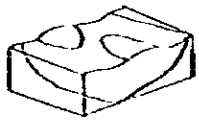

CHAOTIC-FILL
(VARIABLE ENERGY)

48.

3. Interpretation of Echo Sounding

3.1 Slope Correction

P. de Vanssay de Blauous and J.D. Nares (1933) showed that for a sea floor with a constant slope, the slope of the echo trace was less than the sea floor slope and related by the following figure :

Sin Q = Tan a

where Tan Q = true slope of botton

tan a = slope of echo trace

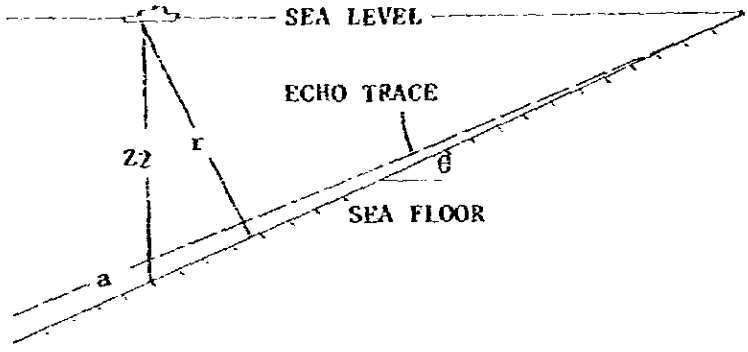

Fig. 1 Echo sounding profile of a sea floor with a constant slope.

This figure below illustrate this relationship. Note that up to a 15 degrees slope, tan Q and tan a are very closed. Even up to 30 degrees, the departure is not very great compared to standard charting errors. In this discussion, it is assumed that the ship is moving directly up or down the slope. For the true depth (Zz) beneath the ship for a constant slope is :

$$Zz = \frac{r}{\text{Cos } Q} = \frac{r}{\sqrt{1-\tan^2 a}}$$

final correction

where r = recorded depth

In general, the sea-floor does not have a constant slope. To obtain the true position and slope of a point from the echogram, we must work with the sea-floor at the point of reflection rather than directly beneath the ship (refer to figure on echo sounding profile of a sea floor with varying slope). Therefore, the information for point A is recorded

while the ship is at point B and not at point C. The true depth at point A is mathematically expressed as

$$Z_1 = r\sqrt{1-\tan^2 a}$$

where tan Q = slope of echo trace at point D

Z_1 = true depth at point of reflection

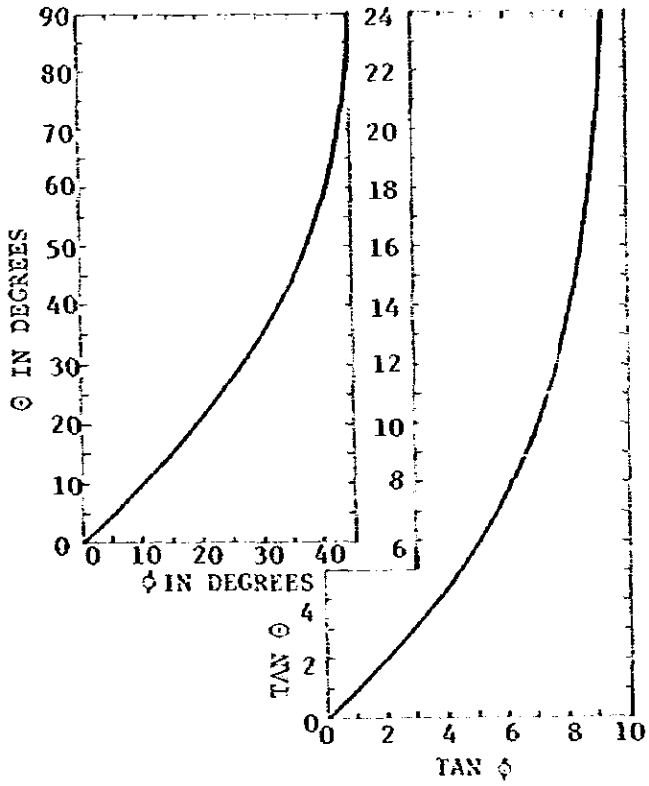

Fig. 2 Plot of the relations of equalation (1). Θ is the slope of the sea floor; ◊ is the slope of the echo trace of the sea floor.

50.

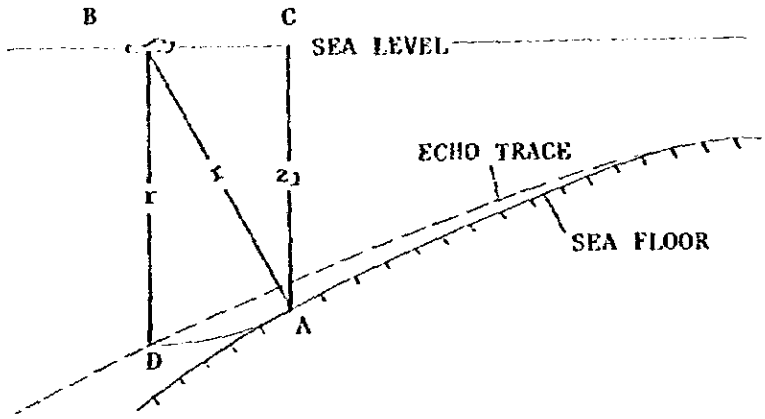

Fig. 3 Echo sounding profile of a sea floor with varying slope.

3.2 Hyperbolic Echo Trace

As shown by Hoffman, any sea peak or sharp change in slope will give a hyperbolic echo trace (please refer to figure on echo trace from a sharp peak) of the form :

$$\frac{(z' + n)^2}{n^2} - \frac{x^2}{n^2} = 1$$

where n = depth to apex hyperbola

z' = Depth of a point on the hyperbola beneath the apex

x = horizontal distance of the point on the curve from the apex

With these two characteristics in consideration, all of the following were derived.

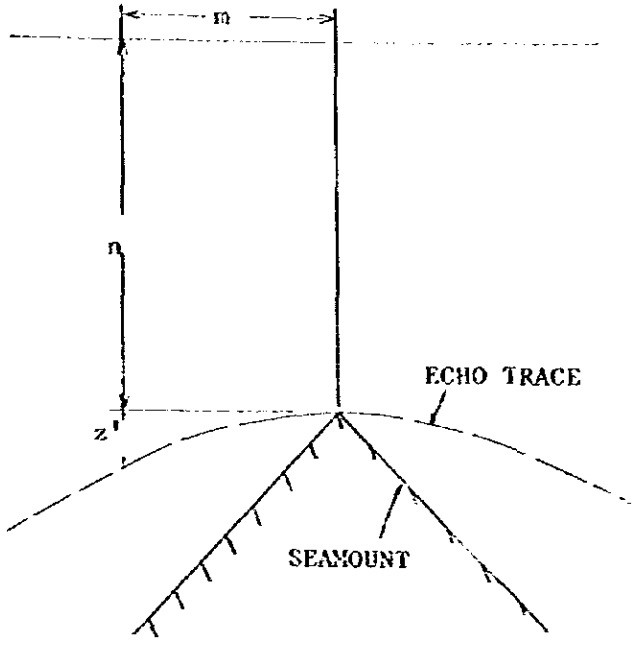

Fig. 4 Echo trace from a sharp sea peak

3.3 Section of Wedge-Shaped Ridge

This is a two dimentional figure (refer to figure on echo trace of a wedge-shaped ridge) and may be regarded as a crossing of a cone directly over its axis or a crossing of a wedge-shaped ridge at right angles to its axis.

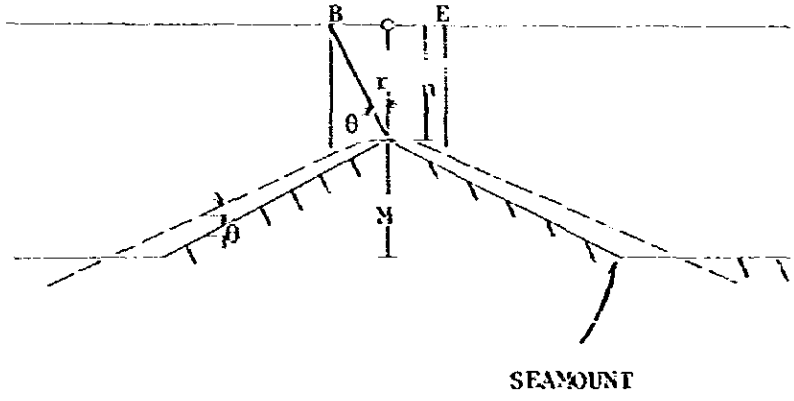

Fig. 5 Echo trace of a wedge-shaped ridge

The formula for the hyperbolic section of the echo trace (between points B and E) follows from :

$$\frac{r^2}{n^2} - \frac{m^2}{n^2} = 1$$

At points B and E, the hypebolic echo from the peak merges with the plane echo from the sides. This intersection occurs as soon as the sound ray becomes perpendicular to the side of the ridge. At point B then :

$$x = n \text{ Tan } \theta$$

and the echo below point B has the form :

$$r = \frac{n}{\text{Cos } \theta}$$

3.4 V-Shaped Symmetrical Notch (simplified trench)

Let the half-width of the notch be (W_2) and (m) be the horizontal position of the ship. Then for $m > W_2$, Z=Zo. For the region, $W_2 > m > x_1$

where $x_1 = w_2 - z_0 \text{ Tan } \theta$

the echo trace is hyperbolic : $r^2 - (w_2 - m)^2 = Zo^2$

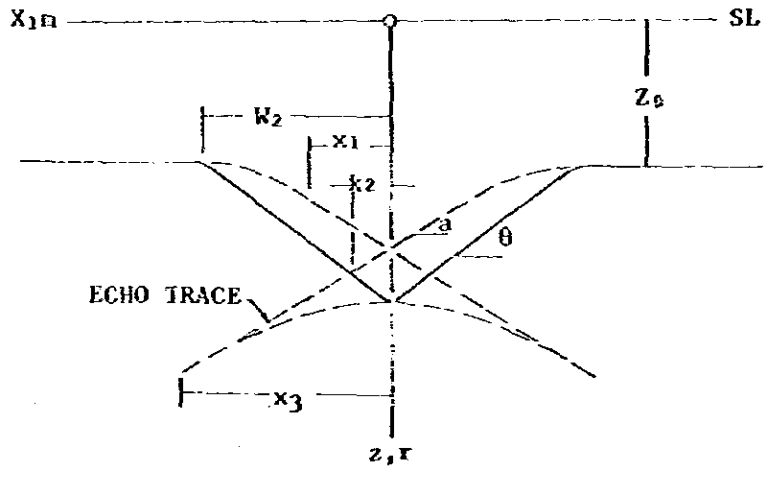

Fig. 6 Echo trace of a V-shaped depression

For the region, $x_1 > m > x_2$, the echo trace is a straight line which carries on beyond (X_2) to (X_3) :

$$r = Zo \cos\theta + W_2 \sin\theta - m \sin\theta$$

In terms of recorded slope of that recorded echo (Tan a)

$$r = Zo \sqrt{1 - \tan^2\theta} + (w_2 - m) \tan a$$

The difference in depth between the crossover depth (ro) and the true depth (Z_1) at the axis of the notch is :

$$(z_1 - ro) = (Zo + w_2 \tan\theta)(1 - \cos\theta)$$

In terms of the slope of the echo :

$$(z_1 - ro) = \left(Zo + W_2 \frac{\tan a}{\sqrt{1-\tan^2 a}}\right)\left(1 - \sqrt{1-\tan^2 a}\right)$$

If we place the origin over the rim (at sea level) instead of over the axis, equation $r^2 - (W_2 - m)^2 = Zo^2$ becomes :

$$r^2 - m^2 = Zo^2$$

Interpretation of the Record from Tokyo Bay

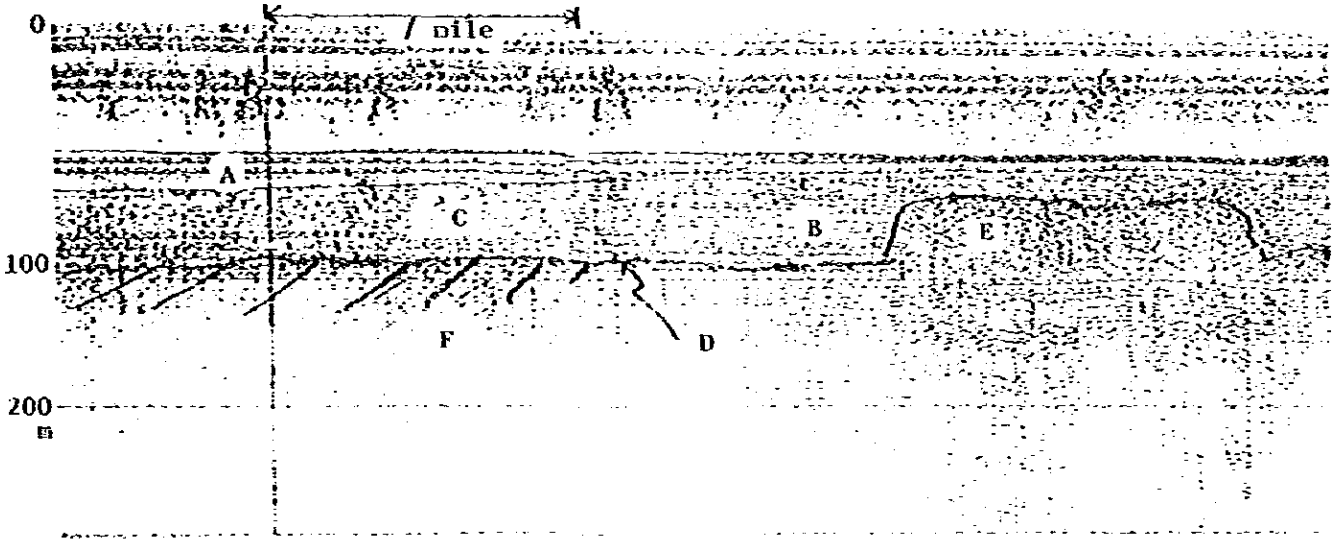

Legend:

A = Low amplitude
marine, no reflection and last channel
B = Slit & Sand
high amplitude and high continuity
C = Composed of mud
Low continuity and variable amplitude
D = Unconformity
E = Procrude (Pull up) conglomerate
F = Pleistocene formation

Acknowledgements

The author wishes to express his thanks to Dr. Hideo Kagami of the Ocean Research Institute, University of Tokyo for his assistance in making this report possible. Valuable information and data were freely furnished by Dr. H. Kagami for the preparation of this reports.

The help extended by Dr. Hiroshi Hasegawa, Mr. Tomosaburo Saito and other personnel of Geological Survey of Japan greatly facilitated the completion of this report.

Finally, the author wishes to express his thanks to Mr. Isamu Hirano, JICA coordinator who patiently and efficiently arranged together with Mr. T. Saito my research work in the Ocean Research Institute, University of Tokyo.

References

1) Dobrin, M.B. (1960), Introduction to Geophysical Prospecting. McGraw-Hill, New York.

2) Krause, D.C. (1962), Interpretation of Echo Sounding Profiles, International Hydrographic Review, vol. 39, no.1.

3) Sangree, J.B. and J.M. Weidmeir (1973), Seismic Stratigraphy and Global Changes of Sea Level, Part 9 : Interpretation of Clastic Depositional Facies. The American Association of Petroleum Geologist vol. 62, no.5.

4) Stacey, F.D. and S.K. Banerjee (1974), The Physical Principles of Rock Magnetism. Elsevier Scientific Publishing Co., Netherlands.

4. Measuring Equipment for Aeromagnetics

Subijantoro*

Summary: The aeromagnetic method has been established in less than two decades as the most useful one in mining and petroleum exploration. This paper takes first the general field operation procedures reviewing the basis of the measuring equipment on boarding the aircraft.

1. Introduction

The airborne magnetic surveying method is one of the other important geophysical methods grows rapidly by developing new instruments and significant techniques.

In comparison with other disciplines, the high rate of coverage and low cost per unit area explored makes it advantageous in approaching the situation of geological structures. The ability to require data regardless of ownership on area accessibility is also profitable.

Since the susceptibilities of sedimentary rock are relatively small, the main response is due to igneous rocks below the sediments.

2. History of the Method

The earliest recorded attempt to used and airborne magnetometer seems to be that of Edelmann, who, in 1910, designed a vertical balance equipped in a ballon. (Heiland, 1932, 1938)

Next, more successfully, pendulum and gyro-stabilized coil-type earth inductors were tried. These rotating coil instruments were built on an ordinary electric generator principle, and were developed as marine and aircraft compassed. The main disadventages of the earth-inductor systen as a magnetometer were low sensitivities, caused by orientation errors and ship ring noise. Even so, Rogachev (1946) used an earth-inductor devise with a sensitivity of about 1000 gammas over the Kursk iron deposits in 1936.

* Directorate General Oil and Gas, Ministry of Mines, Indonesia

It was Victor Vacquir who in Gulf Research and Development Company in 1940 and 1941, prefected a sensitive magnetic saturation type of detector element. Also known as a fluxgate, this sensor formed the heart of the magntic airbone detector, Antisubmarine Magnetometer, and could measure field as weak as 10^{-5} oersted.

In 1946, Hans Rundberg (1947) introduced a stabilized verical-intensity magnetometer, presumably the earth-inductor type, which was successfully used

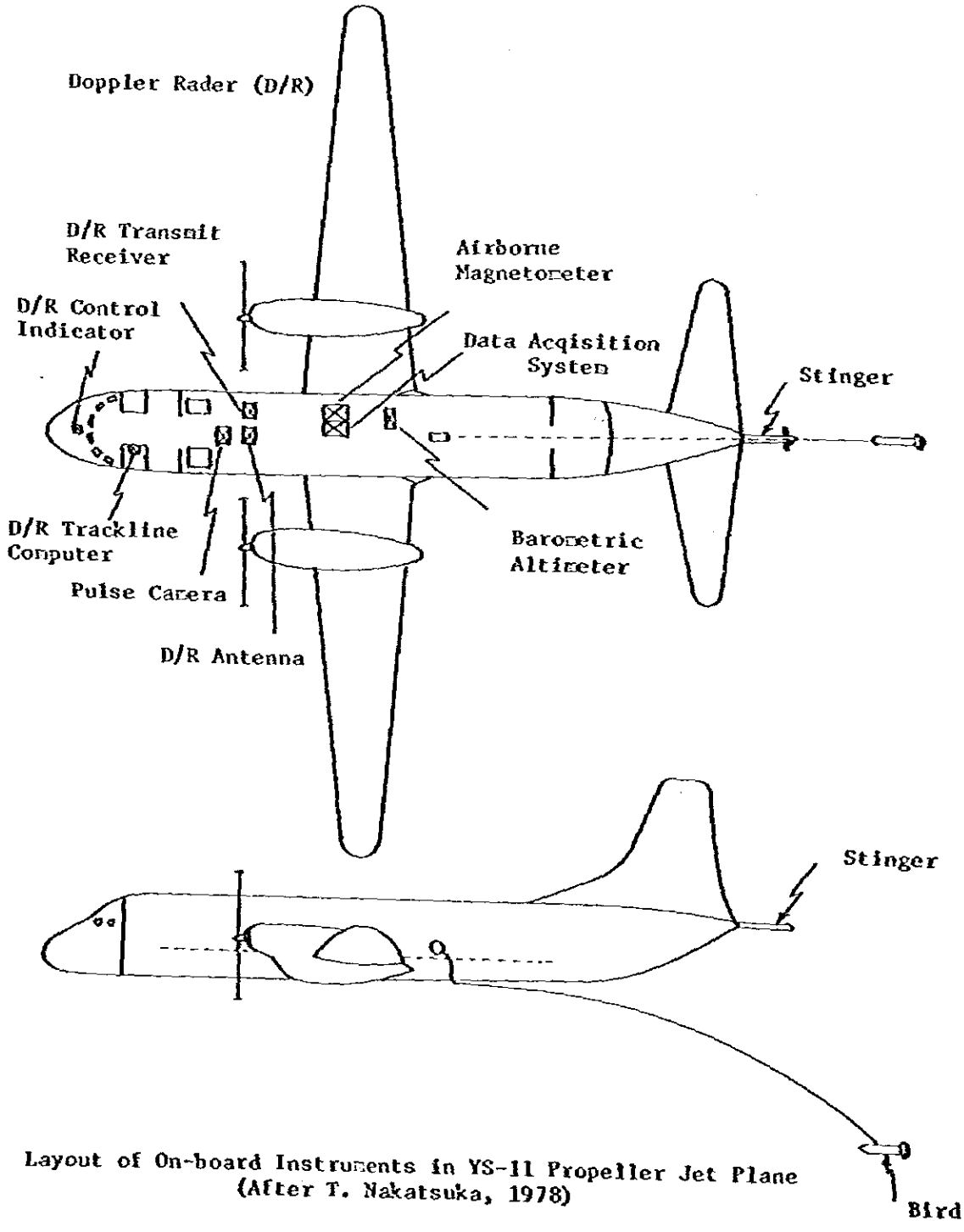

Layout of On-board Instruments in YS-11 Propeller Jet Plane
(After T. Nakatsuka, 1978)

in a helicopter. This device sufficiently sensitive for mining exploration purposes, and was used for several years on contract surveys.

The Elliott aspect electron tube was developed by the U.S. Navy and has since been adapted for used as a prospecting magnetometer (Wagg, 1963) This novel instrument is a magnetron type of vacuum tube in which the earth's field apparently can be measured to and accuracy of about 5 gammas, which is quite sufficient for mining exploration. The Elliott tube total full instrument has been used by his Joint Exploration of Canada on and offer type aircraft in conjunction with airborne electromagnetic Surveying. The International Nickel Company is also reported to have operated instrument of this type.

A good summary of magnetic instruments including flux-gate, proton precession, and Hall effect deviced, is continued in the paper by Whilham (1960).

3. Measuring Equipment

3.1. Electronic Magnetometer

It used for magnetic prospecting. Since electronic magnetometers are free from the effects of rotional acceleration they can be operated on airplanes and ships. As a result of this fact the magnetic incremented field measurement from to point observations in ground with a sensitivity of 5 to 10 gammas continuous the observations in the air utilizing speeds over 100 mph and obtaining sensitivities under 1 gamma.

There were three steps in the development of electronic magnetometers. The fluxgate was originally developed during World War II as submarine detector. The second instrument is the Proton Precession Magnetometer which depends on fundamental properties of an atom. The third instrument uses the spectro of "pumped" alkali vapors.

3.1.1. Flux gate magnetometer

The detector consists essentially of two identical cores of high permeability material placed parallel to each other, and wound with a series opposing primary coils (see Fig. 1). A second winding surrounds the two primary windings. The coils are connected to an A.C. moment, each system has a decrease on its self-induction producing and unbalance in the primary wave form. When the two primaries are balanced, no voltage is induced in the secondary coil. The pre-

sence of an external field along the axes of the cores produces an inbalance by bringing one core to saturation sooner and a voltage pulse is produced in the secondary twice perprimary cycle. The amplitude of the pulse is proportional to the applied field, and the device is capable of measuring its component along the axis of the core. The secondary signals can be shaped, amplified, rectified and recorded.

3.1.2. Nuclear resonance magnetometer

Free precession of protons in the earth's magnetic field was first observed experimentally in 1953 by Packard and Varian (1954). The effect of nuclear resonance had been predicted by Bolch (1946) in consideration of the magnetic-spin properties of atomic nuclei. The total field proton instrument based on this theory was a radical departure from earlier magnetometer which used micro-magnetic substances in their detection and measurement system.

The proton precession instrument operates on the principle that the precessional frequency of oriented protons in a magnetic field is proportional to the field intensity. This can be written as:

$$H = \frac{2\pi pf}{\mu}$$

where

H is the field strength

f is the precessional frequency

p is the angular momentum for protons

μ is the magnetic moment in the direction of p.

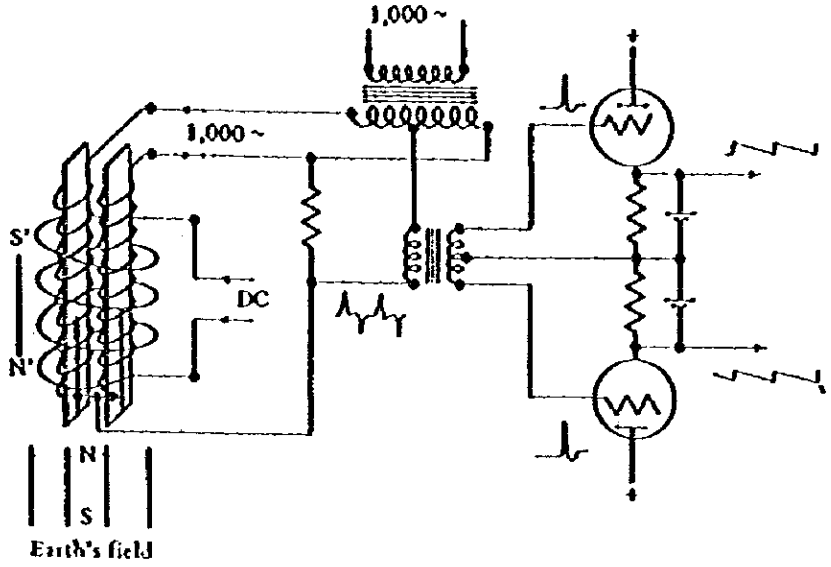

Fig. 1 Schematic diagram of flux-gate magnetometer detector circuit. Secondary voltage is here obtained by the pulse transformer from modification of primary circuits and is equivalent to a single secondary. Secondary winding is shown as helmholtz-coil compensating means, producing a bucking north-south field. (After Nettleton, 1974)

The ratio μ/P is the gyromagnetic ratio, which is a physical constant known for protons to one part in 133,000, and thus determines the absolute accuracy of a field strength measurement.

In practice, the proton continuing medium is polarized by a coaxial coil with about 100 oersted field. The field is then turned off and the same coil pickes up the relaxing audio-frequency precessional field of the protons, which continues until phase incoherence obliterates the signal. The polarization and relation cycle for most instruments is one to three seconds, depending on polarization field, signal level, and characteristics of the proton containing fluid.

3.1.3. Optical absorption magnetometer

The principle of optical pumping of electrons of a gas or vapor was described by A. Kastler and J. Brossel of Ecole Normale Superieur in Paris and F. Bitter of MIT in 1950. The concept of optical pumping in volves the energy transition or "pumping" by optical-frequency radiation of electrons from only one of two closely spaced energy levels to a third higher level, from which they fall back to both of the original two level. When complete pumping is achieved, all of the electrons are effectively transferred to the other one of the two

lower-energy levels. At this point, the gas cell no longer absorbs the pumping radiation, and becomes transparent to it. Redistribution of the pumped electron to the first lower level is accomplished by stimulation from a radio frequency corresponding to the difference in energy between the two levels.

In this fashion the pumping effect is distroyed the cell become apaque and is again able to absorb energy from the pump source. Since this energy difference and, hence, the radio frequency required to nullify pumping are proportional to the ambient magnetic field. This frequency gives the measure of the magnetic field.

Alkali vapors are readily pumped because these elements have one valence electron and, hence well-defined lower energy states. Absorption of polarized light changes the energy of the valence band electron by one unit of angular momentum, which is the difference in energy between the two lower levels described above.

One could view the optical absorption magnetometer effect as being similar to that of proton precession, in that the radio-frequency pulses cause the electrons to wobble, or precess around the field direction at radio frequencies. This wobble produces a flicker to the transmitted light. In the Varian associaties rubidium vapor magnetometer this flicker is detected and fed back to the cell by means of a coil, thus producing a self-oscillating magnetometer whose oscillation frequency is proportional to a magnetic field. For Rb^{87} the constant of proportionality is 0.6996 mc per gauss, for Rb^{85} it is 0.4667 per gaus.

A schematic diagram of a helium magnetometer is shown on figure 2. The energy-level diagram of rubidium showing Zeeman splitting of the ground state is given in figure 3.

The use of nuclear precession and optical pumping magnetometer from mobile platforms requires that consideration be given to minor effects on the devices due to vehicle orientation and rotation, if maximum sensitivity is to be utilized.

The basic output of all these magnetometers is a frequency which varies linearly with total magnetic field. As the angle between the earth's total magnetic field and the magnetometer reference axis is changed, the amplitude of the steady-state output will change. Thus, under these conditions, although this amplitude change alone will not produce an error in the measured field value, this signal level may fall below that required for operation on the electronic circuit. This difficulty may be overcome, in the case of optically pumped instruments, by adding the signals from three sensors whose axis are

mutually orthogonal. In this fashion, the signal amplitude may be contained to lie within certain bounds depending upon the power of the angular orientation dependence.

3.2. Associated Equipment

3.2.1. Frequency meter

Measures the frequency delivered by the magnetometer that is proportional to the magnetic field. With an optical pumping magnetometer using cesium vapor the relation is 1 gamma per 3.490688 Hx. In order to increase the precision of the final measurement, a multiplier is added and the read-out is then multiplied by either 10 or 30.

3.2.2. Digital recording

To make full use of the high sensitivity magnetometer requires digital recording. This permits making an analog record if desired at any horizon. The digital recording is made up regularly of two superposed racks. The upper rack contains the electronics and the controls, and the bottom one contains the actual record, mounted on a shock proof base.

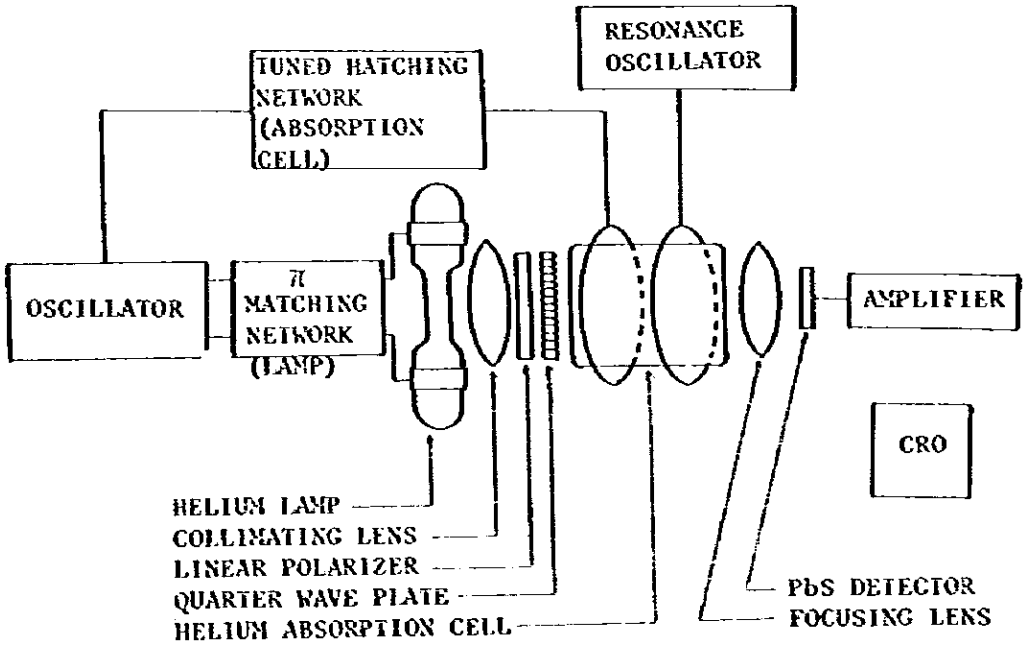

Fig. 2 Schematic diagram of a helium magnetometer

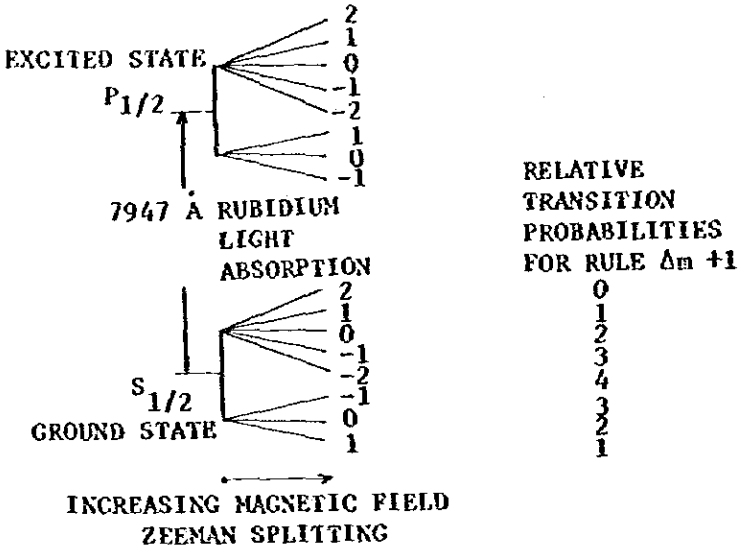

Fig. 3 Energy-level diagram of rubidium, showing Zeeman splitting

3.3. Location System

For a successful airborne magnetic observation it is necessary to locate the flight lines and to correlate the readings at any moment with the ground position. Several location systems are used for this purpose.

3.3.1. Aerial photograph

Many of the onland aeromagnetic surveys are positioned by aerial photograph. The horizontal position of the airplane is determined by recording photograph either by taking a series of intermitted pictures with 35 mm frames at intervals of 1 or 2 second or continuous 35 mm strip camera film. Later, in the office, these are compared with the photomap previously obtained and each argument carefully matched with the picture on the ground.

3.3.2. Electronic posicioning system

In unmaped areas or in regions of water, desert of featureless the photographic method of location cannot be used, and electronic navigation aid are necessary. There are four system in this positioning system:

- Shoran system

- Radio frequency system
- Doppler system and
- Radar system

3.3.3. Altimeter

The third dimension of the position of the aircraft is determined by altimeters, either barometics or radio. The former measures the high above the sea level, and the latter above the ground.

4. Conclusion

Experience shows that offshore surveys carried out with radio frequency system and specially with Toran are more accurate. This is mainly due to the routine use of the radio navigation (controls and efficient calculation of errors) and to the automatic restitution of heights which avoids the errors due to on sight navigation for example.

Specially airborne magnetic surveying is very attractive for reconnaissance because of the low cost per mile and high speed of surveying. This speed reduces the cost per line-mile, as we have been, but also decreases the effect due to the time variations in the magnetic field and instrument drift.

Acknowledgements

The author wants to express thanks to the personal of the Geological Survey of Japan, particularly regard and best wishes to Dr. H. Hasegawa and Mr. T. Saito who celebrated in the preparation of this paper.

References

1) Balsley, Y.R. (1969), Aeromagnetic Surveying, U.S. Geological Survey, Washington D.C., p. 313-325

2) Redford, M.S. and J.S. Sumner (1964), Aeromagnetic Geophysics, vol. 29, p. 482-516

64.

3) Bloch, F. (1946), Nuclear induction, Phys, Rev. vol. 70, p. 461

4) Bloom, A.L. (1960), Optical pumping, Scientific American, October, p. 72-80

5) Nettleton, L.N. (1974), Gravity and Magnetic in Oil Prospecting, McGraw Hill, New York, p. 327-359

5. Experimental Studies on Heavy Minerals

Juan M. Saldarriaga R*

1. Introduction

Concentration of detrital heavy minerals result from normal cycles of erosion of the land surface and economic deposits occur where the rock material has yielded sufficient quantities of the valuable mineral type sand where physiography and climate have provided suitable conditions of transport and accumulation.

During the erosion cycles most of the rock forming minerals are fragmented and otherwise altered by a combination of physical and chemical actions and only the more stable mineral survive.

Heavy minerals are defined operationally as those with a specific gravity greater than 2.85 the S.G. of the bromoform liquid used to separate then from highter quartz, feldspar or calcite.

Although over 100 different minerals have been recorded for sediments, they probably form no more than 0.1-0.5% of the terrigenous fraction of sediments. Despite their small amount, they are great value in studying provenance, transportation and weathering history of a sediment and in correlation and paleographic studies, they represent the accessory and varietal mineral of igneous and metamorphic rock.

Common heavy mineral range from 3 to 5 in specific gravity because of their heaviness, they usually travel with quartz averaging 0.5 to 1.0 size larger this difference is known as the "Hydraulic ratio" and varies for each mineral species, the value is affected chiefly, also by the original size of the mineral grains in the parent rock.

Thus, if a sand has a median of 2.5, tourmaline may have a median 2.9ϕ and, zircon 3.5ϕ when a sand such as this is sieved, the heavy minerals fall in the finer size.

Grades and the heaviest occur at the very finest thus when the heavy minerals are mounted one may find that the 4.0-4.5ϕ grade has 90% zircon and 10% tourmaline, and the 3.5-4.0ϕ grade has 10% zircon and 90% tourmaline.

Sound of different size within the very same bed may consequently have

* Institute of Science & Mining Technology, Ministry of Energy & Mines, PERU

radically different percentages of the several heavy minerals, hence mineral ratios between minerals of different specific gravity or shape are chiefly a function of grain size. One has to use minerals of the same shapes and specific gravity in practice this boils down to marking varietal studies of one mineral, such as tourmaline or zircon. Then when comparing ratios between the different varieties one knows that the specific gravity and shape are essentially the same hence there is no hydraulic factor, differences in varietal ratios will then reflect differences in source area lithology.

Heavy minerals are generally studied in terms of four groups: Opeques, Micas, ultra-stables, metastables.

1. Opaque minerals;

These generally have very high specific gravity, because of their iron content. Little has been done with them; they are more a nuisance than a help, at present.

a. Magnetite and Ilmenite. May form placer of economic value, very difficult to tell apart except magnetically; both moderately stable, but magnetite may alter to hematite or limonite and fairly commonly alters to chalky-looking leucoxene or even fairly large crystals of sphere anatase, or other titanium minerals. Magnetite and ilmenite are more stable under oxidizing conditions but are dissolved readily in a reducing environment.

b. Pyrite is nearly always authigenic: thus occurs in great amounts in some heavy minerals slides, is absent in most others.

c. Hematite and limonite are usually alteration products but sometimes may be detrital.

d. Leucoxene is an aggregate of extremely fine-grained sphene, rutile or anatase and forms as an alteration product usually after ilmenite.

2. Micas;

Percentages unreliable because they do not always sink in bromoform. commonly not counted in heavy mineral studies because of their widely different shape, hence difference hydraulic behavior.

3. Ultra-stable group;

Zircon, tourmaline and rutile. Because the first two are very hard and inert, they can survive many reworkings. When older sediments are reworked to form younger ones, Zircon and tourmaline are about the only ones that can survive. Also, in supermature rocks they are about the only ones that can withstand such prolonged abrasion.
Hence they are the backbone of many heavy mineral suites. An abundance of tourmaline and zircon in a heavy suite then means either.

prolonged abrasion and chemical attack has occurred
the minerals are being reworked from older sediments
both tourmaline and zircon are excellent correlation indicators and
idiomorphic zircon is an indicator of volcanism

4. Metastable group;

Olivine is very rare in sediments, occuring only under dry climatic conditions and rapid erosion. Chiefly from basic igneous rocks.

Apatite is moderately stable commonly it occurs spordically (abundant in a few specimens, sparse in others) then indicates a volcanic source, otherwise it can occur in basic to acidic plutonic rocks.

Horneblende and pyroxene are moderately unstable; may come from either igneous or metamorphic rocks, but when present in abundance indicate volcanics or metamorphic rocks, such as hornblende schist.

Brown oxyhornblende is diagnostic of a basaltic source, glaucophene and tremolite are others less common amphiboles, indicating almost certainly a metamorphic source. Pyroxenes are etched and dissolved rapidly by solution after deposition, hence are rare in porous sands.

Garnet may come from plutonic rocks, pegmatites or metamorphics but in abundance indicates a metamorphic source. Many varieties present, based chiefly on color. Stability variable, depending on the variety; often corroded on sea floor or instrastratally to produce fantastic etch figures. Rapid dissolved in many porous sands, especially those flushed by fresh water.

Epidote, cliuozoisite and zoisite indicate a metamorphic or hydrothermal source, they are moderately stable.

Kyanite, sillimanite, andalusite, staurolite are highly diagnostic of a metamorphic source, they are moderately stable, but usually rather soft.

2. Formation of Beach Placer Deposits

Beach placer are formed when the mechanical or chemical breakdown of rock masses is followed by a redistribution of the material along a continental shelf.

The valuable minerals are generally resistant to weathering and hence become concentrated with the coarser grained sediments the final distribution of values being affected by the sedimentation properties of the particles and the strength and direction of the wind and ocean currents.

Periods of upwards warping of the coastal areas. Eustatic variations in sea level and the migration of wind-blown sand dunes has converted some of these sediments to land formations and, consequently many beach placers occurs at considerable distances in land from the present coastline. Some also become indurated or partially cemented through the agency of ground water.

The most important placer accumulations develop at the base of frontal dunes on open beaches and in the natural traps formed by headlands and other barriers to the free pasage of longshore currents. They are characteristically lenticular in shape and may vary in size up to many hundreds of feet in length and several feet in thickness.

Aeolian placers are formed in conditions where large expanses of beach sand are exposed to the action of the wind. They are characterised by secondary dunal systems wide develop according to the direction and force of the winds the surface contours of the ground and the presence or otherwise of barriers to the drift of the sand. Mineral concentrations within the dunes have developed as pencil thin seams and in more or less disseminated masses during alternate periods of stability and migration. (Fig. 1 and 2.).

Formation of Beach Place Deposits

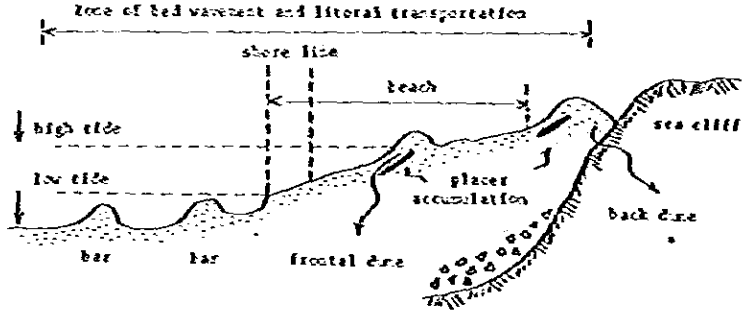

Fig. 1 Showing typical beach pattern with off-shore bars. Lenses of mineral accumulations have formed placer deposits in dunal systems.

3. Exploration of Mineral Reserves

The purpose of boring and sampling is to obtain a set of data whose measurements are reproduceable within required limits, may be permitted for economic reasons during reconnaissance and scout boring.

The constituent parts of each section of the deposit must have equal opportunities of being represented and there must be no possibility of bias in the subsequent calculations.

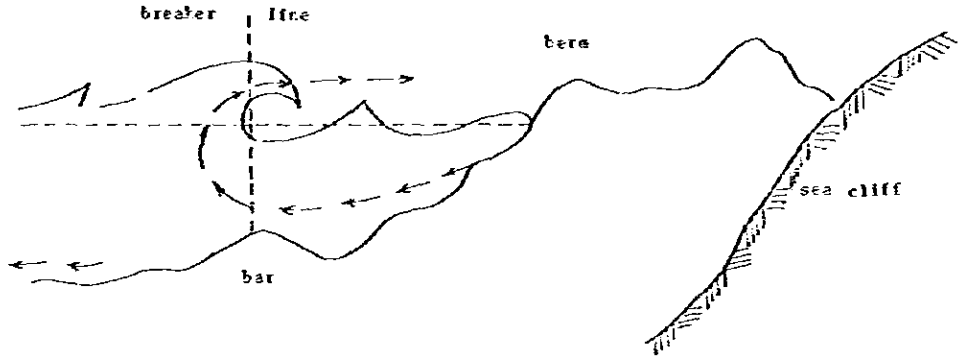

Fig. 2 Showing circulation of water movement of sediments from the berm to an offshore bar along a beach. Density currents are development on sea ward side of breaker line.

Correct conclusions depend upon the number and placement of samples the methods of testing the samples and the techniques used in obtaining them.

4. Actual Procedure of Marking Out

In marking out a line grid for beach mining evaluation the base line is stabilished by theodolite survey as nearly as possible along the longitudinal axis of the deposit. Where the mineralized zones are curved, the base line should be angle appropriately.

Holes which are bored at intersections with the base line are designated 0. for the N-S axial trend as described the bore numbers are prefixed with the letters E or W depending upon whether they are to the east or the west of the base line.

For an E-W axial trend the numbers are prefixed with the letters N or S depending upon their location relative to the base line.

5. Boring and Sludging Equipment

The hand drilling equipment described in table 1 for one team of drillers boring and sludging to depths of 10 meters.

An appropriate additional quantity of casing and aluminium drilling roads is needed for sampling to greater depths.

6. Hand Boring

In most beach mineral placers where the sediments are fine grained and relatively unconsolidated, hand boring provides the cheapest and most reliable

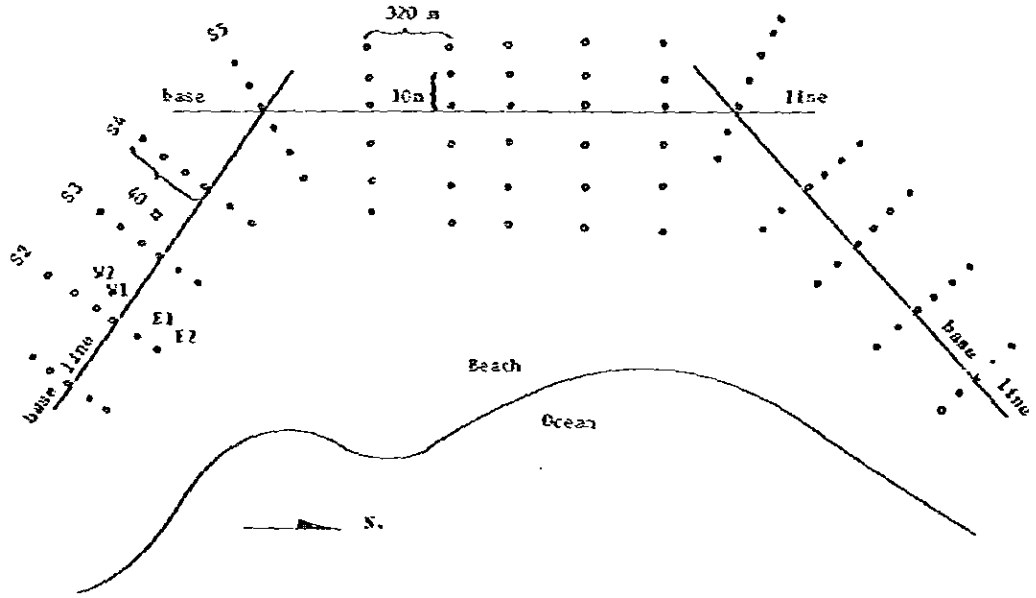

Fig. 3 Represents a scout boring grid with lines spaced at 320 m intervals and holes 40 m apart along lines on an axial trend N-S. The lines are numbered 1-2-3 allowing for 8 intermediate lines in each case at intervals of 40 m. The holes are numbered for intermediate holes to be spaced 10 meters apart. There are 3 separate base line because of the contour of the beach line.

method of sampling.

A number of different auger types are available from various manufacturers but while most of them are reasonably satisfactory the 2 inch (50.8 mm) diameter shell auger described here is considered the best for most conditions.

This auger is 15 inches (38.1 cm) long in the shelll and has a male thread at the end of the handle section for attachment to either the handle or an extension rod. As a unit it is 5 feet (1.524 m) in length for uniformity.

Each extension rod has a male and female end and additional lengths of rod are added as the hole deepens. The rods are made from aluminium for lightness.

Applying slight body pressure, and taking care to keep the tool vertical the auger is rotated by hand some 8 turns.
It is then withdrawn from the hole and the sample cuttings are shaken out on to a 6 ft x 6 ft (2m x 2m) canvas sampling mat.

The process is repeated and the cutting are allowed to accumulate until the desired depth of hole has been sampled. A suitable sample interval is 1.5 m and manufacturers should be requested to produce both their casing and extension rods in 1.5 m lengths for convenience.

Hand augers may be used satisfactorily only in damp and relatively unconsolidated material: dry sand is not retained in the auger and the sides of the hole cave. When this occur water may be introduced into the hole in sufficient quantities to dampen the sand but the accuracy of the sample may then be questionable.
(the upper part of Fig. 4 shows the equipments of hand boring.)

7. Hand Sludging

The limit of accurate shell auger sampling is reached at the water table. Below this level sampling is made possible through the use of the casing inserted into the auger hole and forced down into the water-logged sediments by steady pressure and rotation.

The material inside the causing is removed by means of a sludge pump manually operated so that the bottom of the pump never approaches closer than 50-75 mm above the mouth of the casing shoe. A high level of water is maintained inside the casing to provide a positive hydrostatic pressure and thus prevent surges of material into the pipe. Sludging is usually limited to depths of 10 m for purely physical reasons although depths to 20 m. have been attained by great effort.

While hand boring is usually the most suitable method for beach mining evaluation because of ready portability, low capital cost, low drilling cost accurate sampling in suitable conditions and simplicity of operation, alternative methods must be considered in certain circumstances. For example deltaic

deposits can seldom be tested to their full depth without the use of power equipment and aeolian deposits along desert shorelines may be too dry for auger drilling and may require a vibro drill, air lift drill or even bulk sampling for their evaluation.
(the lower part of Fig. 4 shows the equipments of hand sludging.)

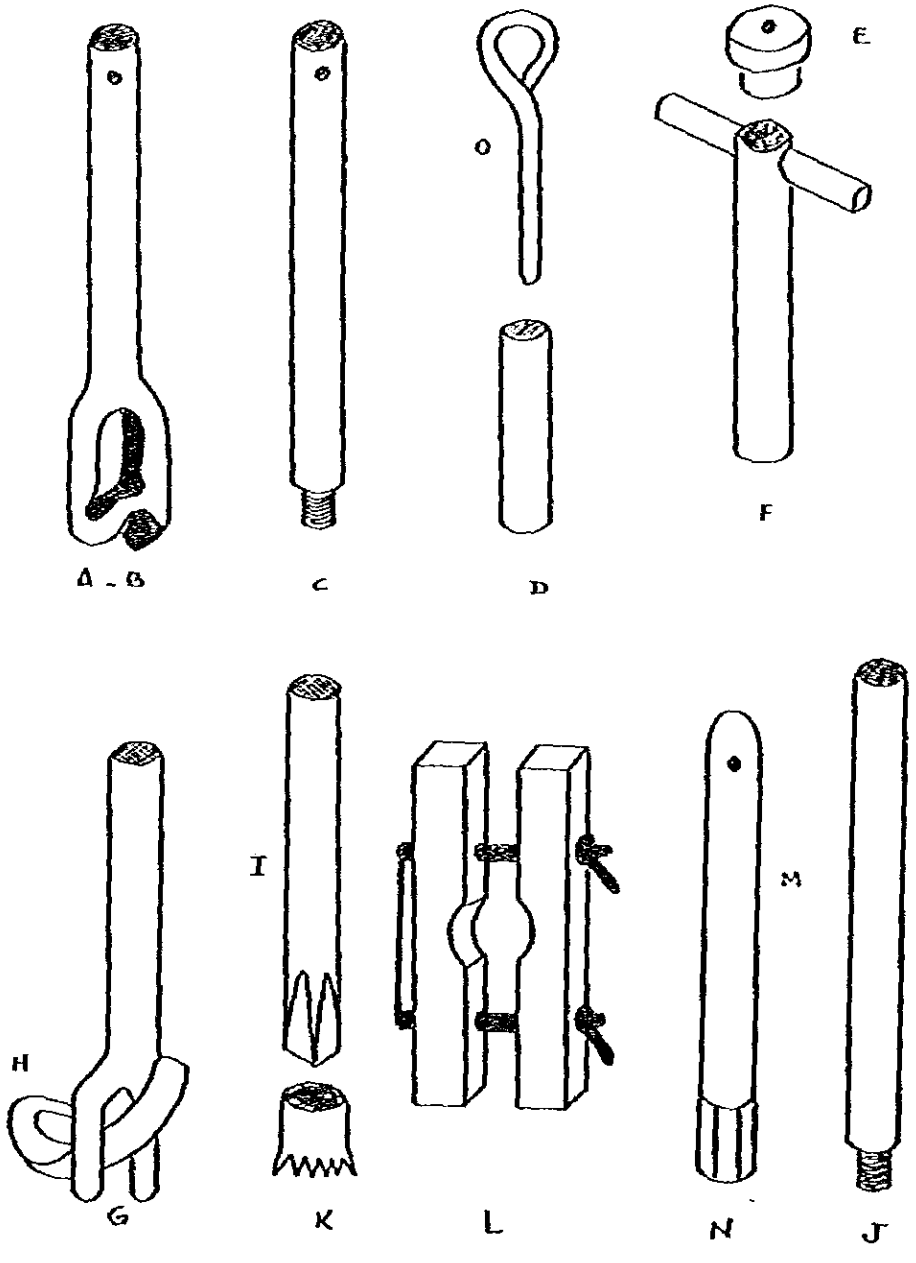

Fig. 4 Equipment for boring and sludging by hand

Table 1 Equipment for boring and sludging by hand

A- Sand boring bits	1 1/2-3" diam
B- Soil boring bits	2 - 3" "
C- Aluminium extension roads	5´(1.5 m) long
D- Handles	
E- Bore protectors	
F- Bushes	
G- Strap wrench	
H- Straps	
I- Star drill	
J- Casing	2" D. 5´(1.5 m) length
K- Casing cutter	H.D for 2" casing
L- Casing clamp	2"
M- Sludge pump barrels	1.5"
N- Replaceable sludge pump rosepieces	1.5"
O- Tommy bars H.T. steel pair	
Accessories including spares	
18" stilson wrenches	4
Small wooden pegs for marking out	200
plastic buckets	6
Rubber sampling mats 3´x3´x1/8"	6
Canvas sampling mat 6´x6´ heavy duck	4
Water containers	20 gal. capc.
Sample bags-calico 9"x6" with tapes	2000
Sample bags-plastic 12"x6"	4000

8. Instrumentation of Chemical Analysis in Laboratory

Adequate facilities for bulk sample entry and for drying and preparation prior to analysis, storage capacity for not reagents and glassware is included, however inflammable materials such as acetone and toluol should be stores separatly.

a) Construction details

Laboratory should provide sufficient ventilation and fume disposal, the

chemical section floor is of concrete mayolic or locets so that in the even of acid the material can be flushed with water and soap.

b) Equipments and chemical materials

- Balance from 160 grs.
- Chemical glassware, funnel separator, probetas 1000 cm^3 funnels, pipetas, gradillas, termometers, micro slide glass, cover glass, specific gravity indicators, paper filter No 2- diameter 11", microscopic
- Hot plate: Electric oven, individual hot plate
- Water supply: tapwater, hot water
- Chemical: Tetrabrom-Ethane (Acetylene-tetrabromide)

  Br_2-CH-CH Br_2-SG=2.904-2.931

  Bromoform -SG=2.86-2.90

  Rigolac (Poliester resine) 2004 W_{M-2} (A)

  Methyl ethyl ketone peroxide 55%

  dimethylphtalate 45%

  active oxigen 10~10.7%

  Parmec-N catalyst (Panic-N Cobalt-N) (B)

  catalyst = 100 grs (A) + 1 gr (B)

  Acetone

9. Preparation and Process of Slide for Heavy Mineral Determination

The method and procedures employed in preparation of samples for heavy mineral determination is given in sequences below, this includes the separation of the heavy minerals from lighter ones utilizing chemical and mechanical procedures up to preparation of slides for microscopic analysis.

1. Divide the raw sample longitudinally into two and put one ~ 200 grs party into a beaker (Fig. 6)
2. Wash the sample with tap water for 6 or more times until the water is clear, this is done to remove the mud and salt from the sample. Be careful not to allow the sand to spill over the older during this process.
3. Prepare 10% HCl solution (10% HCl+90% H_2O) (Fig. 7) care should be taken as you are dealing night acid, wash the bottle containg HCl before and after whing tap H_2O.
4. From each breaker remove the H_2O and then pour 10% HCl solution about 200 cm^3 is enough. Allow about 20 minutes for the solution to react with carbonate

matter (take nots of the reaction upon porting the 1% HCl solution)
Have the solution sample dried on a hot plate and cover the beaker with glass disc while heating for about 30 minutes (Fig. 8a)

5. Wash again the dried sample with water for a number of times to remove the acid and the remaining organic materials.
6. Have the washed sample completely dried on a hot plate (Fig. 8b)
7. Sieving then follows the dimension of the sieves utilized are 100, 200, 300, 400 mesh (fig. 9) coarse grains (100 mesh) and the finest (400 mesh) are discarded. The remaining grain-sized sample are recovered for the succeeding determination about 3-10 grs. of 200 and 300 mesh samples are placed in an envelop for weighing about 3 grs. of sampler.
8. Put the 3 grs sample into the filtration funnel then your heavy solution tetrabrom-ethane SG=2.904-2.931.

   One sample for each funnel agitate the solution by are of glass rod then allow some minutes for the heavy minerals to settle wash the sides of the funnel by tetrabrom-ethane.
9. Open the value of the funnel and let the heavy minerals only to flow into a breaker. Get another breaker for the light minerals then wash the funnel with tetrabrom-ethane to recoverer the other light mineral grains.
10. Filter the heavy minerals and the light minerals separately the filter should be coashed with acetone for 3 or more times to recover all the grains scattered in the filter paper, the filter paper containing the heavy and light minerals are properly folded.
11. Dry the filtered sample (heavy and light minerals) placed in a porcelain plate over a hot plate heat for 3 hours or more at 100°C.
12. Weigh about 3 grams of the heavy minerals
13. Separate the magnetite grains from other heavy minerals by use of a magnet (cover the magnet with paper for case in detaching the magnetite grains) Record the wight of magnetite grains, do the same for other samples.
14. After this process proceed to the recovery of tetrabrom-ethane. Put the used heavy solution into a large graduated cylinder and dilute with water then throw the water.

    The sure not to spill the heavy liquid, continue the process for 5 times or more to eliminate the acetone.

    Then again water and allow to stay fou one day, then separate the heavy liquid from the water by use of filtration funnel, the usual recovery is from 80% to 90% of the tetra-bromethane.

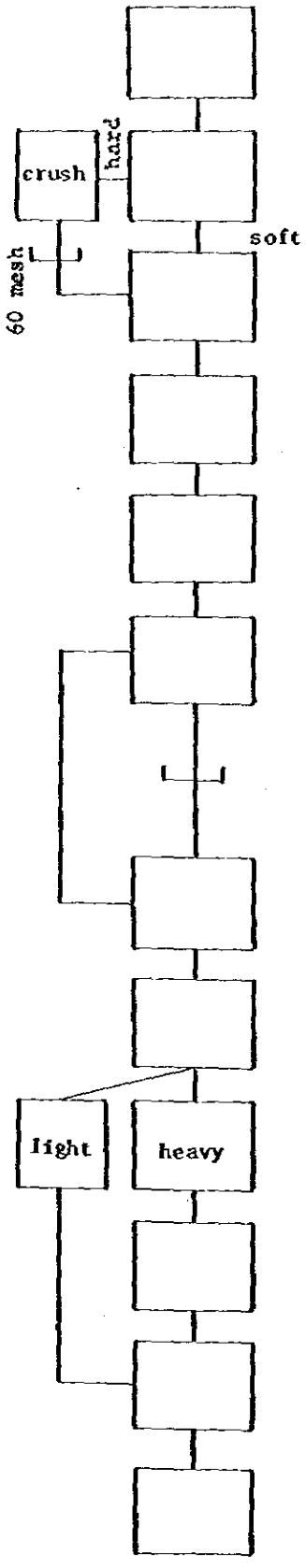

Original Sample

Splitting

Sample (100 ~ 200 gr)

Wash by decantation 20°, 10 cm, 29 second
Remove mud (<0.06 mm)

HCl treatment (10% HCl)
Boil about 15 minutes

Wash by decantation
more than 8 times

Dry in a oven

60 mesh

splitting

Sample (2 ~ 10 gr)
weighing

Heavy liquid separation
(tetrabrom-ethane S.G=2.95)

Heavy Mineral
weighing

Remove magnetite (bar magnet)
weighing

Mounting (Rigolac)

Microscopic stidy

Fig. 5 Heavy mineral analysis

10. Mounting of Heavy Minerals

In mounting the heavy minerals grains the following are needed, glass slide and cover glass, rigolac, catalyst and acetone. For each sample two slides are used, one for the heavy minerals and another for the lithg mineral.

The Procedures of mounting of heavy mineral are as follows:

1. Prepare a mixture of rigolac 2004 W,5 and catalyst Panic-N y Cobalt-N to retard the harding of preparation of other samples.
2. The proportion of the mixture is 10 grams of rigolac to one gram of catalyst.
3. Firstly clean the micro-slide glass and cover glass with acetone and put the tag of the sample on the side of the slide. Then put a small amount of the heavy mineral over the slide by used of roman pencil and press the glass cover and move the cover glass by gyrating motion to remove the air bubble and make the grains in one plane without over tapping.
   Allow the processed slide for one day, then clean it with acetone which drier up rapidly slide then are ready for microscopic analysis (Fig. 5).
   This processing technique was applied to original samples gathered is one offshore area of Japan.

11. Use of Microscope

Firstly one has to provide himself with a catalog for identification of slides used in the processing of mineral samples, this catalog provides a table for comparison of the principal mineral like zircon, garnet, topaz, staurolite so on with the mineral under study.

The method is a follow: In this study the microscope utilized is a NIKON-POH that has 10x10 - 10x40 - 10x100 for the identification of the minerals it is recommend that 10x10 and 10x40 should be used.

Table 2 Samples analized cruise hakurei maru

Sample No.	× ○ ⊙ ●	Sample weight	Heavy mineral weight	etic weight
107	○	5.245	0.130	0.003
108	●	6.815	0.399	0.008
115	×	5.968	0.528	0.112

Sample No. / Heavy Minerals	107	108	115
Hornb lend	110	160	150
Epidote	-	-	2
Staurolite	85	140	149
Apatite	30	50	90
Monzonite	45	46	35
Kyanite	20	30	-
Rutile	35	40	36
Total	325	466	462

Table 3

Heavy mineral / Sample	A Kyanite	B Staurolite	C Rutile	D Apatite	E Monazite	F Epidote	G Magnetite	I Others	Total
107	20x3.6 72 5.9%	85x3.7 315 25.9%	35x 4.24 148.4 12.2%	30x3.2 96 7.9%	45x5.1 229.5 18.2%	-	2.3%	110x 3.2 352 28%	99.7
108	30x3.6 108 6.3%	140x3.7 518 30.4%	40x 4.24 196.6 10%	50x3.2 160 9.4%	46x5.1 234.6 13.8%	-	2%	160x 3.2 512 30%	99.9
109	-	149x3.7 551.3 33.3%	36x 4.24 152.64 9.2%	90x3.2 288 17.4%	35x5.1 178.5 10.8%	2x3.36 7.2 0.4%	0.37%	150x 3.2 480 29%	99.7

107 = A + B + C + D + E + I = total

72 + 315 + 148.4 + 96 + 229.5 + 352 = 1213

$$\frac{72 + 315 + 148.4 + 96 + 229.5 + 352}{1213} \times 100$$

108 = A + B + C + D + E + I = total

108+518+169.6+160+234.6+512= 1702

$$\frac{108 + 518 + 169.6 + 160 + 234.6 + 512}{1702} \times 100$$

115 = B + C + D + E + F + I = total

$$\frac{551.3 + 152.64 + 288 + 178.5 + 7.2 + 480}{1657.6} \times 100$$

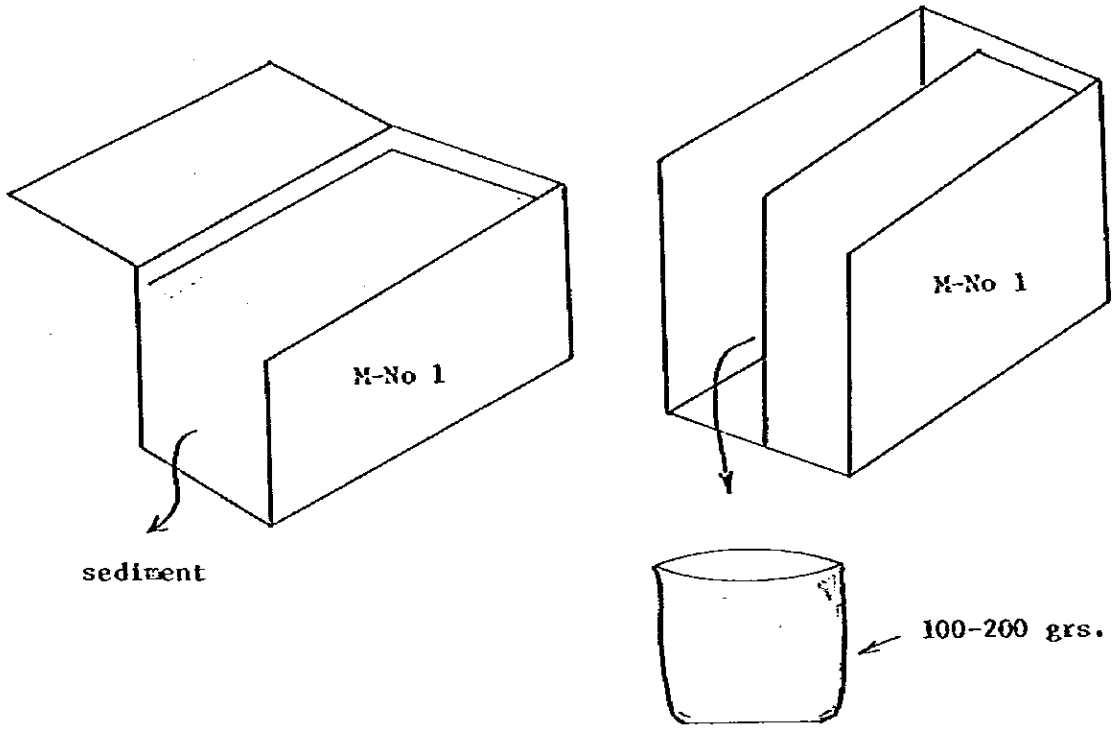

Fig. 6

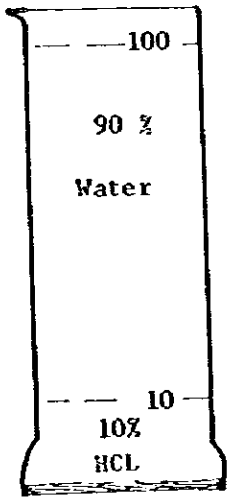

Fig. 7

80.

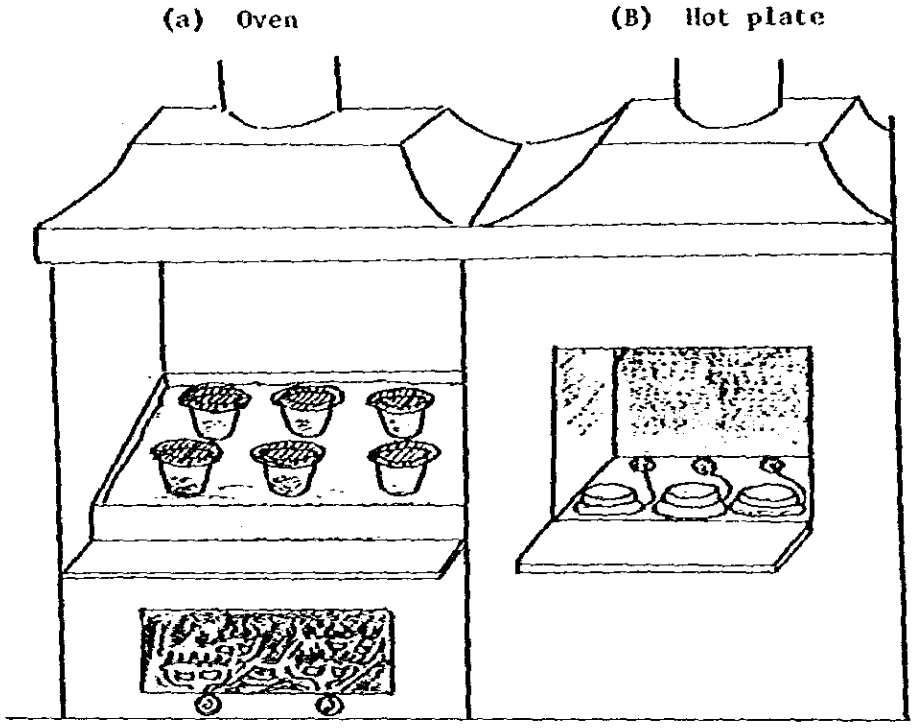

Fig.8

Sieves

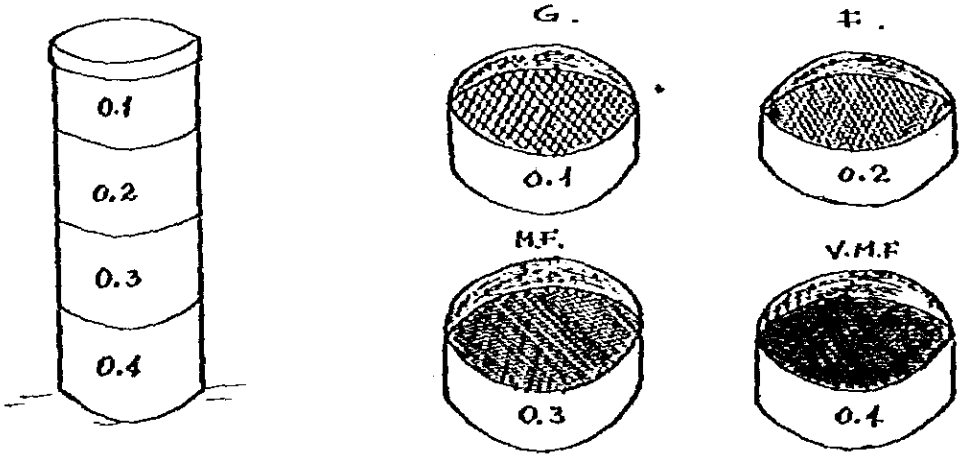

Fig.9

Mounting

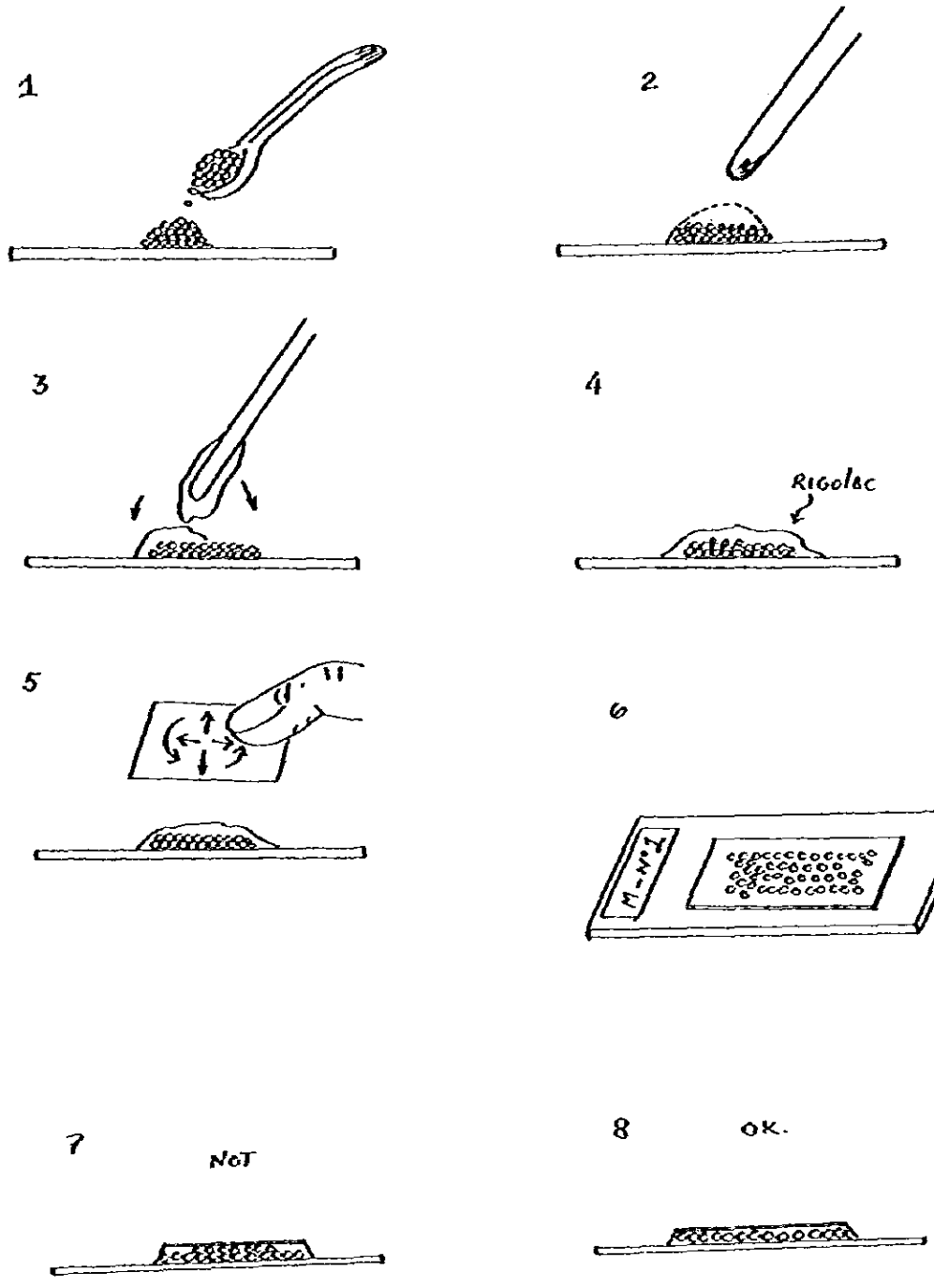

Fig. 10

82.

Tourmaline.

- $(Na\ Ca)_{R3}\ (Al,\ Fe)_6\ B_3\ Si_8\ O_{27}\ (O,\ OH,\ F)_4$

  R = Mg, Fe^{II}, Fe^{III}, Al, Li, Mn, Cr
- SG ± 3.0 - 3.3 D_c = 5 - 6
- Hexagonal-rhombohedral, striated prismatic, cleavage lacking or poor (1120) and (1010) basal parting.
- Yellow-brown, dark brown, Indigo to black.
- Extinction parallel to length, elongation negative
- Detrial tourmaline occurs as elongate prismatic grains, more commonly irregular fractured pieces and well rounded, oval grains the prismatic grains, generally with fractured ends and well-marked striations and markedly pleochroic, pleochroism of irregular to well-rounded grains variable to lacking.
- Derived from pneumatolytic rock, pegmatites, schists, gneisses, marbles.

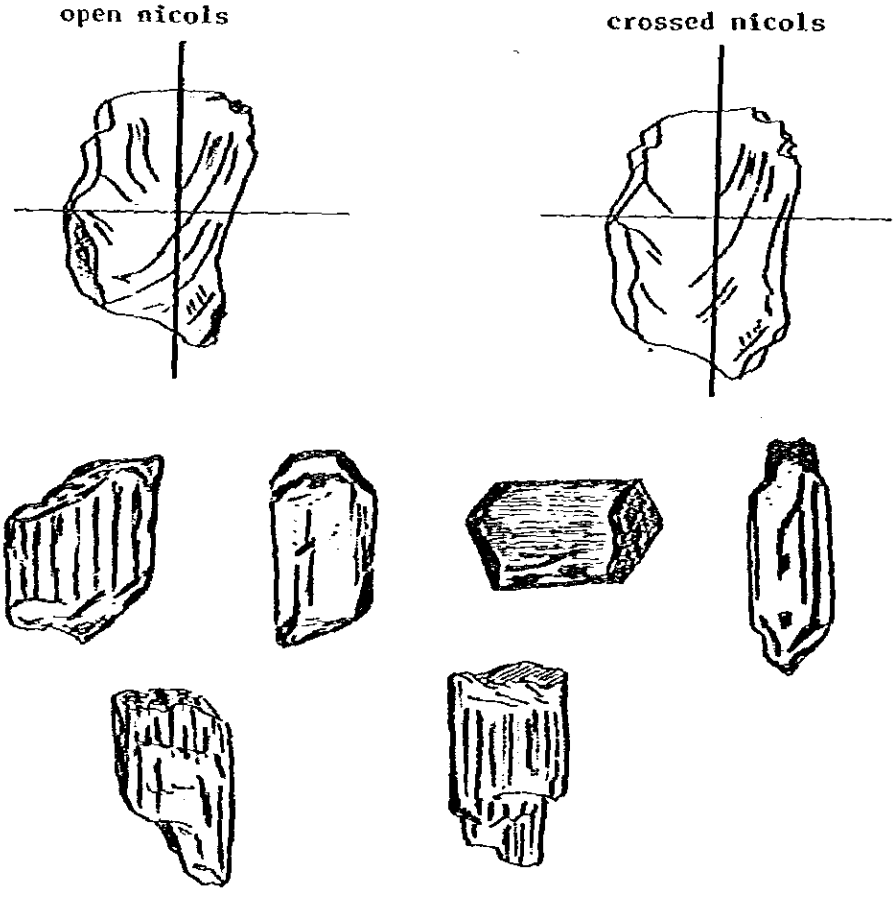

Fig. 11

Garnet.

$R''_3\ R2'''\ (Si\ O_4)8$ where $R'' = Mg_1\ F_e{}''$, Ca, Mn

$R'' = A\ell,\ F_e{}'''$, Cr

- SG = 3.5 - 4.3 Dc = 6 - 8
- Isometric: Dodecahedra, trapezohedra
- Conchoidal fracture
- Colorless: pale pink, red, orange, apricot-yellow, amber
- Garnet is variable in color, form and inclusions, it is commonly in well-rounded grains, but in many cases it appears in angular, sharp-cornered, irregular grains bounded by conchoidal fracture surfaces, Euhedra rare. Garnet is characterized by high relief, isotropism, conchoidal fracture, the several species of garnet can not be distinguished except by careful determination of index and specific gravity.
- Derived from igneous and metamorphic rocks, especially the crystalline gneisses and schists.

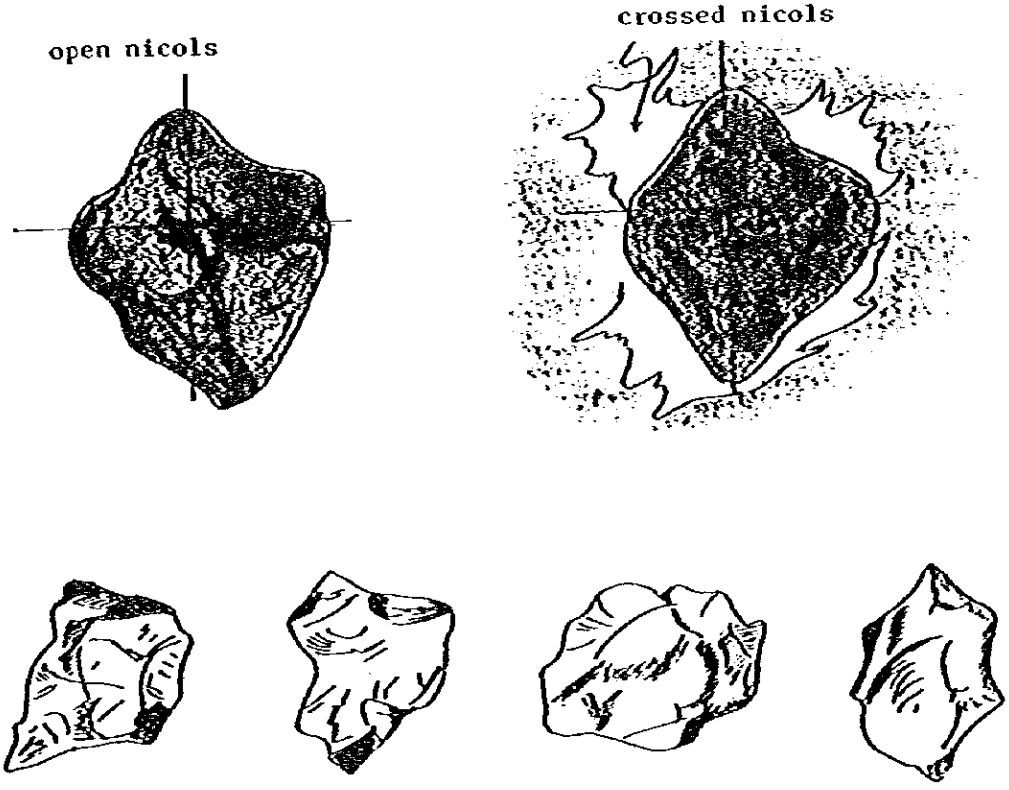

Fig. 12

84.

Topaz.

- 2 (Al F) O Si O_2
- SG = 3.58 DC = 6 - 7
- Orthorhombic: Elongation C, often vertically striated perfect (001) cleavage, imperfect (201) (021)
- Irregular fractured grains, basal grains, common on which well-centered interference figures are readily obtained, Interference colors bright.
- Marked by high relief (in balsam) fracture, and optic character.
- Derived from pegmatitic, granites and greisen

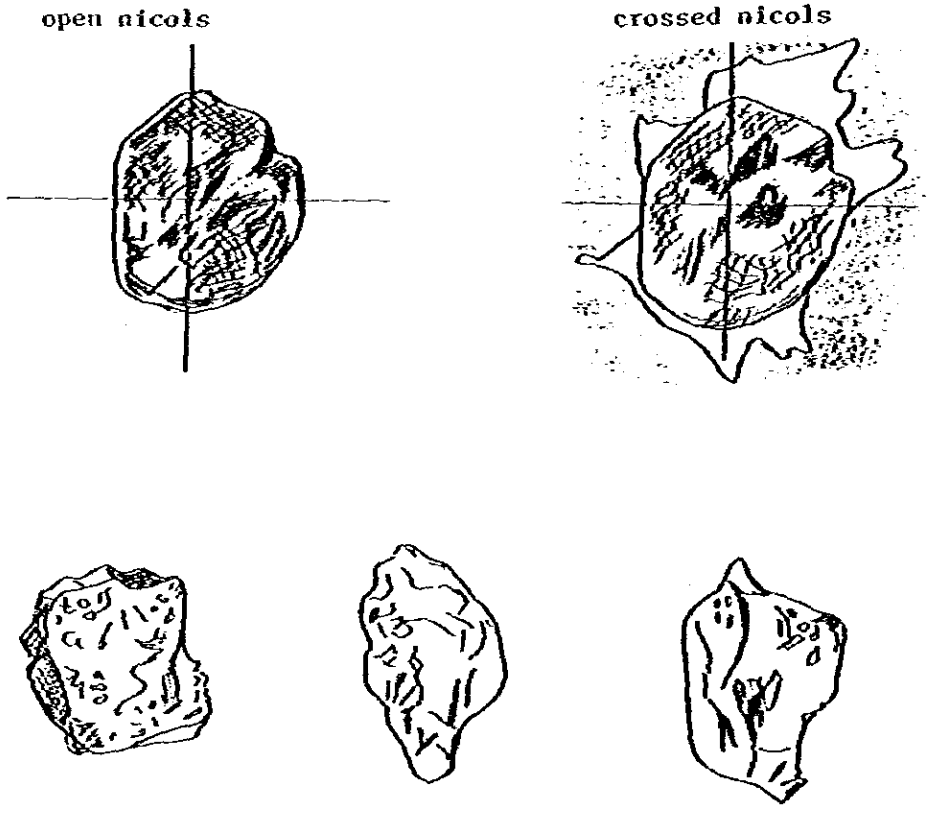

Fig. 13

Staurolite.

- $2\ Fe\ 0.5\ Al_2\ .\ 4\ Si\ O_2\ .\ H_2O$
- SG = 3.7 DC = 6 - 7
- Orthorhombic: short prism parallel to c.
- Cleavage (110) imperfect
- Hackly fracture
- Yellow, gold, brown
- Irregular, some what platy grains, determined by cleavage, marked by hackly to subconchoidal fracture, well formed crystal rare. Inclusions numerous, sometimes imparting a porous (swiss cheese) appearance to the grains. Minerals found as inclusions are garnet, tourmaline, rutile, biotite and carbonaceous matter. Inclusions more abundant in deeper-colored varieties.
- Derived from crystalline schists.

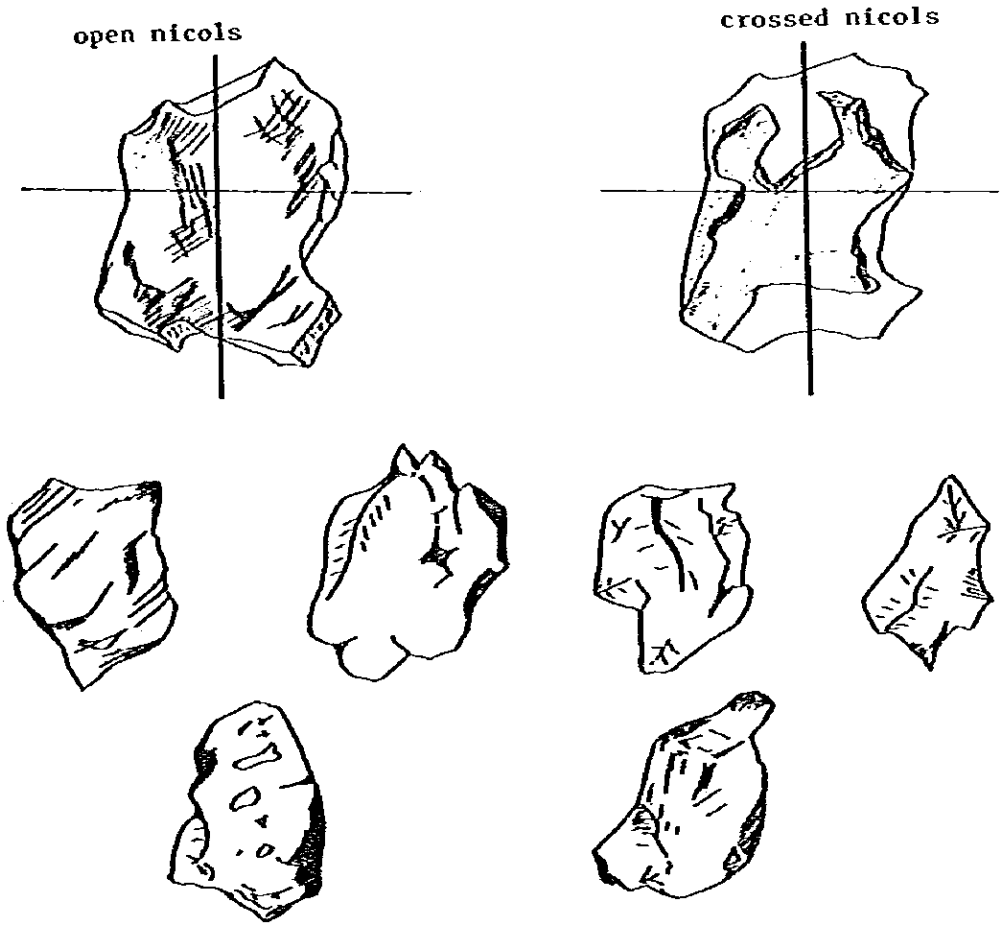

Fig. 14

86.

Manazite.

- $(Ce, La, Nd, Pr)_2 O_3 P_3 O_5$
- SG = 5.1 - 5.2 DC = 7 - 8
- Monoclinic, tabular parallel to (100)
- Colours, yellow, brown, red
- Grains rounded, equidimensional, often lying on (001) such grains yield good interference figure, Euhedra rate. They exhibit the same color between crossed nicols as in ordinary light owing to their high birefringence.
- Derived from granites.

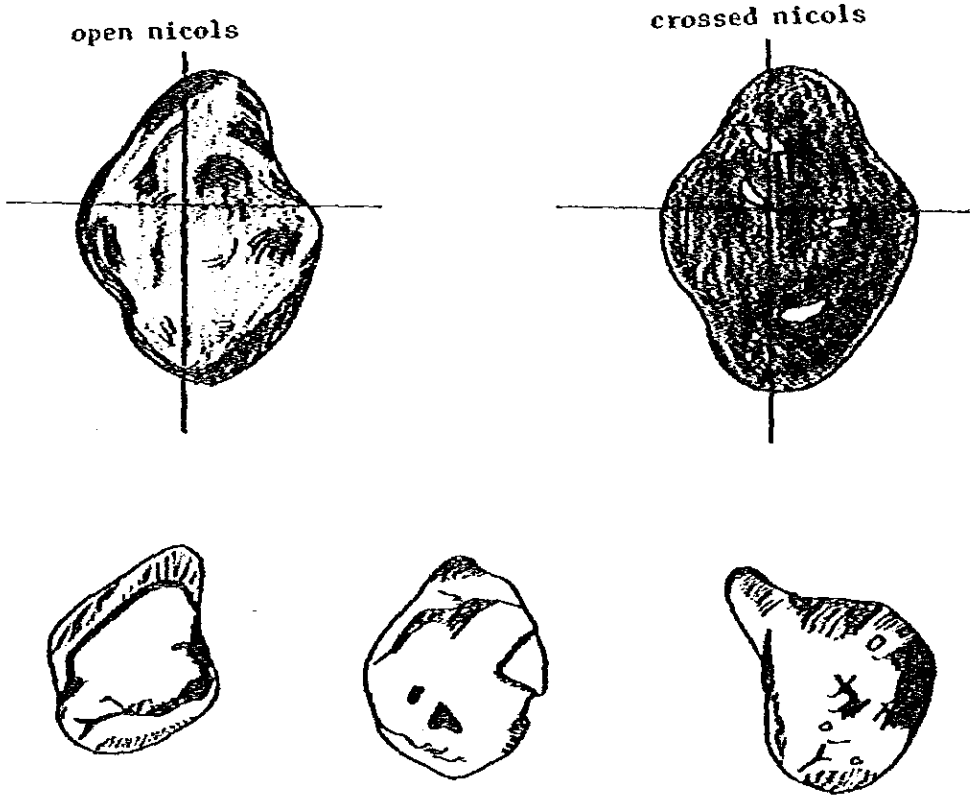

Fig. 15

Zircon.

- ZrO_2 SiO_2
- SG = 4.6 - 4.7 DC = 6 - 7
- Tetragonal: short prisms with pyramids (110) cleavage rare (111) poor.
- Usually colorless, some grains are mauve, yellow to brown strongly colored varieties are pleochroic.
- Extinction parallel

  Zircon often shows euhedral form even in far-traveled sands with well-marked crystal facets, commonly prisms (100) or (010) or both with pyramid terminations (111) contains large rod-shaped inclusions of other minerals and large liquid or gas inclusions.

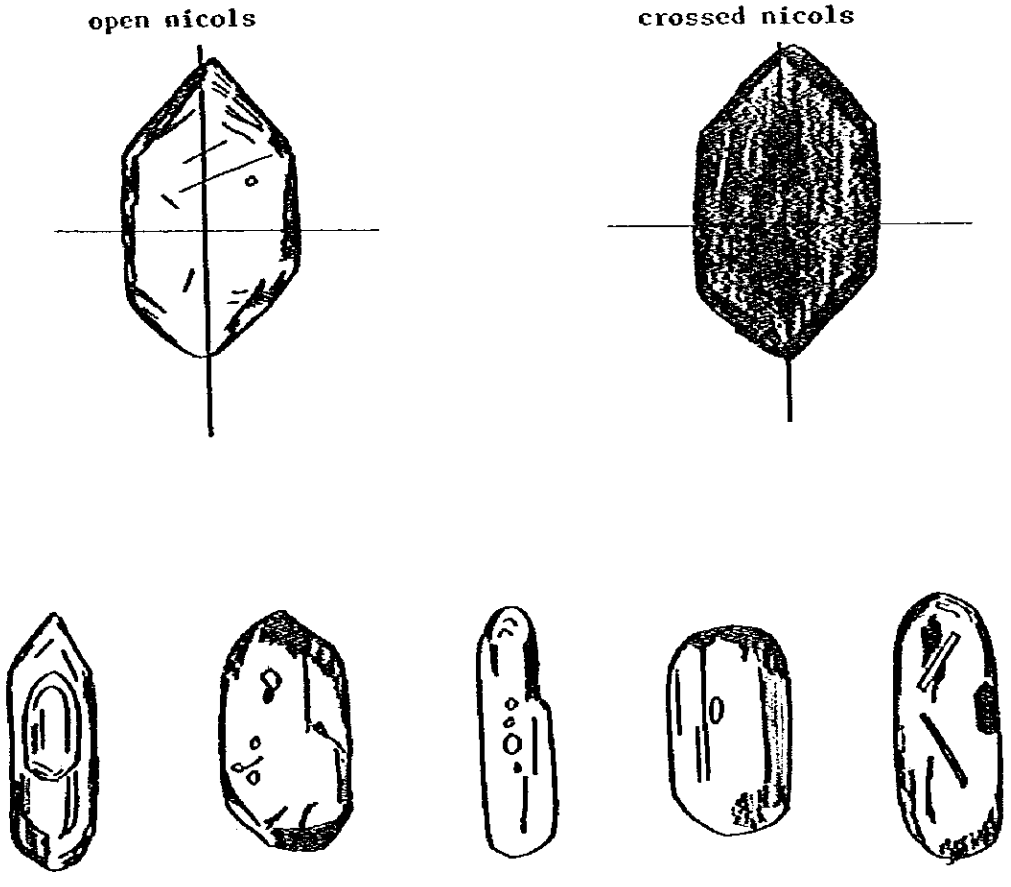

Fig. 16

88.

Rutile.

- TiO_2
- SG = 4.24 DC = 5 - 6
- Tetragonal: prismatic, geniculate twins
  distint (100) (110) cleavage, also (111)
- Yellow, reddish brown, red
- parallel extinction
- Grains irregular, generally elongate, prismatic forms with rounded pyramidal ends common, twinned crystals rare. Rutile shows the same color under crossed nicols as in ordinary light owing to its extreme birefringence. Deep red-brown varieties nearly opaque, has very high relief in any medium and therefore broad dark bourders around the grains.
- Derived from acid igneous rocks and crystalline metamorphics.

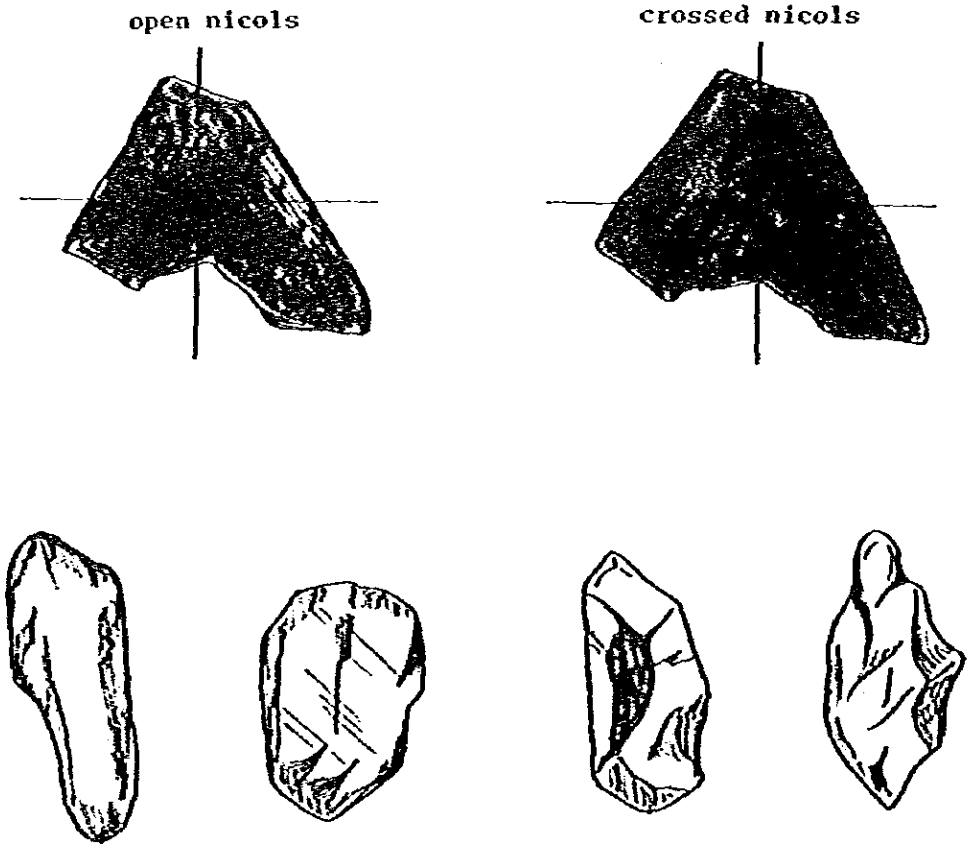

Fig. 17

Apatite.

- Ca_5 (F.Cl) $(PO_4)_3$
- SG = 3.16 - 3.22 DC = 5 - 6
- Hexagonal: long to short prismatic, terminated by base or pyramid. Imperfect basal (0001) cleavage
- Grains oval or nearly circular in plan to slightly worn elongate prismatic form. Often contains inclusions arranged in rows or plans
- Marked by detrital form and low birrefringense, may be wholly removed from a sediment by acid digest since it is soluble in HCL
- Derived from acid igneous rocks and pegmatites.

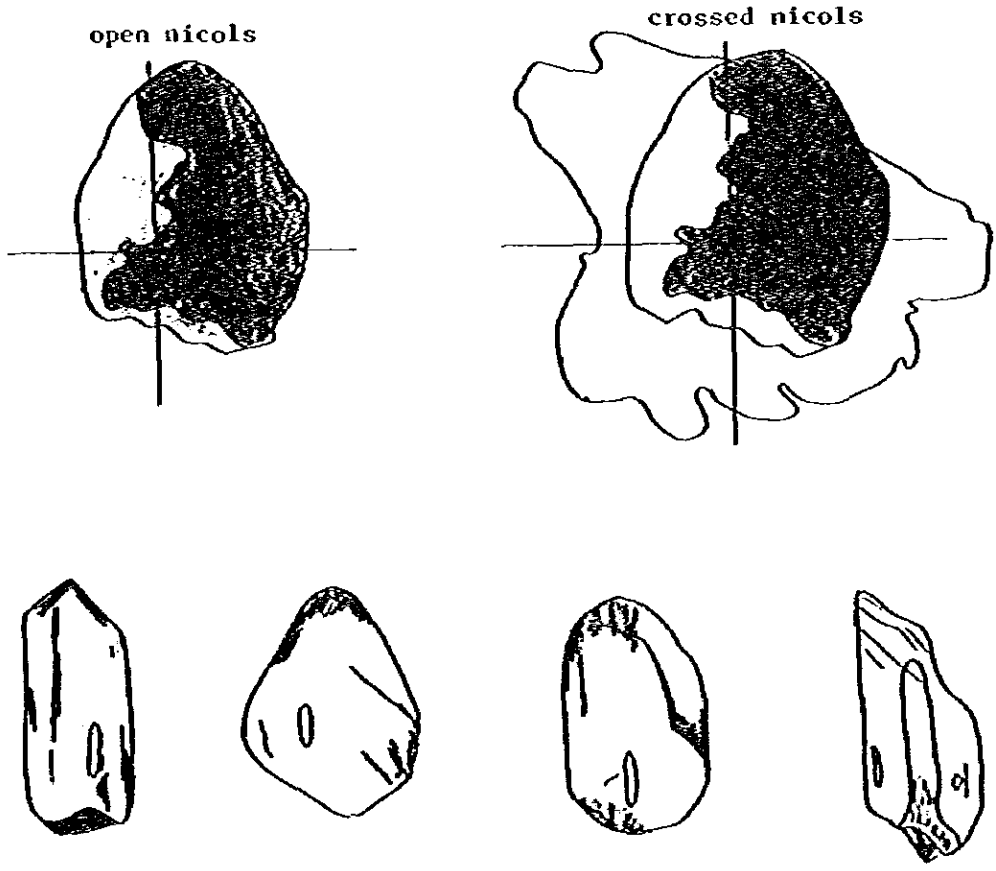

Fig. 18

90.

Epidote.

- $Ca_2 (Al, Fe)_3 Si O_{12} (OH)$
- SG = 3.36 DC = 6 - 7
- Monoclinic, elongate parallel to b.
  Cleavage perfect basal (001) imperfect (100)
- Pale greenish, yellow to lemon-yellow
- Equidimensional sharply angular to subrounded grains of characteristic greenish yellow. Grain very often yield centered optic axis or one bar interference figure. Bar nearly straight. Such grain are non-pleochroic most grains exhibit high-order interference color therefore appear much the same under crossed nicols as in ordinary light.
- Derived from metamorphosed igneous rocks.

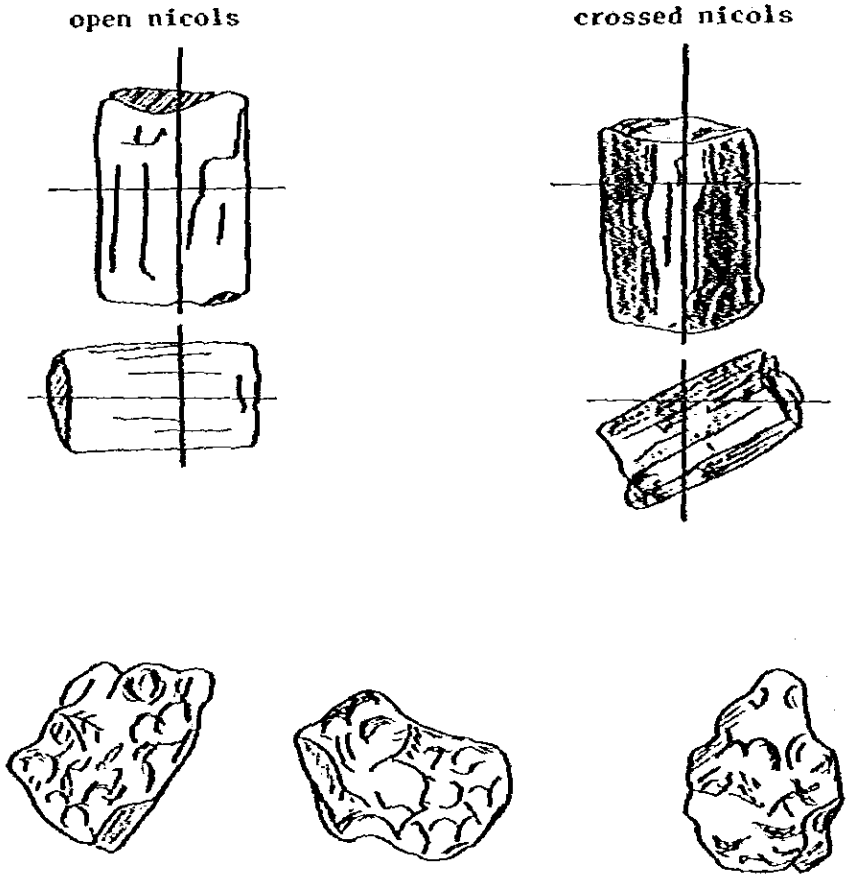

Fig. 19

Kyanite.

- $Al_2 SiO_5$
- SG = 3.6 DC = 7 - 8
- Triclinic, bladed
- Perfect pinacoid (100) and (010) (001) parting
  nearly at right angles
- Colorless rarely pale blue
  usually colorless, decidelly elongate grains of marked rectangular outline to short, moderately rounded elliptical grains.
- Conspicuous cross cleavage associated with step-like, carbonaceous inclusions frequent, grains may be altered along edges to micaceous material.
- Marked by cleavage-controlled rectangular detrital form, by low birefringence, inclined extinction, centered interference figure
- Derived from schists and gneisses.

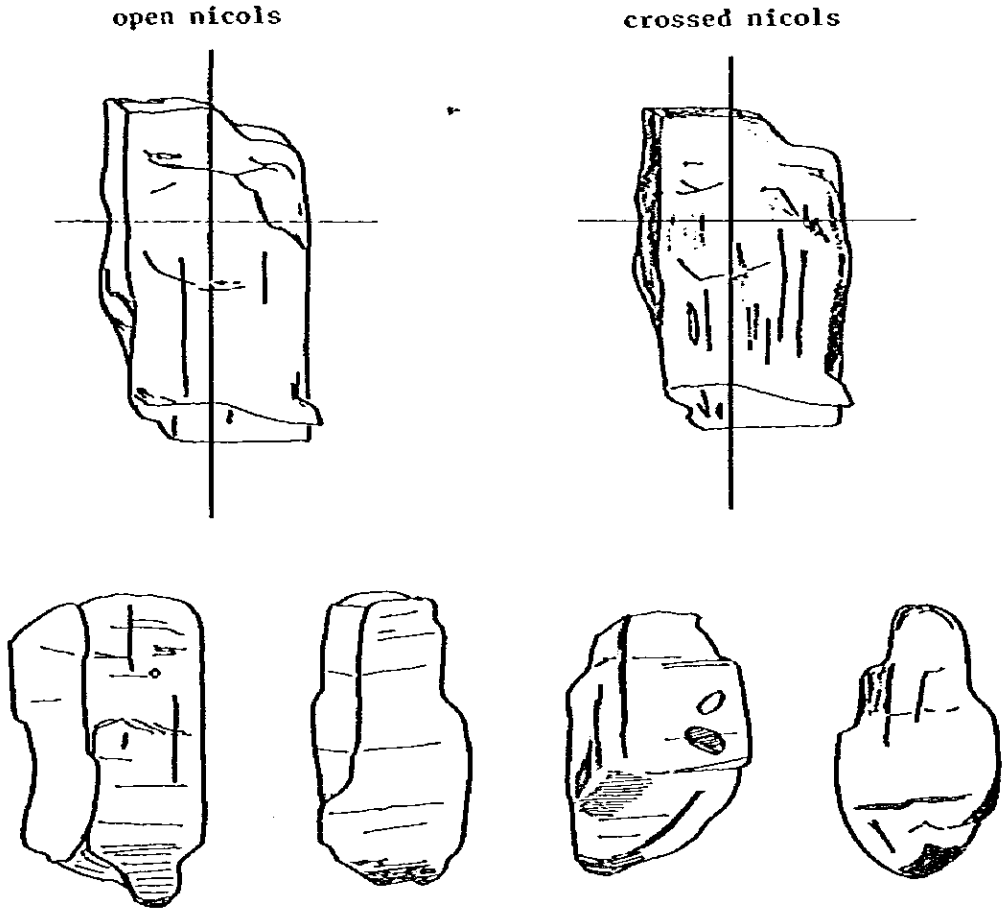

Fig. 20

92.

Magnetite.

- FeO. Fe_2O_3
- SG = 5.17 DC = 3 - 3.7
- Metalic luster, blush black in reflected light
- Angular and well-rounded grains abundant, crystal facets noted on some grains. Distinguished from ilmenite with difficulty, marked by strong magnetic character and crystal form.

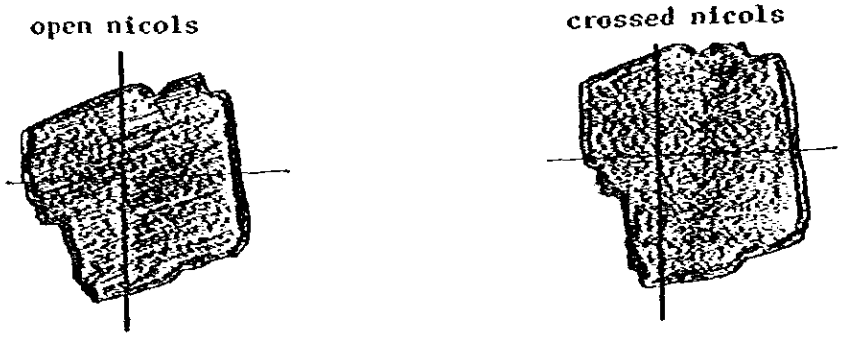

Fig. 21

Marcasite.

- FeS_2
- SG = 4.8 DC = 3 - 3.7
- Metalic luster, pale yellow in reflected light, often furnished dull
- Small grains irregular, readily descomposed, radial structure common authigenic

Pyrite.

- Fe S_2
- SG = 5.02 DC = 3 - 3.7
- Metalic luster, pale brass-yellow in reflected light, readely farnished. commonly well crystallized detrital euhedral rare, in sediments often as globular to irregular aggregates, or cluster of globules, also as nodules and small concretions, authigenic for the most part.

Ilmentite.

- $FeTiO_3$
- SG = 4.6 - 4.9 DC = 3 - 3.7
- Orthorhombic
- Metalic luster, Brownish to purplish black in reflected light
- Common in sediments as irregular to well-rounded grains of ten in part altered to leucoxene.

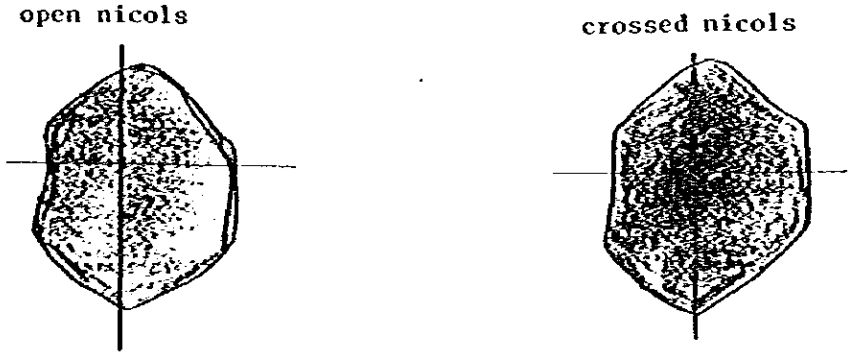

Fig. 22

Hematite.

- Fe_2O_3
- SG = 5.2 DC = 8
- Hexagonal-rhombohedral
- Metalic to earthy luster, indian red to black in reflected light
- Common as microscopic inclusions, also as irregular powdery aggregates, as oolites and pseudomorphs after fossils, rarely minutely botoyoidal, also as grain coatings.

Limonite.

- $Fe_2O_3 \cdot n\ H_2O$
- SG = 3.8 DC = 6 - 7
- Amorphous
- Earthy to metallic luster, ochre yellow, brown to brownish black in reflected light.
- As rounded granules or as powdery aggregates and coatings also pseudomorphs and discomposition product of pyrite, marcasite and glauconite.

12. Conclusion

Based on the preceeding discussions, the importance of conducting studies and investigation on heavy minerals become eminent. From this experimental studies, the processes involved in the disintegration of rocks transportation and disposition of sediments, as well as the present condition of the basin lay bare the economic possibility of heavy mineral exploration.

Acknowledgements

The writer is grateful to the geological survey of Japan for the various kinds of help rendered during his training. Special thank are indebted to Dr. H. Hasegawa and Dr. E. Inoue. He is also grateful to Ing. Lee Youn Oh, who made available to him all the references for preparing this report.

References

1) Mac. Donal, Manual of Beach Mining Practice

2) Folk, Robert L., Petrology of Sedimentary Rocks

3) Tickell, Frederick G., Development in Sedimentology

4) Krumbein, W.C. and F.J. Pettijohn, Manual of Sedimentary Petrography

6. Application of Koulomzine Method to One of the Aeromagnetic Anomalies of Panay Islands, Philippines

Jose R. Bustamante *

Summary: This is an approach in the interpretation of one of the aeromagnetic anomalies in Panay Island, Philippines through the application of the Koulomzine method of analysis of a field profile. The method employed can be considered as one of the outstanding processes based on its practicability and rapid solution of an aeromagnetic anomaly by determining the depth of burial, the width and, the dip of the anomalous body through comparison of the field profile to a set of six master curves.

In this report the total intensity map has been corrected by application of I.G.R.F. From the resulting residual map, a field profile is decomposed into its symmetrical and antisymmetrical components which are then analyzed separately. In the case of a dike or bed-like structures, the entire procedure takes place for some minutes.

1. Introduction

Aeromagnetic surveys become only concrete, if and when, a logical interpretation of the magnetic profile is made and thus, its usefulness for solving geological problems is attained. Outstandingly, we need a general idea of the shape of the body, the depth of burial, and the dip of that body imparting the anomaly. This again, becomes reasonably and effectively useful if a field profile is constructed from a properly corrected aeromagnetic map, and primarily, if the method employed gives a good view of a model considered in the interpretation. For this problem, the Koulomzine method of separate interpretation of an infinite dike provides ample, if not all, solutions of the parameters necessarily needed for interpretation.

The theoretical aspects, the mechanics of analysis and the I.G.R.F. correction, applied in the analysis of the aeromagnetic map of an anomaly in a portion of Panay Island is cited. The final results of the determinations of the parameters, depth, width, and dip, from a field profile are compared to

* Bureau of Mines, Department of Natural Resources, Philippines

a set of six master curves.

2. Theory of I.G.R.F. (International Geometric Reference Field)

The reference field is a series of spherical harmonics in geometric spherical coordinates with the magnetic potential V and intensity components given by

$$V = \sum_{n=1}^{n=8} \sum_{m=0}^{m=n} \left(\frac{a}{r}\right)^{n+1} \cdot \left(g_n^m \cos m\lambda + h_n^m \sin m\lambda\right) P_n^m (\cos \phi)$$

$$X = (1/r)\, dV/d\phi, \quad Y = (-1/r \sin \phi)\, dV/d\phi, \quad Z = dV/dr.$$

where X, Y and Z represent the north ward, the eastward, and the downward components of the intensity in geocentric coordinates, a is the radius (6371.2 km) of the reference sphere, r is the radial distance from the center of the reference sphere, ϕ is the geocentric colatitude measured from the north pole, λ is the geocentric longitude measured east from Greenwich, $P_n^m(\cos \phi)$, an associated Legendre fuction of degree n and order m and of the Schmidt quasi-normalized type, g_n^m and h_n^m are spherical harmonic coefficients, of which there are eighty, up to $n = m = 8$, for the main field as well as for the secular variation. The scalar intensity $F = (X^3 + Y^2 + Z^3)$; the horizontal intensity $H = (X^2 + Y^2)^{\frac{1}{2}}$; the declination $D = \tan (Y/X)$; the inclination $I = \tan^{-1} (Z/H)$.

For the earth's surface the international ellipsoid is used: equatorial radius 6378.160 km and flattening 1/298,25.

Below is a table showing the I.G.R.F. coefficients which apply to the period 1975.0 - 1982.0.

3. Theoretical Formulas and Curves

Firstly, we consider the general case of the tabular body of infinite length and depth, oriented and magnetized in any direction. Secondly, consider a magnetometer measuring the intensity of the magnetic anomaly along a given orientation. The value of the intensity of the anomaly ΔF, measured when the instrument is moved along the axis normal to the body which is given by the formula.

$$\Delta F = 2M \cos D' \cdot \cos \delta \cdot \sin \rho (\epsilon \sin (\psi + k') + \ln r_1/r_2 \cdot \cos (\psi + k') \quad \text{--- (1)}$$

or by its expanded form

$$\Delta F = 2M \cos D' \cdot \cos \delta \sin \rho \, (\sin (\psi + k') \cdot \tan^{-1} \frac{2hb}{x^2 + b^2 + h^2} + (\psi + k') \cdot \frac{1}{2} \ln \frac{(x - b)^2 + h^2}{(x + b)^2 + h^2} \quad \text{---------- (2)}$$

Table 1. IGRF 1975 coefficients

n	m	Main field, nT		Secular change, nT/year	
		g	h	g	h
1	0	-30186		25.6	
1	1	-2036	5735	10.0	-10.2
2	0	-1898		-24.9	
2	1	2997	-2124	0.7	-3.0
2	2	1551	-37	4.3	-18.9
3	0	1299		-3.8	
3	1	-2144	-361	-10.4	6.9
3	2	1296	249	-4.1	2.5
3	3	805	-253	-4.2	5.0
4	0	951		-0.2	
4	1	807	148	-2.0	5.0
4	2	462	-264	-3.9	0.8
4	3	-393	37	-2.1	1.7
4	4	235	-307	-3.1	-1.0
5	0	-204		0.3	
5	1	368	39	-0.7	1.2
5	2	275	142	1.1	2.3
5	3	-20	-147	-1.6	-2.0
5	4	-161	-99	-0.5	1.3
5	5	-38	74	1.0	1.1
6	0	46		0.2	
6	1	57	-23	0.5	-0.5
6	2	15	102	2.0	-0.1
6	3	-210	88	2.8	-0.2
6	4	-1	-43	0.0	-1.3
6	5	-8	-9	0.9	0.7
6	6	-114	-4	-0.1	1.7
7	0	66		0.0	
7	1	-57	-68	0.0	-1.4
7	2	-7	-24	0.0	-0.1
7	3	-7	-4	0.6	0.3
7	4	-22	11	0.9	0.3
7	5	-9	27	0.3	-0.7
7	6	11	-17	0.3	0.1
7	7	-8	-14	-0.5	0.8
8	0	11		0.2	
8	1	13	4	0.3	-0.2
8	2	3	-15	0.0	-0.4
8	3	-12	2	0.2	-0.2
8	4	-4	-19	-0.4	-0.3
8	5	6	1	-0.3	0.4
8	6	-2	18	0.6	-0.3
8	7	9	-6	-0.3	-0.6
8	8	1	-19	-0.1	0.3

Formula (2) shows that x is the only independent variable which changes when the magnetometer is moved perpendicular to the length of the dike. The remaining quantities are either already known (D,I) and arbitrarily fixed (δ,k) or the values are to be determined from the profile gathered in the field, such as, p, ψ, h, and b. In figures 1 and 2, the symbols are illustrated and the definitions are stated below.

D is the true magnetic declination, D' is the projection of D/vector D.

M is the intensity of magnetization.

ρ is the angle of the dip of the dike measured clockwise from the north.

$\psi = I' - \rho$ is the angle between the projected magnetic inclination I' and the dip of the dike. I' is the projection of the true magnetic inclination I on the dike. Both p and I' are measured from the positive side of the axis, i.e., in the north, northeast, or northwest directions.

$b = W/2$ is the horizontal half-width of the dike, W being the total width.

h is the depth to the top of the dike.

x is the variable distance of the point of measurement from the vertical projection of the center of the upper plane of the dike.

ε is the angle between r and r while, reading from the point of observation to the corners of the dike (Figure 3).

$B = b/h$
$X = x/h$ are the normalized values of b and x.

$\lambda = \text{cotan}\ (\psi + k')$

δ;k are angles that define the orientation of the magnetometer sensor element. with respect to the xz plane normal to the dike.

δ;k' are projections of the angles o and k on the plane containing both vectors ΔF_k and $\Delta F_{k'}$ on the plane xz.

k, k', δ and δ are angles defined on Figure 2.

4. Determination of the Position of X=0

The position of X=0 critically depends on the values of ΔZ maximum and ΔZ minimum, quantities which can be assigned accurate numerical values only if the neutral datum of the magnetic field is known (Figure 3).

A working equation is established by rewriting the equations (1) and (2), then substituting $\lambda = \text{cotan}\ (\psi + k')$ and expressing b and x in units of depth of burial, $B = b/h$ and $X = x/h$. From here, we obtain

$$\Delta F = \tan^{-1}(X+B) - \tan^{-1}(X-B) + \lambda/2 \ln\left((X-B)^2 + 1\right) - \lambda/2 \ln\left((X+B)^2 + 1\right) \quad \text{----- (3)}$$

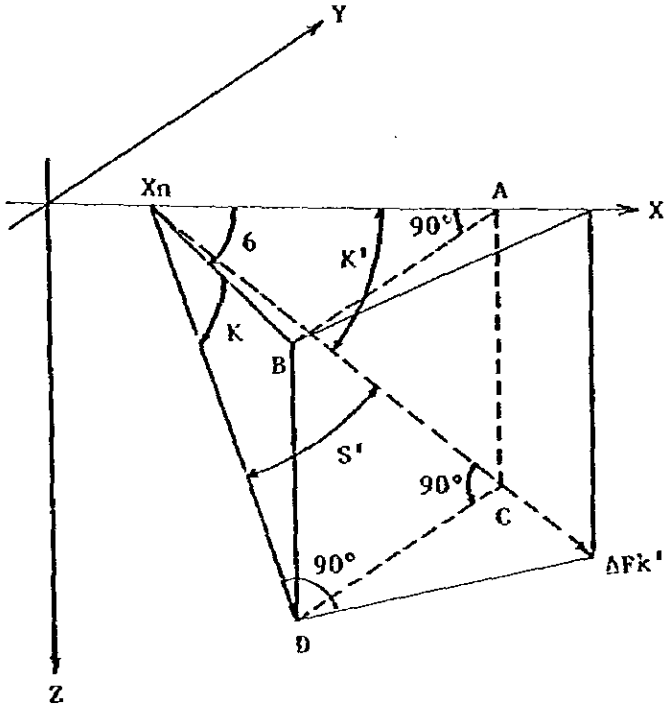

Fig. 1 Relationship between $\Delta F_k'$ the anomaly in the xz plane, and $\Delta F_k'$, the anomaly actually measured in the vertical plane of the magnetometer.

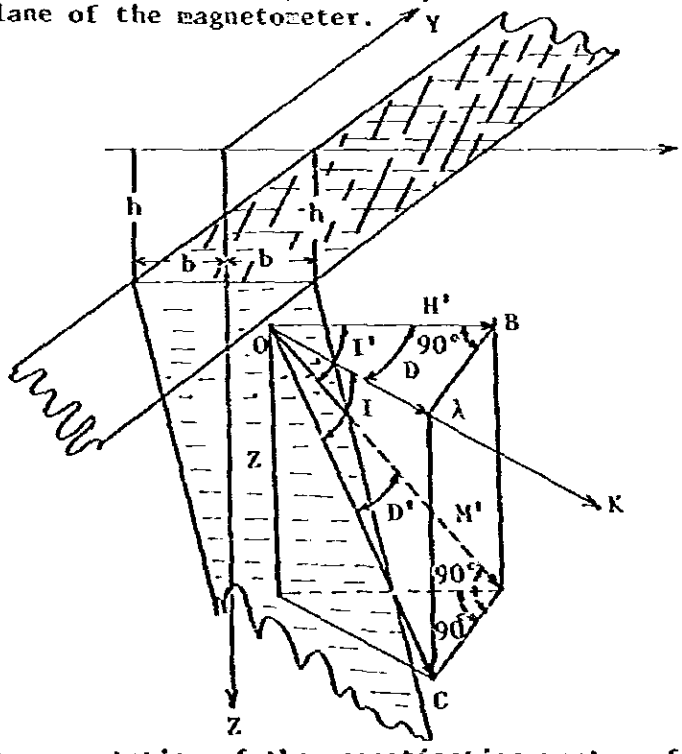

Fig. 2 Representation of the magnetization vector affecting any point O within the dike. The coordinate system chosen has its axis, along which the measurements are taken, normal to the dike. M may or may not be along the magnetic meridian depending on the orientation of the remanent magnetization, if any, which is included in M. M' is the projection of M into the xz plane.

We break down ΔF into its symmetrical and antisymmetrical parts to form another equation

$$\Delta F\ (X_1) + \Delta F\ (X_2) = \Delta F\ (0) \qquad \text{----- (4)}$$

Considering the symmetrical part of equation (3) and we let X_1 and X_2 be two abscissae, we get

$$S(X_1) + S(X_2) = S\ (0) \qquad \text{----- (5)}$$

It follows that

$$\tan^{-1}(X + B) - \tan^{-1}(X - B) + \tan^{-1}(X + B)$$
$$- \tan^{-1}(X - B) = 2\tan^{-1}(B). \qquad \text{----- (6)}$$

If we apply the formula for the sum of two arctangents and by further simplifications, we arrive to this new equation

$$X_1 \cdot X_2 = \pm (1 + B^2) \qquad \text{----- (7)}$$

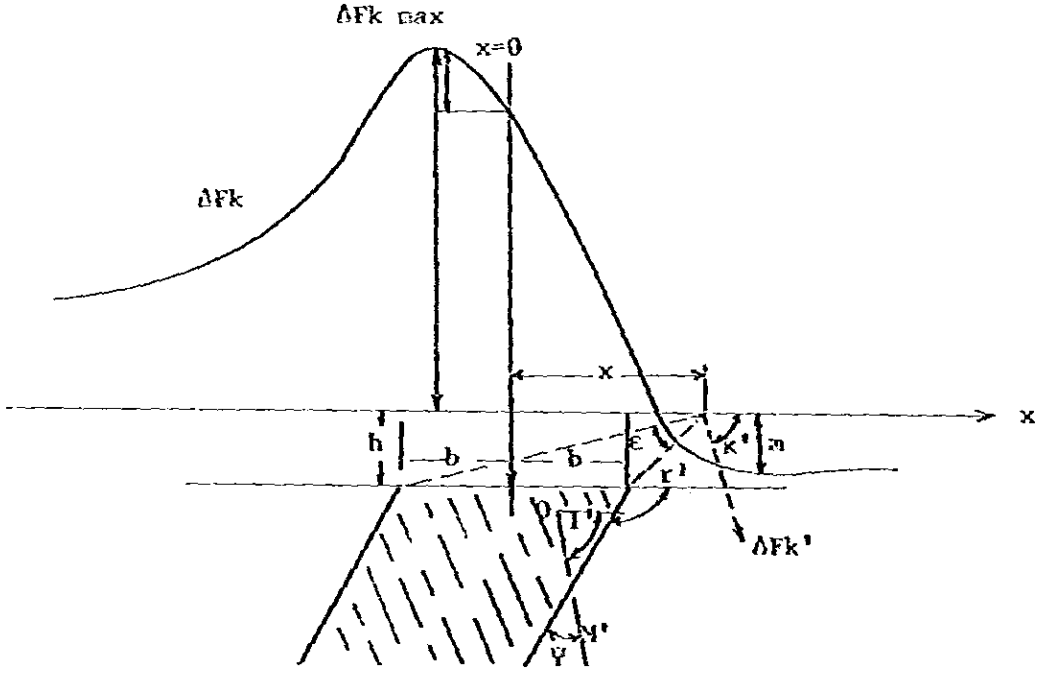

Fig. 3 Representation, on the xz plane, of the field vectors and orientation angles. Angle Ψ is the difference between the projection of the magnetization vector and the dip of the dike. k' is the projection of the arbitrary dip; k, of the magnetometer sensor. If the vertical component of the magnetic field is measured, $k'=90$ degrees. If a self-orienting, total intensity magnetometer is used, $k=I$ and, therefore, $k'=I'$.

The antisymmetrical part of the field curve can be extracted by the use of the following formula

$$A(X) = A/2 \ln \left[\frac{(X-B)+1}{(X+B)+1} \right]$$

First of all, we find the abscissae of the maximum and minimum of A(X) by differentiating the above formula and find the values of Xe and Xe corresponding to A'(X) = 0, then transform the resulting formula to get

$$A'(X) = A/2 \cdot \frac{4B\,(X^2 - B^2 - 1)}{(X^2 - B^2)^2 + 2\,(X^2 + B^2) + 1}$$

It should be noted that the denominator should always be positive, and, $A'_X(X)=0$ when $X_e^2 = (1 + B^2)$, so that, when $X_e^2 = b^2 + h^2$, $X \pm (b^2 + h^2)^{\frac{1}{2}}$

If we return to equation (9), we note that equation is valid for any value of X and, that of $X\frac{3}{4}$ is the value of the abscissa corresponding to a value of three-quarters of the maximum of the function, that is, $S(X\frac{3}{4}) = \frac{3}{4} S(X)$ maximum. Further substitution and by application of the double and triple arctangent formulas, then dividing by B, we get

$$(3-B^2)\, X_{\frac{3}{4}}^4 + 2\,(1 + B^2)^2 \cdot X_{\frac{3}{4}}^2 - (1 + B^2)^3 = 0.$$

Substituting $(1 + B^2) = X_{\frac{1}{2}}^2$, and $X = x/h$, we find that

$$h = \frac{x_{\frac{1}{2}}\,(x_{\frac{1}{2}}^2 - x_{\frac{3}{4}}^2)}{2\,x_{\frac{3}{4}}}, \qquad b = x_{\frac{1}{2}} \frac{[4\,x_{\frac{1}{2}}^4 - (x_{\frac{1}{2}}^2 - x_{\frac{3}{4}}^2)^2]^{\frac{1}{2}}}{2\,x_{\frac{3}{4}}^2}$$

If we use a new variable, $\dot{\psi} = \frac{x_{\frac{1}{2}}}{x_{\frac{3}{4}}}$, where $\dot{\psi}$, being a quotient, is scalar and independent of any measurement units, and substituting this to the above formulas for h and b, we obtain

$$h = x_{\frac{1}{2}} \cdot \frac{(\dot{\psi}^2 - 1)}{2}, \text{ and } b = x_{\frac{1}{2}} \cdot \frac{[(4 - (\quad - 1)^2]^{\frac{1}{2}}}{2}$$

and in the form used in the master curve,

$$h = 2x_{\frac{1}{2}} \cdot \frac{(\dot{\psi}^2 - 1)}{4} = 2x_{\frac{1}{2}} \cdot f(\dot{\psi}) = 2x_{\frac{1}{2}} \cdot D,$$

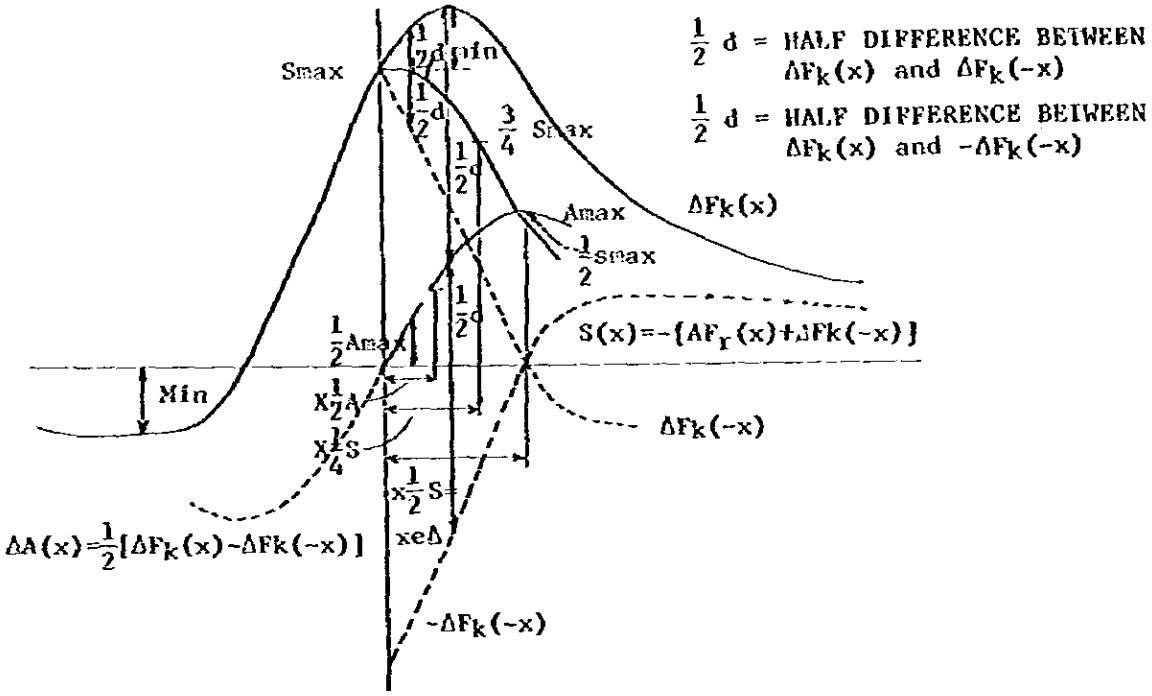

Fig. 4 Separation of a field curve into its symmetrical and asymmetrical components after the location of x=0. The plot of the symmetrical curve is the locus of the mid-points between $\Delta F_k(x)$ and $\Delta F_k(-x)$. The antisymmetrical component can be constructed either by replotting 1/2 d as ordinates or as the locus of mid-points between $\Delta F_k(x)$ and $-\Delta F_k(-x)$ obtained by a 180 degree rotation of the $\Delta F_k(-x)$ part of the original curve. Abscissae x1/2, x3/4, and x_e, $x_e/2$ enter into the calculation of the parameters of the dike by the Koulomzine method.

symmetrical part of the function ΔF (X). Here, at the abscissa x=0, A(x) must have a zero value.

$$A(X_1) + A(X_2) = 0 \qquad \text{----- (8)}$$

By expressing it in logarithmic form and then extracting the root we can find that $X_1 \cdot X_2 = -(1 + B)$ is the only relationship satisfying both the conditions imposed by equation (5) for the symmetrical and (8) for the antisymmetrical function.

5. Koulomzine Method of Separate Interpretation of an Infinite Dike

For this method of separation of the field curve into its symmetrical and antisymmetrical components after the location of the position of x=o, we take as example, one of the anomalies in Panay, Philippines (Figure 7).

From the field profile, $\Delta F(x) = S(x) + A(x)$, we consider first the symmetrical branch S(x) which can be expressed in two forms:

$$S(x) = \tan^{-1}(X + B) - \tan^{-1}(X - B) \text{ or}$$
$$= \tan^{-1}(B + X) + \tan^{-1}(B - X), \text{ from here, we get}$$

$S(X)$ maximum $= 2\tan^{-1}(B)$, at $x=0$.

If we assume, $S(X) = \frac{1}{2} S(X)$ maximum, and we apply the formula of the sum of two arctangents, the resulting equation will be

$$\tan(B) = \tan^{-1} \frac{2B}{1 - B^2 + X_{\frac{1}{2}}^2}, \text{ and } B = \frac{2B}{1 - B^2 + X_{\frac{1}{2}}^2},$$

$$X_{\frac{1}{2}} = \pm (1 + B)^{\frac{1}{2}}$$

as $B = b/h$, $X_{\frac{1}{2}} = x_{\frac{1}{2}} / h$, $X_{\frac{1}{2}} = \pm (h^2 + b^2)$.

$$W = 2x_{\frac{1}{2}} \cdot \frac{(4 - (\psi^2 - 1)^2)^{\frac{1}{2}}}{2} = 2x_{\frac{1}{2}} \cdot f(\psi) = 2x_{\frac{1}{2}} \cdot W.$$

The limits of these parameters are the following:
b is always real and positive and therefore, $\psi \geq 1$. In the liniting case of $= 1$, h = 0, the depth of the overburden is nil. Then $x_{\frac{3}{4}} = x_{\frac{1}{2}}$, i.e., the side of the S(x) curve becomes vertical and b is equal to $x_{\frac{1}{2}}$. For a thin dike, b = 0, which occurs when $\psi = 3$. In this case, h is equal to $x_{\frac{1}{2}}$, thus $1 \leq \psi \leq 3$.

W and h are fundamental to the interpretation of the symmetrical component of the magnetic field curve. D and W are independent scalars, and can be plotted as master curves (Figure 5).

6. Determination of the Parameters h and W of the Symmetrical Curve of a Dike

1) Values of $x_{\frac{1}{2}}$ and $x_{\frac{3}{4}}$ are scaled off the symmetrical curve;

2) $\psi = x_{\frac{1}{2}} / x_{\frac{3}{4}}$ is calculated;

3) D and W corresponding to the ψ are read off the master curves of Figure 5 and values of h and W are obtained by multiplying D and W by $2x_{\frac{1}{2}}$ expressed in the units of measurements employed.

A somewhat similar procedure can be adopted to interpret the antisymmetrical

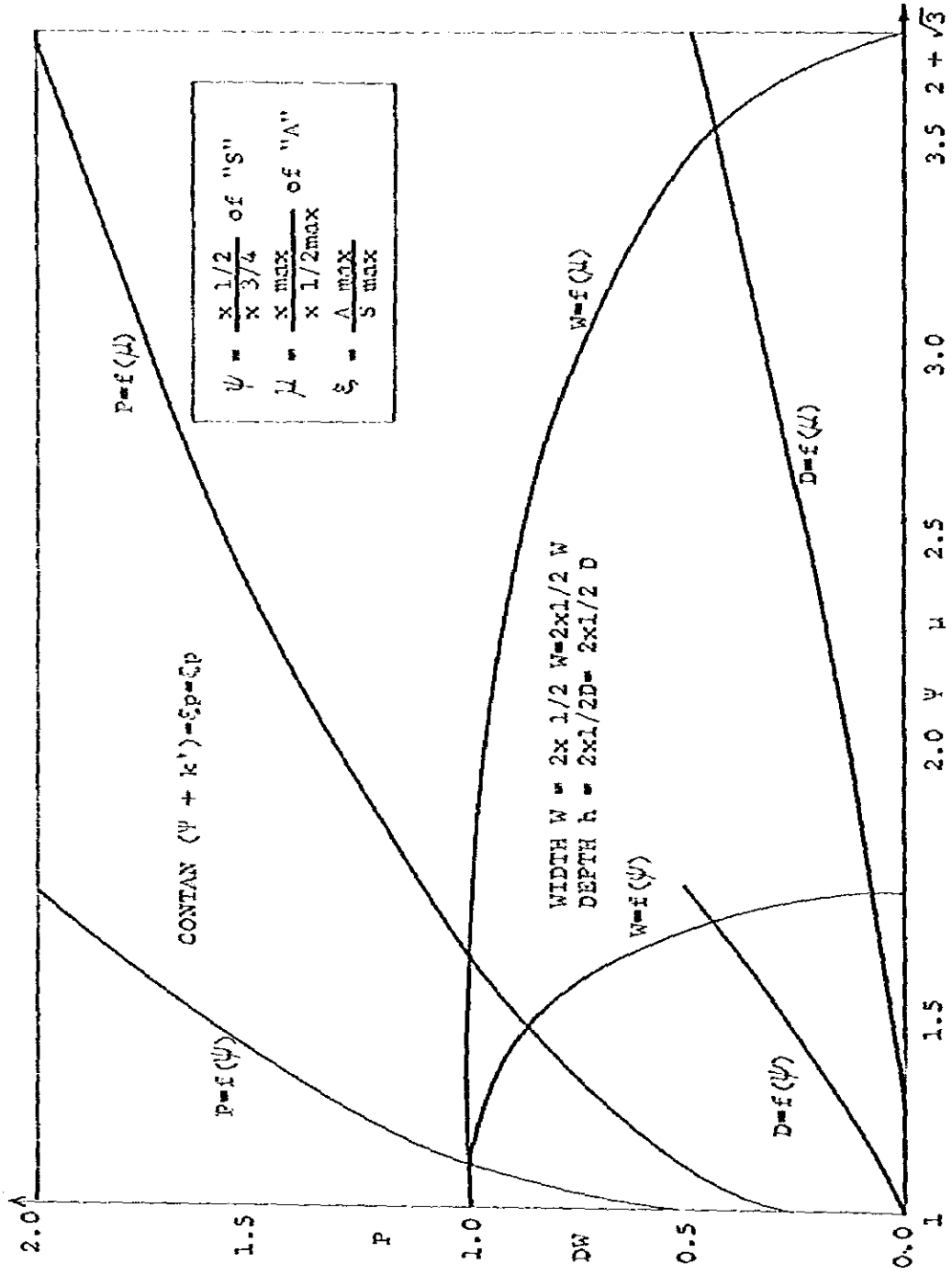

Fig. 5 Master curves of the scalar functions used in the Koulomzine method. Ratios Ψ, μ, and ξ are obtained from the field curve decomposed into its symmetrical and antisymmetrical components.

component of the field curve which is given by the formula

$$A(X) = \frac{\lambda}{2} \ln \frac{(X - B)^2 + 1}{(X + B)^2 + 1} \quad .$$

7. Graphical Solution for x=0, S(x) and A(x)

A graphical solution to determine the position of x=0, and the symmetrical S(x) and A(x), c the antisymmetrical A(x) components of the field curve $\Delta F(x)$ is illustrated in the analysis of one of the aeromagnetic anomalies of Panay Island (Figs. 6 and 7).

7.1 Actual Procedures of the Graphical Solution for x=0

The graphical solution in establishing x=0, of the field curve $\Delta F(x)$, (Fig. 8) is discussed below.

1. Establish a line tangent to the maximum and minimum, respectively, of the field curve $\Delta F(x)$.
2. Set two conjugate points, M,A, along $\Delta F(x)$, and project these points downward along the minimum tangent line, scale off the distance of this and then transfer the measured value to the maximum. The distance should be reckoned from the maximum tangent line to the corresponding points along $\Delta F(x)$.
3. Project the established points as illustrated in Fig. 8. By projecting, we get the point of intersection R, due from points M,A,R,I,K, and O is the point where succeeding measurements will be reckoned.
4. Project R downward to intersect $\Delta F(x)$, and designate point R'. Then extend line R,R' downward, this equals x=0.
5. Scale off the distance from R and R', and transfer the measured value from the minimum line to a point along $\Delta F(x)$, connect and extend horizontally. The resulting line equals the anomaly zero level.

7.2 Determination for S(x) and A(x).

The determination of the symmetrical curve S(x) and the antisymmetrical curve A(x) is graphically illustrated in Figs. 4 and 8.

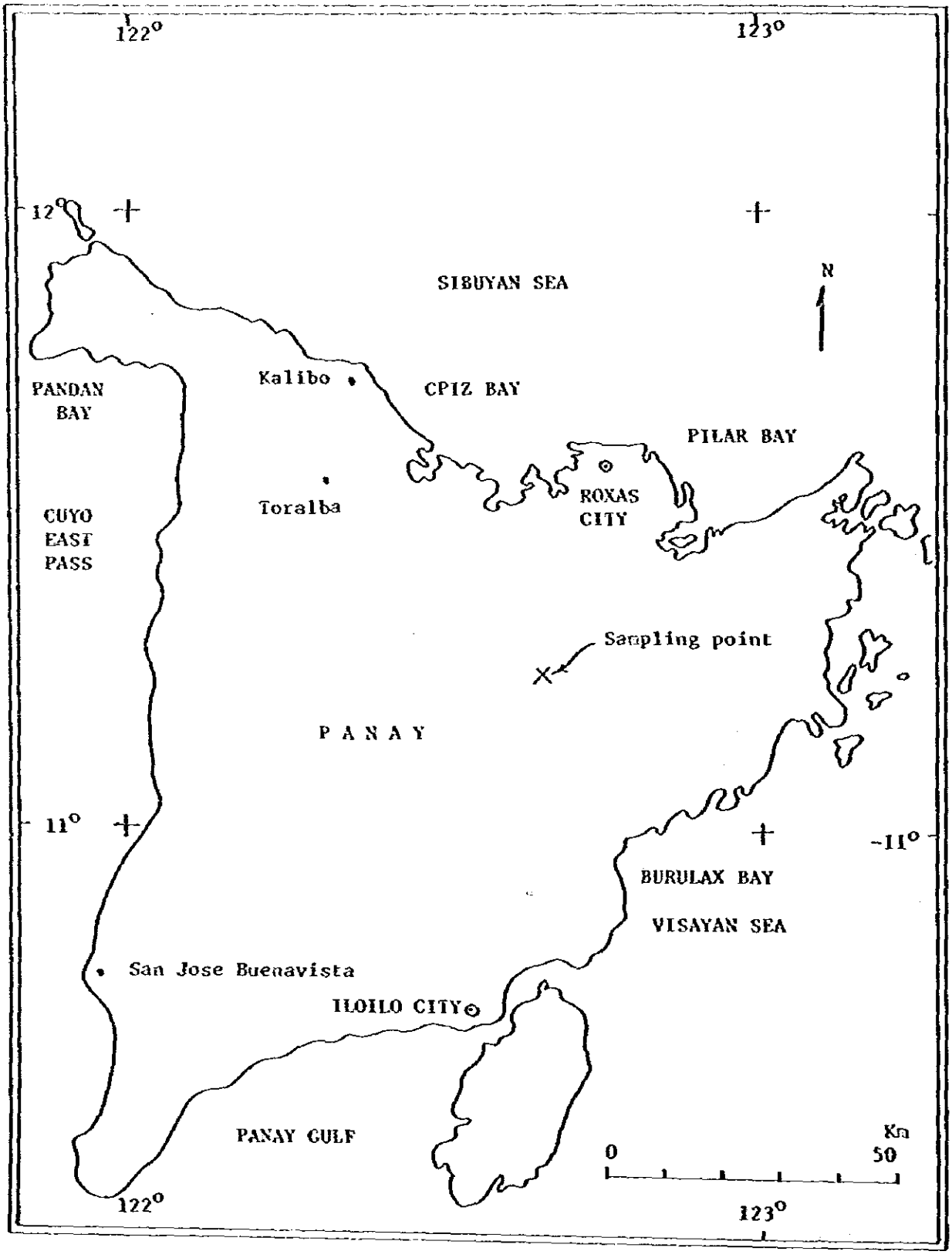

Fig. 6 Location map of Panay Island, Philippines

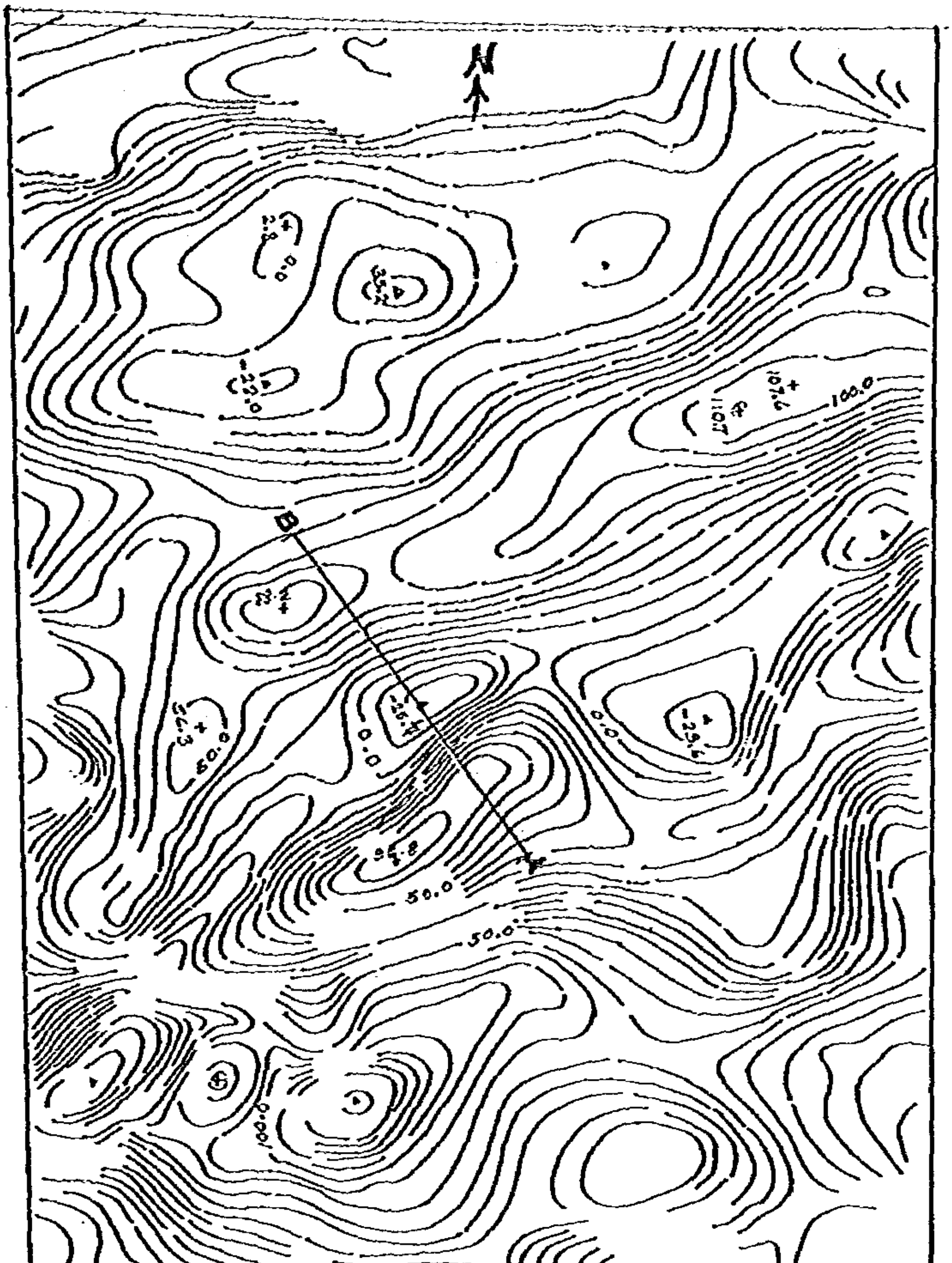

Fig. 7 I.G.R.F. residual map of a portion of the aeromagnetic survey of Panay Island, Philippines

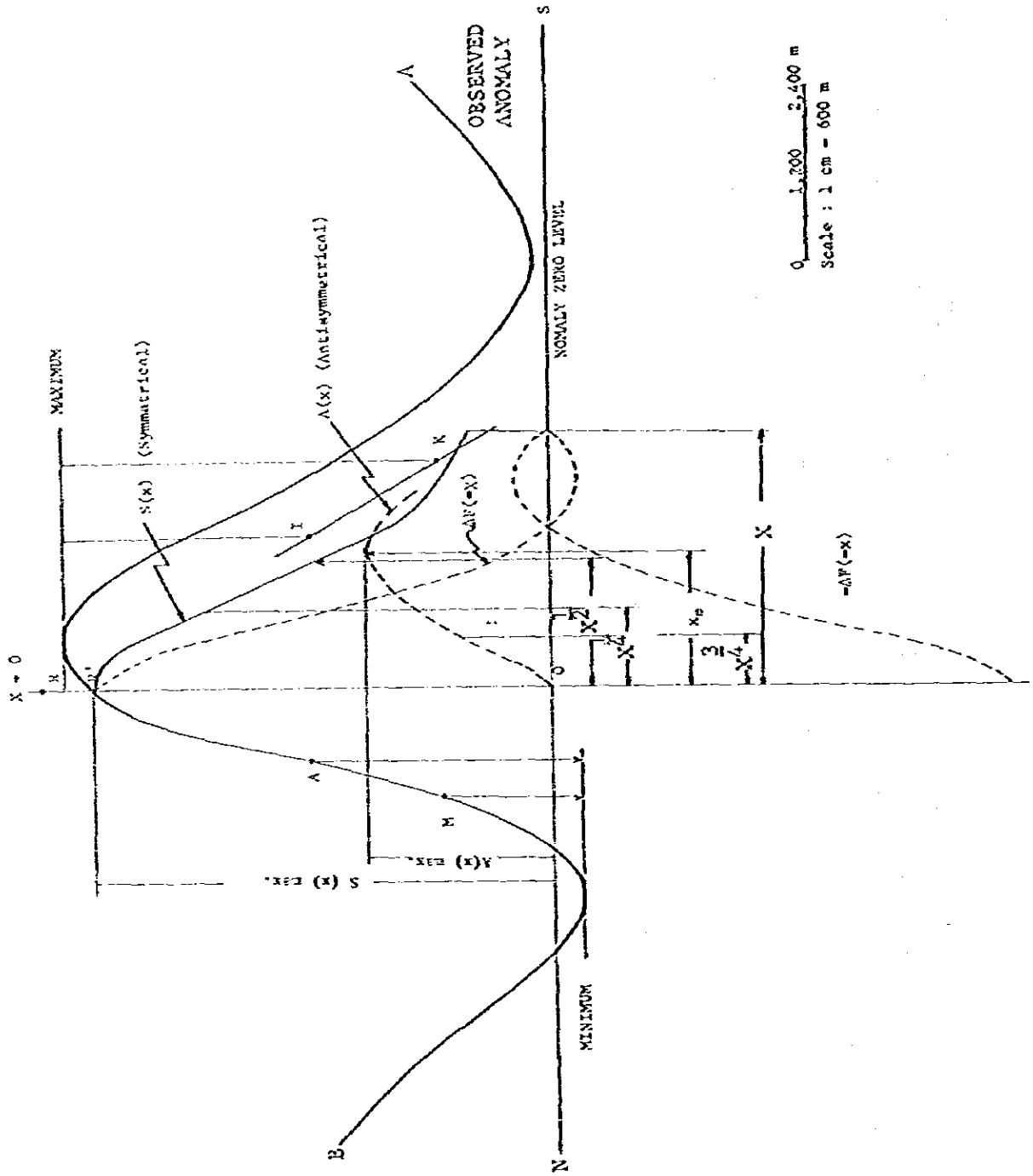

Fig. 8 Analysis of one of the aeromagnetic anomalies of Panay Island, Philippines

8. Actual Application of the Koulomzine Method

The actual application of the Koulomzine method to the aeromagnetic field curve of one of the anomalies in Panay Island, Philippines is discussed below.

Firstly, the location of the position of x=0 is established by utilizing the procedures previously explained.

Secondly, the field profile is separated into two components namely, the symmetrical S(x) and antisymmetrical A(x).

Thirdly, the maximum and minimum of each component is determined.

Fourthly, the position of $x_{\frac{1}{2}}$, and $x_{\frac{3}{4}}$ from the symmetrical S(x) and X_e, $x_e/2$ from the antisymmetrical A(x) components are located. These points are projected to the zero anomaly level and distance is measured for each from x=0 along the said level.

Finally, the determination for the depth of burial h, the width w, and the angle of dip p is done by comparing to a set of six master curves (Fig. 5). The calculations are shown in the succeeding section.

9. Calculation of the Depth of Burial, Width of the Dike, and Dip of the Dike in One of the Anomalies (aeromagnetic) in Panay Island

Symmetrical method S (x)

$x_{\frac{1}{2}} = 2.9$ cm

$x_{\frac{3}{4}} = 1.8$ cm

$\psi = \dfrac{x_{\frac{1}{2}}}{x_{\frac{3}{4}}} = 1.6$

$D = f(\psi) = 0.38$ $\qquad h_s = 2.1$

$W = f(\psi) = 0.60$ $\qquad w_s = 3.4$

Antisymmetrical method A (x)

$x_e = 3.1$ cm

$x_{e_{\frac{1}{2}}} = 1.2$ cm

$u = \dfrac{x_e}{x_{e_{\frac{1}{2}}}} = 2.58$

$D = f(\mu) = 0.28$ $\qquad h_a = 1.74$

$W = f(\mu) = 0.83$ $\qquad w_a = 5.1$

Getting the mean values,

$h = \dfrac{h_s + h_a}{2} = 1.92 \times 600 = 1{,}152$ m. (depth of burial of the dike).

$w = \dfrac{w_s + w_a}{2} = 4.25 \times 600 = 2{,}550$ m. (width of the dike).

110.

For the dip (p)

$$\varepsilon = \frac{\text{A maximum}}{\text{S(x) maximum}} = \frac{10.1}{4} = 2.52$$

$P_S = f(\psi) = 1.84$ $\quad\quad$ $\lambda_S = \xi \times P = 1.84 \times 2.52 = 4.64$

$P_A = f(\psi) = 1.58$ $\quad\quad$ $\lambda_A = \xi \times P = 1.58 \times 2.52 = 3.98$

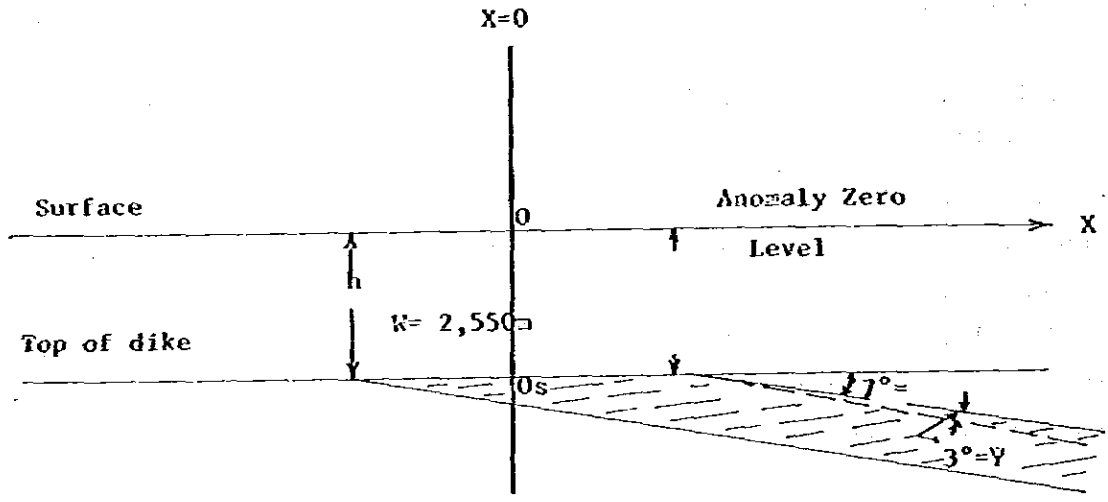

Fig. 9 Fig. 9 Final model of one of the anomalies of Panay Island, Philippines, using the Koulomzine method of interpretation. The dip of the anomalous body tends to be horizontal; h and w represent the depth of burial and width of the body, respectively.

Here, k'=I' = 10 degrees (known value).

cotan $(\psi + k') = \lambda_S$ ----- (+ k') = 12° 10' (λ_S = 4.64).

cotan $(\psi + k') = \lambda_A$ ----- (+ k') = 14° 05' (λ_A = 3.98).

Therefore, $\psi_S = 2$ and $\psi_A = 4°$.

ψ = mean of ψ_S and $\psi_A = 3°$.

and the dip (ρ),

$\rho = 10 - 3 = 7°$, which is almost flat-lying.

10. Conclusion

Koulomzine method of interpretation is analytically correct and fast in terms of the determinations for the depth and width of an infinite dike. However, in the case of our application to the analysis of one of the anomalies in Panay,

we found out that extra care should be given in dealing with the dip of the model. For example, when the dip tends to be nearly horizontal, some ambiguity comes out. This would have been clearly shown if other anomalies were processed. But the usefulness and practicability of the Koulomzine method in the solution of an aeromagnetic field profile provides us great convenience in determining the depth of an overburden, which a very important factor in exploration, as well as, the width and the dip of the anomalous body. Therefore, the separate method of interpretation of an infinite dike provides us with sufficient, if not all, solution of the parameters necessarily needed for interpretation.

Acknowledgement

The writer wishes to express his thanks and gratitude to Dr. Hiroshi Hasegawa, Mr. Tomosaburo Saito and Mr. Hiroji Tsu, all of the Geological Survey of Japan, for the help they extended to him. To Mr. Isamu Hirano, of JICA, an efficient and accommodating coordinator, for his invaluable service to the participants of the Offshore Prospecting Course. And to those people who in one way or the another, exerted their efforts during the training period, thanks are due them.

References

1) Geophysics, Vol. 35, No. 5, 1970, p. 812-830.

2) F.S., Grant and West, G.F. (1965), Interprestation Theory in Applied Geophysics.

3) Geophysics Research Journal, Vol. 74, No. 4, 1978.

4) Geophysics, Vol. 29, No. 4, 1969, p. 482-516.

7. Aeromagnetic Data Compilation, Analysis and Interpretation

Neoman B. Dela Cruz*

1. Introduction

Geophysical prospecting is the art involving the search for concealed deposits of oil and gas or economical minerals by physical measurements from the earth's surface. Information on the physical properties of material within the earth may be extracted from these measurements from where interpretation may be made to locate mineral deposits.

Magnetic prospecting which is the oldest method of geophysical exploration is used in oil prospecting primarily to determine the thickness of the sedimentary section or to map structural features on the basement surface that may influence the structure of the overlying sediments.

Airborne magnetics has steadily increased after the end of the Second World War. Nearly all magnetic exploration for oil and magnetic prospecting for minerals are now carried out with aeromagnetic instruments. The speed, economy, and convenience of airborne technique have made this method a popular one for exploration.

2. Aeromagnetic Field Operations

Aeromagnetic flight pattern usually consists of a series of primary flight lines with fixed spacing, usually, about half the depth from the survey elevation to the basement but usually is not changed within a given survey even when large variations in basement depth may be found. The main flight lines are tied by crosslines with the common dimensions of the rectangles formed by the flight and tie lines usually 1 by 6 miles, 2 by 10 km., 2 by 10 miles, etc.

Band flying rather than widely speced single lines are usually preferred for reconnaissance surveys over very large areas. In this method two or some times three parallel lines are flown at normal spacing with a greater spacing between bands. Resulting magnetic field can be contoured within the bands and the trend directions established for making azimuth corrections in the inter-

* Bureau of Mines, Department of Natural Resources, Philippines

pretation process. This gives more accurate basement depths than can be derived from single widely spaced lines.

Flight lines during the course of the survey should be held as much as possible on a straight line at constant elevation. It is the usual practice for basement mapping to maintain the flight at a constant elevation usually about 1,000 feet above the average surface elevation. Areas with wide range of topographic elevation may be subdivided into blocks, each area to be surveyed at a fixed elevation, with some overlaps between blocks to make the map continuous. The magnitude of the vertical gradient as a result of the difference of elevation may be approximated as -0.047 Ho in gammas/meter where Ho is the value of the total intensity in oersteds. A line can be drawn on the map at the boundary between the two elevation blocks and contours on each side drawn to this line with a discontinuity corresponding to the vertical-gradient effect to make a continuous map.

2.1. Flight Line Orientation

Principal or the more closely speced flight lines should be oriented perpendicular to the expected geological strike or the tectonic trends of the area which may be obtained from regional geologic or tectonic maps. This alignment means that magnetic features of geologic origin are crossed so that azimuth corrections which are part of the basement-depth calculations are smaller and more accurately determined. Where the survey is conducted in low magnetic latitudes where a simple source produces a complex anomaly with a low on the north side it may be preferable to fly on a north-south direction because the magnetic character is better determined.

2.2. Location Systems

The location of the flight lines and the correlation of the readings with a ground position is necessary in mapping airborne-magnetometer observation. The control of the aircraft and its positioning must be very exact to retain the detail of high-sensitivity recordings.

2.2.1. Aerial photography positioning

Aerial photography positioning involves the drawing of lines on a photomasaic cut into long strips with the copilot calling course corrections to the pilot and

making necessary notes. Horizontal positioning of the survey craft is determined by positioning photographs taken during flight by a continuous 35 mm strip-camera film taken at intervals of 1 or 2 seconds. The continuous-strip record is compared with the photomaps and each frame are matched with the ground picture. Total magnetic field values after removal of the earth's normal field are then transferred from the record to the map.

2.2.2. Electronic positioning system

The electronic positioning of flight lines are commonly employed by several systems and is very necessary when survey is conducted in offshore areas or where photo mapping is not available.

a) Radar. This is used in marine surveys where suitable reflecting objects such as towers or floating buoys using corner reflectors are available. This operates at a frequency range of 3,000 to 10,000 KHz.

b) Shoran. This system depends on transponders mounted on towers at fixed shore positions or on anchored boats responding to a signal from a moving craft. Sharply pulsed signal is sent by the equipment on the moving craft and when this signal reaches a transponder a responding signal is activated which is picked up by the moving station equipment. The transmission time from the moving station to the transponder and vice versa is a measure of the distance between the moving vehicle and the transponder.

2.2.3. Radio-frequency systems

These system depend on patterns of standing waves maintained accurately with respect to fixed shore operations. In the circular mode, standing waves are formed by interference between a signal from a fixed base station and a transmitter on the moving vehicle which form a set of circles of equal phase centered at the base station. Two sets of such circles centered at two base stations give location coordinates. In the hyperbolic mode, two sets of circular standing waves in space are formed by interference of signal between the base stations. Two phase meters on the moving vehicle measure phase changes giving a set of location coordinates.

2.2.4. Doppler navigation

This system is self-contained within the survey craft and does not depend

on auxiliary reference stations. It works on the Doppler principle that wave travelling between two locations moving in relation to each other change in frequency in proportion to the relative velocities of the source and the receiver. For aircraft survey the source is the aircraft, and the receivers are the ground traces of the transmitted beams. In turn, the ground as reflector becomes a source and the aircraft the receiver with the phase difference between transmitted and reflected signal measuring velocity. A variation of the Doppler principle using sound waves in water (Sonar Doppler) is used for sea navigation.

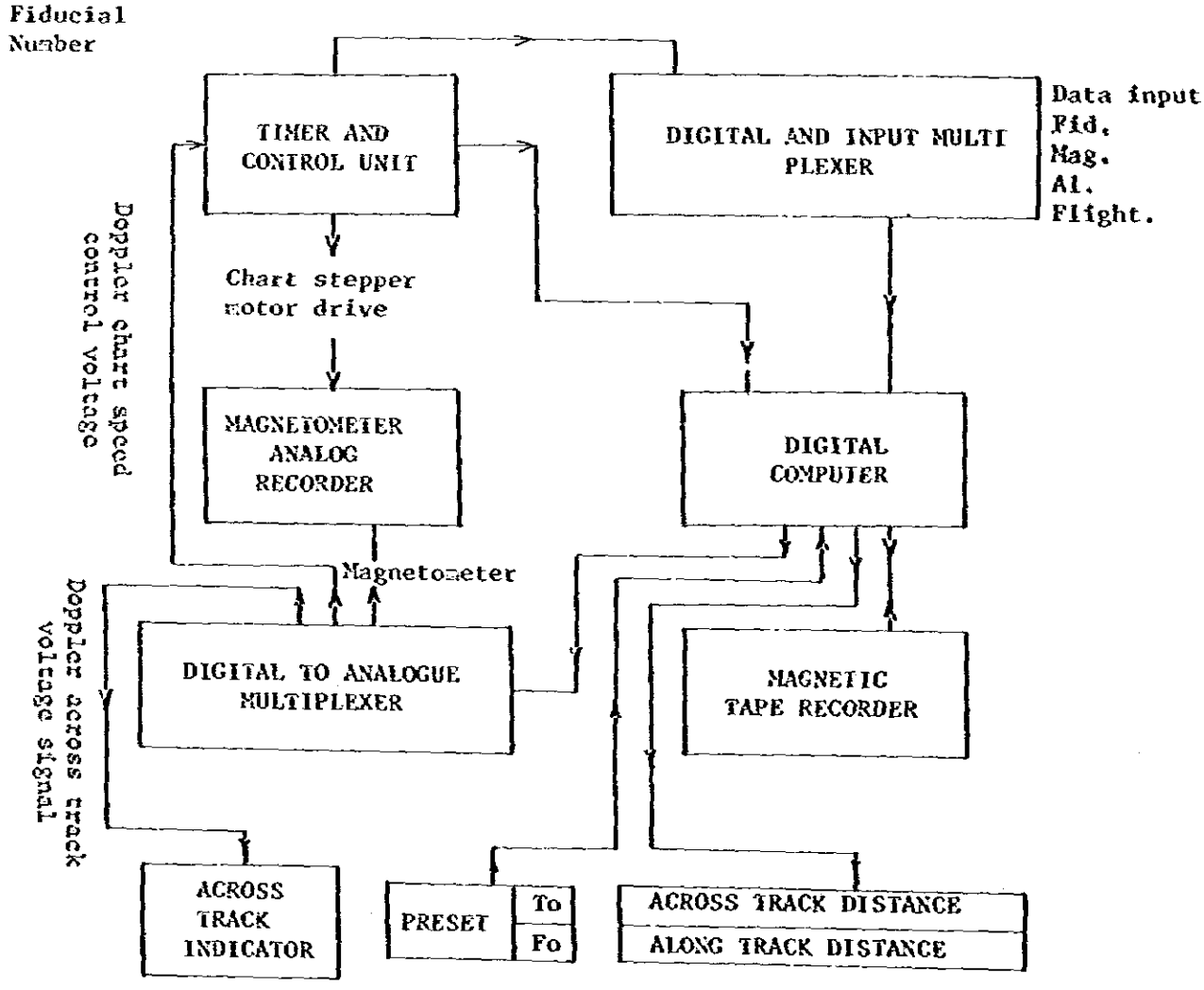

Fig. 1 Flow chart of data acquisition

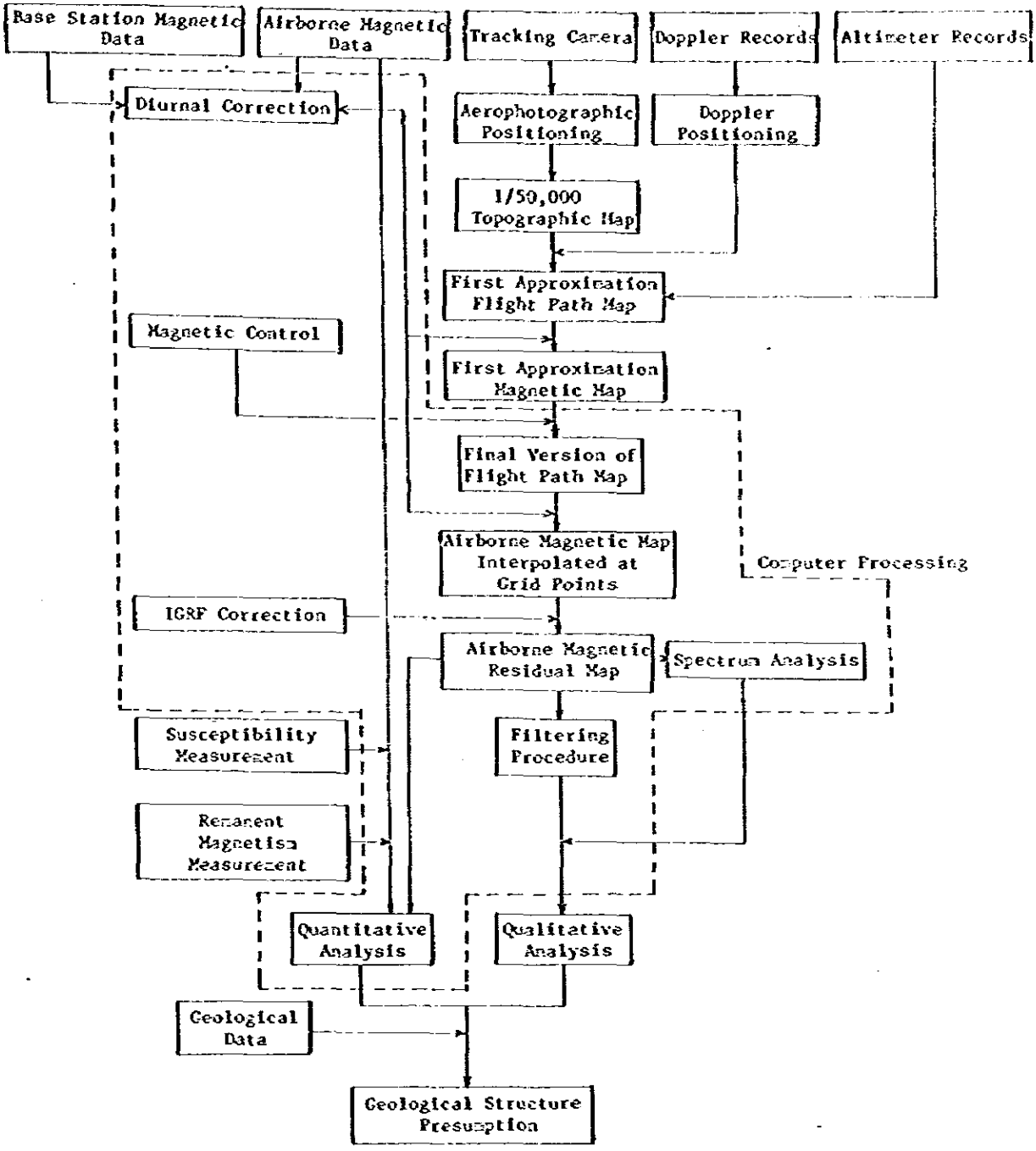

Fig. 2 Flow chart of data processing and analysis

3. Data Reduction Systems

The preparation of a contoured map form airborne magnetic data starts with the recording in the survey craft of magnetic, elevation, and position data. Various sources of errors committed in the mapping process have to be noted and appropriate corrections be made.

Modern data processing involves the various steps in eliminating errors and making final maps through the use of digital computers.

3.1. Corrections to Magnetometer Observations

The sum of all contributions to the magnetic field at the time and place of observation affects the magnetometer reading. It is absolutely essential that to attain a satisfactory image of magnetic anomalies of small relief, extraneous effects to the total magnetic field must be eliminated.

The total field measured at a given time and place represents: inner field of the earth due to the basic properties of the earth as whole, external field due to sources above the surface (diurnal variations), and anomaly field due to sources within the outer part of the earth's crust. In petroleum exploration only the last component is of interest, and the first two components must be removed and the field operations carried out in such a way that these corrections can be made in data processing and mapping.

3.1.1. Normal corrections

This corresponds to the latitude correction of gravity values and are made to remove special variations of magnetic intensity due to the eart earth's inner field. Corrections are determined empirically from the following magnetic charts of tables.

For large surveys normal corrections should be determined from smooth normal contours based on these figures. In the mapping of airborne surveys normal corrections can be determined from the IGRF charts. If the map is compiled from the analog records, normal magnetic change from the tables can be drawn as nearly straight lines on the records and the values mapped are then departures from these lines..

3.1.2. Diurnal corrections

Magnitude of diurnal variations of earth's magnetic field range from 10 to 100 gammas or more. For ground magnetometer surveys data for diurnal corrections can be made by returning the instrument at intervals during the day to the same point or to points between which magnetic intensity differences have been previously determined and the variation in these readings is a measure of the magnetic change during the day.

For airborne surveys the diurnal change within the span of 3-5 minutes, the time it requires the survey craft to make rectangular closed loops on the flight pattern. While start time diurnal changes may occur in the closure adjustments it is a common practice for a continuously recording monitor magnetometer to accompany the survey. This is done to show the general nature of the magnetic weather and when diurnal changes exceed certain rates, operation is discontinued. This ensures that records made during times of magnetic storms or at times when changes are very irregular will not be used in the normal data-reduction procedure.

4. The Nature of Magnetic Anomalies

In magnetics, total intensity of the field is in a direction which varies from nearly vertical near the magnetic poles to horizontal at the magnetic equator (0 degree contour at Fig. 4) to near vertical near the south pole. The form of the magnetic anomaly from a given body depends on all the following factors: geometry of the body, direction of the earth's field at the location of the body, direction of polarization of the rocks forming the body, orientation of the body with respect to the direction of the earth's field, and the orientation of the flight line with respect to the axis of the body.

4.1. The Geomagnetic Field

Geomagnetic field at any particular point in space consists of several time varying components of widely separated origin and may be summarized as follows:

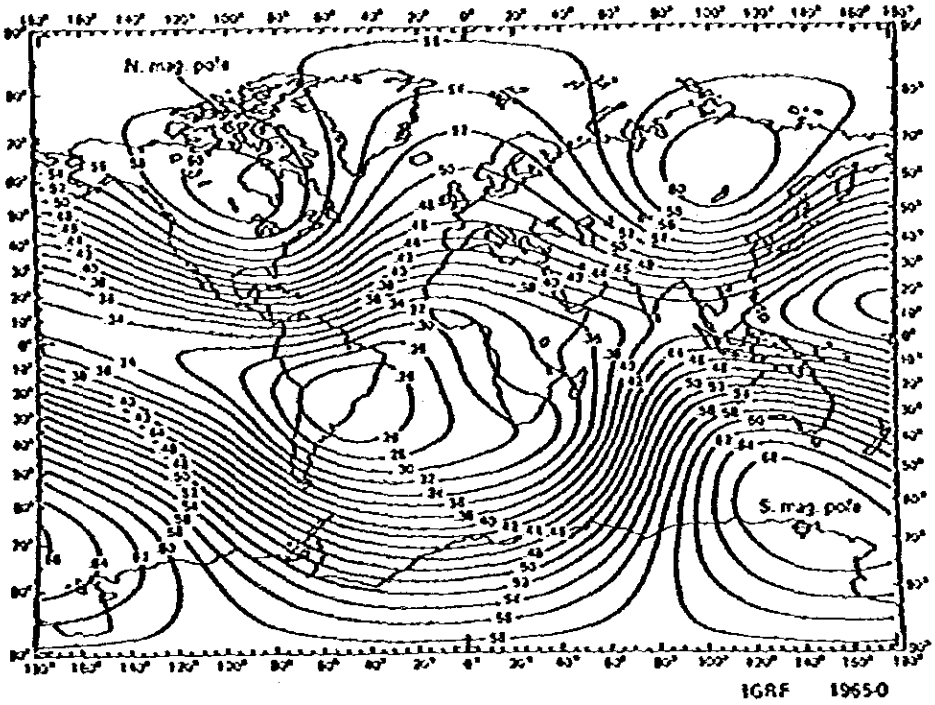

Fig. 3 Contours of the total intensity of the earth's magnetic field in oersteds. (from Leaton, 1971)

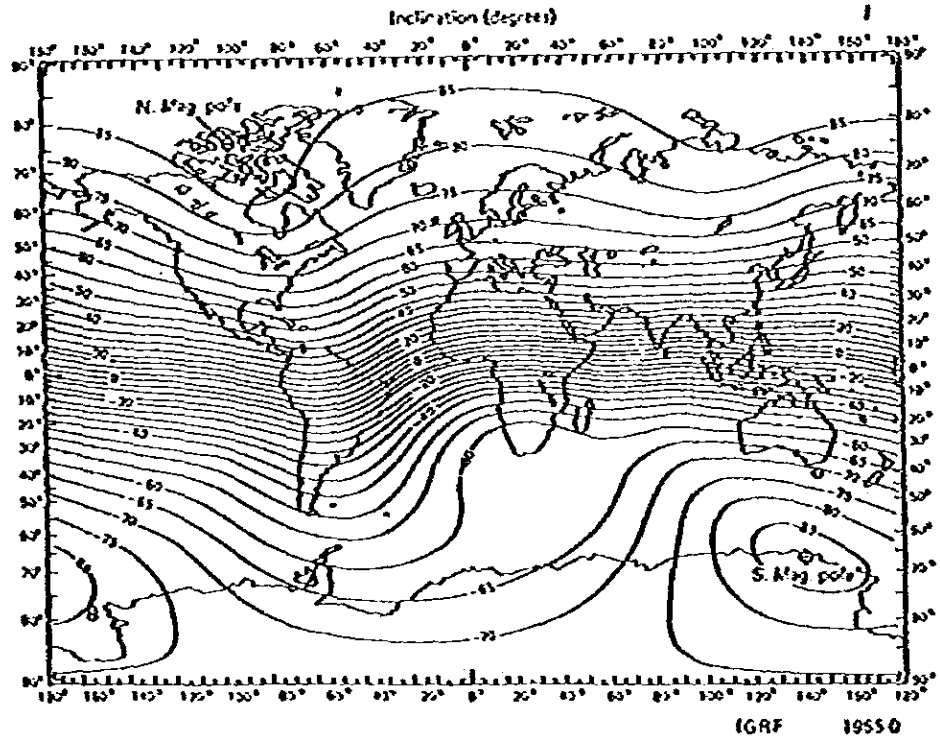

Fig. 4 Contours of the inclination of the earth's magnetic field in degrees from the horizontal. (from Leaton 1971)

Table 1. Components of the geomagnetic field

Name	Source	Time dependence	Space dependence	Typical amplitude
Dipolar	Deep internal	Slowly decreasing	Approximately dipolar	25,000 - 70,000 γ
Secular	Earth's core (3,000 km)	1 - 100 years	Random but drifts westward	±10 - 100 γ per year
Diurnal	External - associated with sunspots	24 hours (Period 27 days, 12 months, 11 years)	With magnetic latitude and sunspot activity	10 - 100 γ
Micropulsations	External	0.002 - 0.1 Hz	Same as diurnal plus magnetic storms	Usually 1 - 10 γ but up to 500 γ
AFMAG	External	1 - 1,000 Hz	Same as diurnal plus thunderstorm activity	0.01 γ per sec.
Telluric current effects	Shallow internal	0.002 - 1,000 Hz	Geologic	0 - 0.01 γ per sec.
Induced magnetization of rocks	Shallow, internal down to Curie point geothermal at 13 miles	Secular	Geologic - varies with % magnetic in rocks	0 - 50,000 x 10^{-6} emu/cc
Remanent magnetization of rocks		Some decay with geologic time	Geologic	0 - 200,000 x 10^{-6} emu/cc

5. The Interpretation of Magnetic Maps

Immediate purpose of magnetic surveys is to detect rocks or minerals possessing unusual magnetic properties which can be identified by causing disturbances or anomalies in the intensity of the earth's magnetic field.

5.1. Magnetic Maps

Interpretation starts with the observed field which is usually the total intensity map.

5.1.1. Second derivative maps

The second-derivative map prepared from the observed total-intensity or vertical-intensity maps acts as a filter, emphasizes the expression of local features and removes the effect of large anomalies or regional influences. Its principal use in interpretation is to indicate the outlines of individual intrabasement blocks or the edges of suprabasement disturbances. These indications serve to suggest features on the individual flight-line profiles which can be used for basement-depth determinations and also to determine the strike of the edges of the bodies and the angles between the flight lines and those edges which are used to make the azimuth correction to the depth determinations.

5.1.2. Continuation calculations

Upward continuation is used to simplify the appearance of magnetic maps by suppressing local features. The abundance of local magnetic anomalies often obscures the regional picture with an abundance of detail and upward continuation smoothen out these disturbances without impairing the main regional features.

Downward continuation is used for a purpose exactly opposite to upward continuation, namely, to increase the resolution of weak anomalies.

5.1.3. Reduction to the pole

This mapping procedure which is very helpful in magnetic anomalies interpretation was developed by a Frenchman, V. Baranov. This mathematical procedure is carried out on a grid of values written from a contour map or computer derived mathematical interpolation, similar to that of contouring procedures, from ob-

served values not on a grid. The purpose of this is to correct for the variation in the appearance of an anomaly depending on its magnetic and the corresponding variation of the dip angle of the magnetization vector in the body.

5.2. Determination of Basement Depths

Magnetic exploration in the petroleum industry is primarily intended for the determination of the depths to the basement surfaces. Most basement rocks have more magnetite and are more magnetic than nearly all sedimentary rocks and in a general way the magnetic effect recorded by an airborne magnetometer (and to lesser degree ground magnetics measurement) is substantially the same as it should be if the sediments were not present. Therefore, determining the depth to the source of the recorded magnetic anomalies is generally equivalent to determining the thickness of the sedimentary section. Since the occurrence of oil is expected only in sedimentary rocks a reliable determination of the depth to the basement rocks gives a measure of the volume of sediments and is a first limitation on its potential as a source of oil.

5.2.1. Slope and half-slope methods for estimation of basement depths

The principles of the half-slope and maximum-slope distance parameters are indicated in the following figure:

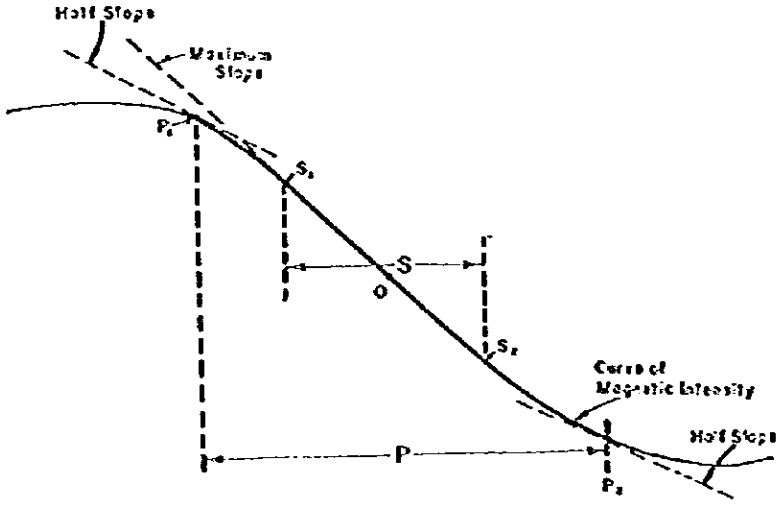

Fig. 5 Idealized magnetic profile showing measurements for slope (S) and half-slope (P) parameters used for basement-depth estimation.

124.

The application to a portion of an actual magnetic profile is shown in the following:

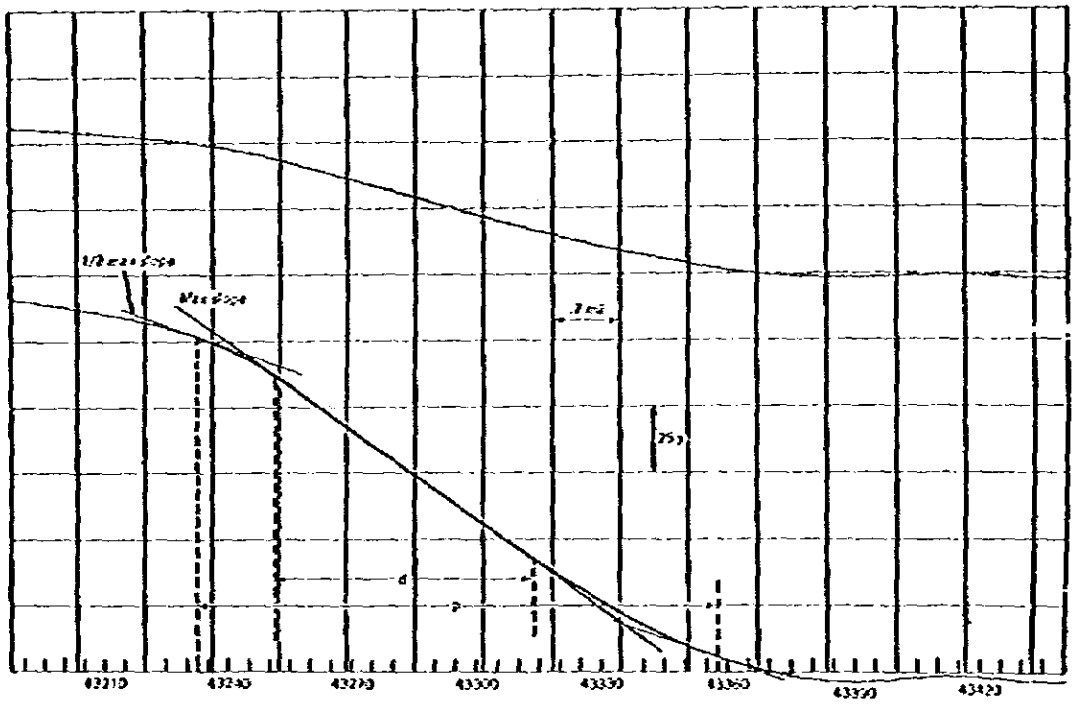

Fig. 6 Portion of an aeromagnetic profile showing measurement of slope and half-slope distances.

On a magnetic profile, either a portion of the actual record from the survey or drawn from contours on a map, a line of maximum slope is drawn through the point of inflection, 0. The points of tangency P_1 above and P_2 below the point of inflection are drawn. The half slope parameter P represents the horizontal distance between these two points. In actual practice, the maximum slope coincides very closely with the magnetic profile for a certain distance then breaks away from the straight line at consistently measurable portions S_1 and S_2. Distance S between these points is the slope parameter.

5.2.2. Depth estimation by other methods

The general principles of other selected systems for basement-depth or model-depth estimation are based on the properities of magnetic curves calculated for geometric bodies. Some of these have been developed for determination of

he depth and dimension of the bodies, and others have been developed primarily or estimation of depth to the top of the body.

Been in the following figure gives a graphical note based on inflection and half-slope points. Upper part of the figure shows the essential parameters for a two-sided anomaly while the lower figure shows a broad or one-sided anomaly such as a zone of steep gradients on a map without any obvious boundary. Defining points are the inflection points 0 and 0', and the half-slope points P1, P2 on

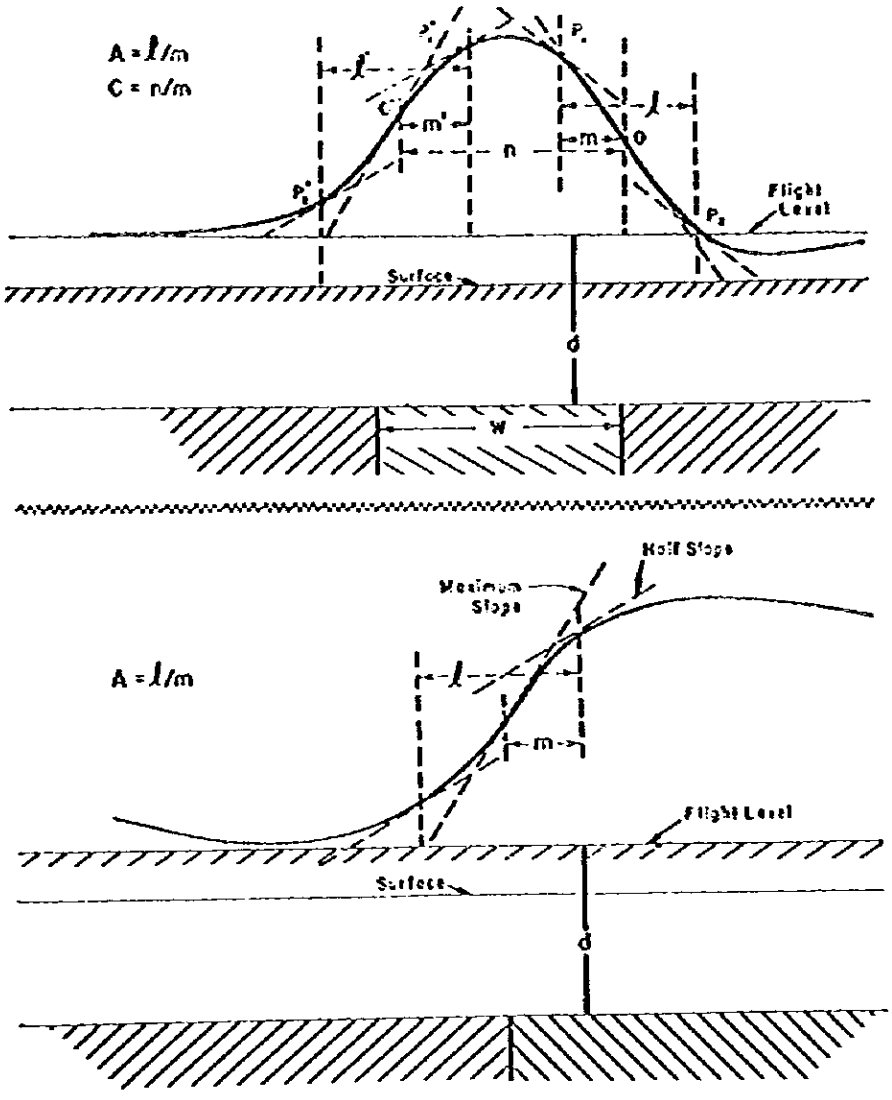

Fig. 7 Assumed magnetic profiles showing quantities measured in Bean's method of depth estimation.

the right and P_1', P_2' on the left. Measurements are made for distances l, m, and n with one value recorded for n, with m and l measured on both sides. From the measurements the ratios a=l/m and C=n/m are determined.

The principle of Koulomzine, Lamontague and Nadeau is an elaborate mathematical analysis based on the two-dimensional dipping dike model where the model curve is transformed into symmetrical and anti-symmetrical components. This process depends on locating certain points and distances on the anomaly curve and the critical parameters of the model (width and depth to top) are determined from the measurements on the anomaly.

5.3. Corrections to the Depth Estimates

Most basement-depth estimation are commonly carried out directly on magnetic records or as reproduced from digital recordings thus giving distances on the recording tapes which must be corrected to give depths used in making the basement map.

5.3.1. Scale correction

Magnetometer recordings made in the survey craft are on at a constant rate and therefore on time base is so that the scale with respect to ground distances is variable dependent on the speed of the craft which can vary as one flies against or with the wind. Scale of the record corresponding to known distances on the ground (between some points) to give a factor for conversion. In modern recording, scale variation is eliminated by controlling the recorder by Doppler distance measurements or by computer coupling with the location data when recorded digitally.

5.3.2. Correction for azimuth

Generally, flight line is not perpendicular to the magnetic contours and the distances determined from the record are greater than they would be if it were meaning the distances measured on the record must be shortened by multiplying the cosine of the angle between the direction of the contours and the flight line. Contour direction of the particular feature being used for depth calculation is usually better determined from a second-derivative map than from the total intensity map.

5.3.3. Flight elevation

Basement maps are usually made with depths below sea level while the parameters measured on the record apply at the flight elevation. It is necessary, therefore, that after determining the depth of a given point from the record, the sea level elevation of the flight line be subtracted to give the depth on a sea level datum.

Acknowledgements

The author wishes to express his gratitude to JICA and the Japanese Government who were responsible for the financial support given in the course of the traineeship and in the preparation of the report.

The valuable moral support extended by Dr. H. Hasegawa, Mr. T. Saito and personnel of the Overseas Geology Office, Geological Survey of Japan also greatly facilitated the completion of this report.

Finally, the author wishes to express his gratitude and appreciation to Mr. I. Hirano, JICA coordinator for all the assistance given.

References

1) Dobrin, M.B. (1960), Introduction to Geophysical Prospecting, McGraw Hill, N.Y.

2) Grant, F.S. and G.F. West (1965), Interpretation Theory in Applied Geophysics, McGraw Hill, N.Y.

3) Nagata, T. (1961), Rock Magnetism, Maruzen Co. Ltd., Tokyo

4) Nettleton, L.L. (1976), Gravity and Magnetics in Oil Prospecting, McGraw Hill, N.Y.

5) Stacey, F.D. and S.K. Banerjee (1974), the Physical Principles of Rock Magnetism, Elsevier Scientific Publishing Co. Ltd., Netherlands

8. Impact of the (Z) Continent on Continental Drift and Offshore Mineral Resources

S. A. Njare. *

Summary: It was at the beginning of 20th centuary, when Edward Suess brought up the idea of the Gondwana continent linking Africa with America, India, Madagascar, Australia, and Antarctica together. Then, in 1912, Alfred Wagener revived the idea by suggesting the existance of the great continent of Pangaea and the drifting of continents. Synthesis of studies on paleontology, paleomagnetism, petrology, mantle convectional currents, earthquakes, volcanic lava, ash, and fumeroles, had conviced many earth scientists of our time, to draw up a conclusion that continental migration based on plate tectonics was indeed a fact. The drift theory, has reasonably served to explain the many perplexing physical phenomenon on the earth's surface; such as mountain building, earthquakes, volcanoes, mid-oceanic ridges, etc.

The (Z) Continent, here-under discussed is made up of what others call as the Philippine plate, much of the western half of the Pacific plate, and much of Indonesia. The paper, also touches upon the possibilities of the mineral deposits and hydrocarbon occurrences based on alignments and other circumstances brought about by consequences of the continental drift. Serious considerations have been aired in respect of the roles of the mid-oceanic ridges and mantle convectional currents.

1. Introduction.

The interlocking similarities between the coastlines of the western Africa and South America, amused Alfred Wagener so much that he became convinced by 1912, to suggest that America and particularly South America was once joined to Africa and that, from Jurassic, say the continents began to part away from each other toward their present positions. Indeed, during Wagener's time, the knowledge about the indepths of oceans was not quite understood. The only evidences available to support his arguments were deduced from the rudimentary and controversial similarities

* State Mining Corporation, Exploration and Economic Geology Department, Tanzania.

of fossils and rocks found from the continents.

When Columbus told his discovery of America and the outstanding civilization of the Red Indian, it was seemed at first almost incredulous story in the Old World; and then, Cook, the great English captain, was startled to discover people in remote Australia, New Zealand, and the tiny islands of the Pacific. If the pattern of human migration and habitats have baffled science; then it remains, therefore, highly contestful to rely on the distribution of fossil plants and animals as a verifying basis for mated continents. However, the distribution of such fossils, like the Glossopteris flora during the Permo-Carboniferous period in Africa, South America India, and Australia; could only suggest that the climate over much of these areas was, approximately, much the same.

During and after the First and the Second World Wars, the development of the submarines, ships, seismic equipments, etc. has intesified the study of oceanography. The discovery of the deep trenches, seamounts and plateau's, oceanic deeps, etc. had been made. The modern radioactive dating techniques has helped the chronology of the non fossiliferous rocks.

The discovery during the 1950, in England, of reversed paleomagnetic property of rocks, encouraged and accelerated similar findings in other places of the earth's surface, including the Deccan plateau in India, Japan, etc. Some interesting interpretations emerged: that, over the years, the earth's magnetic polarity had changed repeatedly so that in Silurian and/or Devonian, the magnetic pole had been located somewhere in the north central United States. In other areas, the contrasts which had been quite drastic had been attributed to land tilting or drift.

The correlative discovery that the Pamir knot and the great Himalayan range, otherwise just known as the roof of the world, had similar origins with the well studied Alpine mountains of western Europe, sparked interest as to the nature of formation of these world-wide distributed mountain system. Old classical geology attributes orogeny of the folded mountain system to result from the large depositional depressions or synclines which must have been subjected to vertical and compressional forces.

The Pacific Ocean has been the central talking point for many a generation of scientists. Some early geologists had thought at time that the moon had originated or detached from there. Even, Alfred Wagener, when trying to explain his famous continental drift theory, kept a blind eye on it. The fact that the great expence of the land covered by oceanic waters, is made up of both the ocean and the (Z) Continent (The Pacific

continent).

Mid-oceanic ridges, discovered and traced along the centre of the extensive oceans and the waters of the Pacific, Indian, and Atlantic; have indicated the partition of the oceanic islands, along the peak lengths. Islands situated near the ridge appeared to be younger in age than those which are a distance further away from it. Some authoratative scientists, attribute to the mid-oceanic ridges the motive force behind the movements of the large land masses across wide and long journeys to their present positions we no know them to be. Ocean floor spreading is also largely connected with the mid-oceanic ridges. The role of the mid-oceanic ridges as buffer zones, along which the large continental masses could rhythm and suppress fragmentations of land on impact, has been largely overlooked. In some parts of the great oceans, the ridges are noted to possess crater

Seisrology and the Internal Structure of the Earth

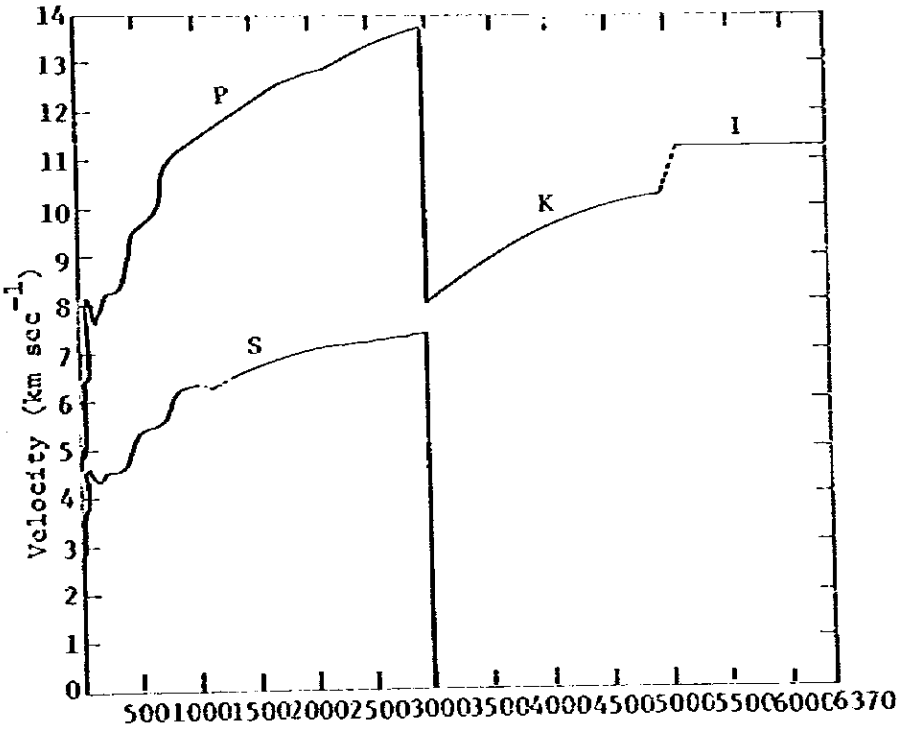

Fig. 1-a: Velocities of P and S waves within the Earth. Mantle velocities are based on data by Gutenberg (1958a), Toksoz et al. (1967) and Anderson (1967b).

INTERNAL DENSITY AND COMPOSITION

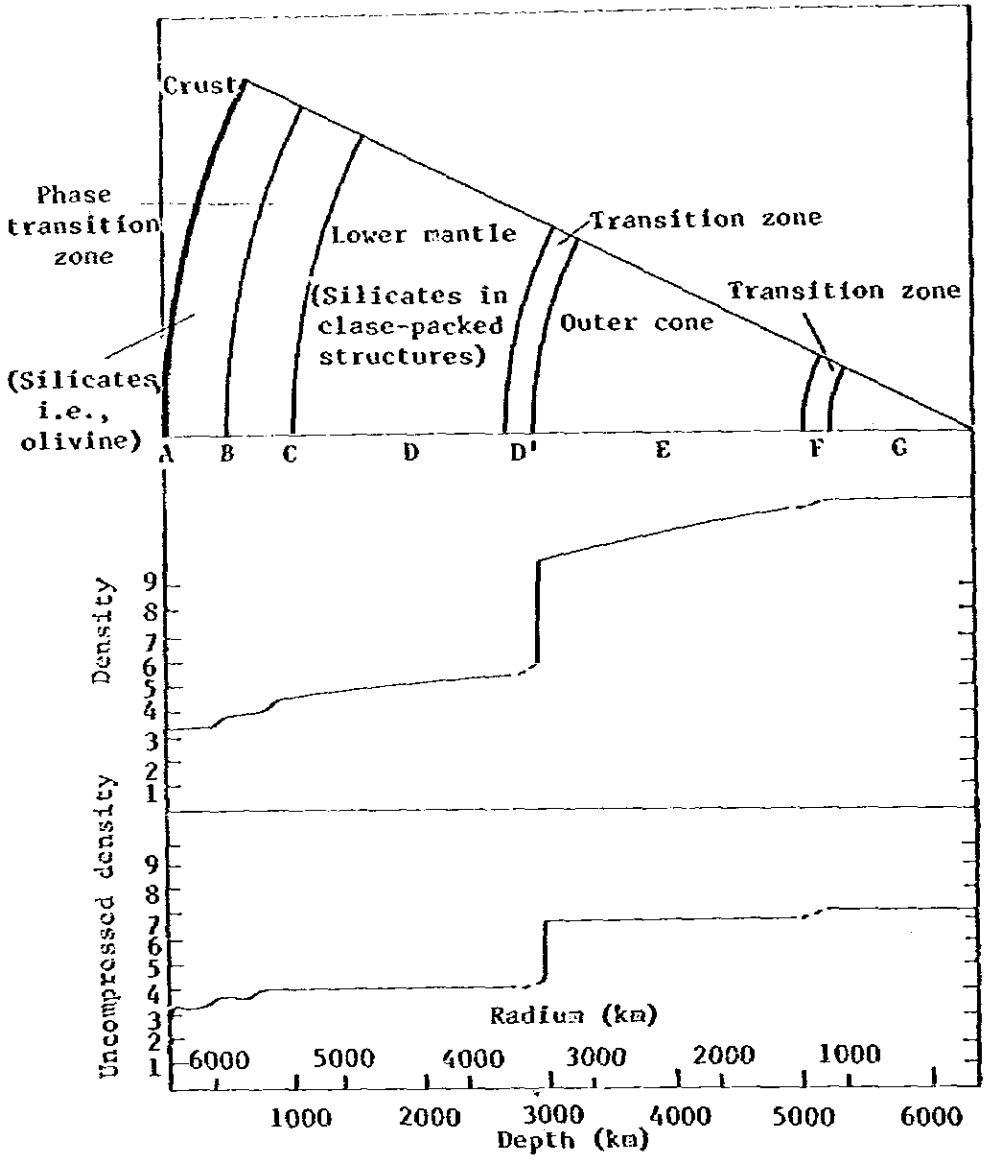

Fig. 1-b: Major subdivisions of the Earth's interior with estimated densities. Absolute values of uncompressed density are less certain but indicate clearly the differences in phase and chemical composition.

like median while in others the median is done shaped and associated with the continental rise.

The classical, vertical and basculating movements known in geology as being responsible for the uplift and sinking of lands as a result of which new sedimentary coatings could be worn on the continents, have been taking place as far as recent times in the Pacific areas. Subduction of

the great Pacific plate is an indisputable phenomenon, observable and marked by the fiery peripheral activity of the strong earthquakes and volcanic eruptions along the western continental coast of America and the island arcs of eastern Asia. Note of significance in the subduction of the Pacific area, is the invasion of the oceanic waters over much of the (Z) Continent which has subsequently lost much of its glorious economic importance in the area but, certainly, exerts tremendous physical influence over much of the area and echo reaction for the rest of the Globe. The surface of the (Z) Continent is marked by numerous deep trenches adjacent to the elongated ridges, some of which are oceanic; some plateau's and seamounts; and numerous islands of which some are of volcanic origin.

The significance of the idea of mantle convectional currents can not be under-rated in trying to describe the so many perplexing phenomenon taking place in the interior and on the surface of the Earth. Seismology favours the existance of the mantle with a transistional contrast to Earth's crust (Fig. 1-a and 1-b).

World concern for mineral resources, makes it imperative to mention the possible avenues by which efforts could be made to bring up many possible discoveries of minerals and oil, in areas whether to not seriously considered, but to be exposed in light of the critical analysis of the continental drift theory.

2. The (Z) Continent.

The (Z) Continent, as viewed in this article, forms part of the land in the Pacific region, much of which is deeply submerged by invading waters of the Pacific Ocean.

2.1. Location of the (Z) Continent

The (Z) Continent encompasses the areas of deep identification by the oceanic trenches adjacent to the high ridges of the island arcs in the north and north west. The northern most tip is marked by the convergence of the Kuril with the Aleutin trench, at about 54°N. The eastern rim is marked by the island chain of the Hawaian range and Tuamotu peninsula curved at approximately, 165°W and 145°W respectively. In the south the boundary runs across

the Touarotu archipelago, the Chatham plateau, down to south of the isles of New Zealand. The western boundary runs as from the north west through the Kuril trench, the Japanese trench, the Rukyu trench, to disappear gradually south of the Luzon-Palawan trench in the China Sea where continuation appears possible through a great transversal fault running across the western part of Borneo and between Java and Sumatra. In the south west, an extension of the Java trench and across the Arafura and Torres Sea, downwards through the eastern barrier reef trench and the trought west of the Lord Howe rise; separates the (Z) Continent from the Australian continent (Fig. 2).

2.2. Existance of the (Z) Continent

Classical geology prophesies that the surface of the globe in which we live had been receiving at different periods of time, coatings of eroded and residual materials.

Ocassionally, diformational forces especially on the earth's surface caused by the delatesional, compressional, vertical, subductional and

OCEAN FLOOR

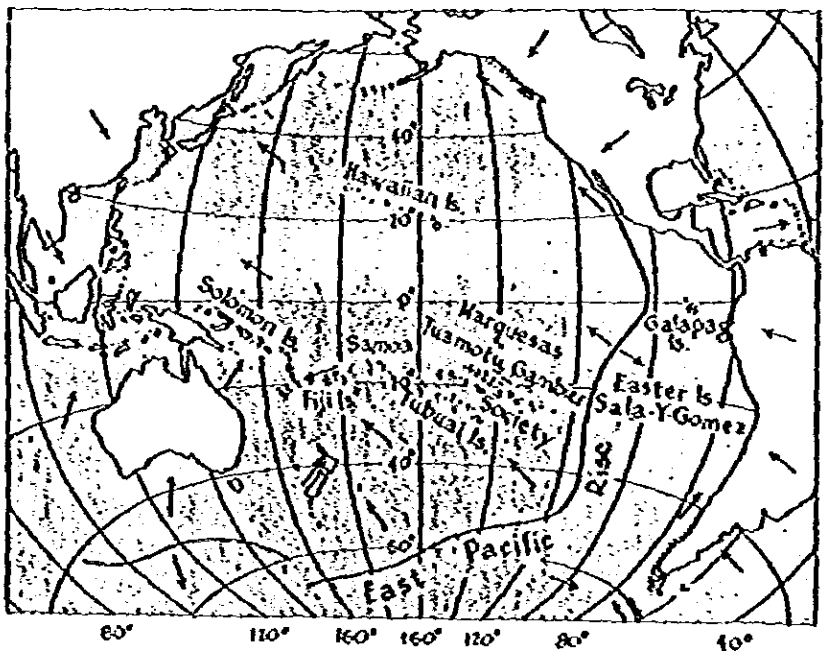

Fig. 2 Boundary of the (Z) Continent as inclosed. Pacific islands. The arrows show the probable directions of convection current flow. (After figure on P. 14 in Continental drift, by J. T. Wilson.)

basculating movements; have interfeared with the stratification of the residual materials. There is therefore, substance to argue that the (Z) Continent, whose continental linkages to the west are marked by deep trenches due to subductional movements, is, but receiving a new coating of sediments brought about by marine transgression.

The floor of much of the present western Pacific Ocean is distinctly platformic. It is indented in many area by mountainous ridges, mounds and platforms as found in the dry continents. Elsewhere, the (Z) Continent reveals itself in a number of hundreds of islands; for example, the Philippines, New Guinea, New Zealand, Fiji, Tonga, Guam, etc.

The rocks represented in the dry lands of the (Z) Continent range from the intrusives and metamorphics of Pre-Cambrian to the Tertiary sediments and volcanics. However, the existance of granites, always sought out to prove the continental crust, in the ocean covered parts of the (Z) Continent could be a subject of controversial discussion, but certainly, its presence over some of the discussed areas is not excluded.

If ecology and evolution of species could also be taken into consideration, for the (Z) Continent, then there is ease for the explanation of the mysterious distribution of human life and pre-historic animals and reptiles found in many of the widely scattered and which could appear in the past quite incomunicable islands.

2.3. The Physical Features of the (Z) Continent

The surface of the (Z) Continent resemble somehow to that of the central Asian continent where the many folded mountains and plateau's could be compared with the ridges and depressions - many of which are burried by oceanic water. Among the most conspicuous feature in the north is the Emperor seamounts which also marks the north eastern boundary and encloses the plateau like structure with the Kuril and the Japanese trench. Sparsely scattered mounds in the north give way to the high rising ridges and platforms towards south, notable among these are the Mariana islands, Marshals, New Hibrides, Tuamotu, Lord Howe, Chatham, etc.

While water cover on the continent is deep in the north, it is much shallower in the southern part of the platform, excepting in places

where the rugged features are associated with the deeply indented trenches, some of which even attain the greatest oceanic depths. Towards the south west, some land is spared of the water cover as in the Philippines, New Guinea, Borneo, Java, Celebes, etc.

2.4. Some Geological Considerations

The geology of the (Z) Continent become much more complicated as one moves from the Indonesian islands of the south west towards the north and east. The sequence of the Pre-Cambrian, Paleozoic, Mesozoic, and Neogene rocks are well represented on the islands of the south west and south respectively; represented by the Philippines, Celebes, New Guinea, etc. It is, therefore contentful that much of the high rise plateau's and ridges of the south and the south west bear such sequense.

The often deep rooted crystaline and compact rocks of the Pre-Cambrian and Paleozoic era can be encountered in the high rises of the oceanic rounds, ridges and plateau's. In parts of the plateau's enclosed by the Emperor seamount and the Japanese - Kuril trench, the probability of encountering the granitic layer on the surface are minimal because the platform is under great depth of oceanic water and hence become liable to attack by the convectional currents which subjects the layer to erosion by the mantle and probably become assimilated into the basaltic layer. Subduction of the (Z) Continent, especially in parts of the north and north west will be observed to be associated with a thinner and thinner layer of granitic rocks as an approach further north is made. Most of the islands found in the eastern periphery of the (Z) Continent are mostly of volcanic origin, e.g., the Hawaians, Marquesas, Tuamotu, etc. The proximity to the intensive activity of the mantle convectional currents of the periphery of the (Z) Continent accounts for the phenomenon.

2.5. Subduction of the (Z) Continent

Subduction of the (Z) Continent cannot be properly explained without considering platformic movements for the whole of the Pacific region which will be explained later on the consideration of the Continental drift theory. However, the downward trend of the (Z) Continent at the north and the upward trend at the south could be partly attributed to

the bascule motion brought about by the mid-oceanic rise in the south and eastern Pacific; and subduction into the island arcs in the north and north weast across the trenches.

There are strong reasons to believe that the areas marked by the subductional zones of the (Z) Continent may still be active even today, from the fact that a chain of the volcanic eruptions, earthquakes, tremors, lava flow, and gaseous emanations are a very common feature around especially the north and the western boundaries of the continent. It can be argued, however, that the subduction of the (Z) Continent has been responsible for the formation of the fold mountains of the central Asia and the island arcs.

3. Continental Drift Theory in View of the (Z) Continent

In 19th centuary, Edward Suess postulated about the existance of the great Gondwana continent which linked up Africa with South America, Madagascar, India, Australia, and Antarctica; but later as from the Jurassic. it slit up into the present land configuration. later on, Alfred Wagener, Runcorn, Brackett, and others argued about the separation of the American continent from the Euro-African continent.

Of recent, discoveries of the mid-oceanic ridges, paleomanetism, radioactive dating, and theories on mantle convectional currents, have revived the interest on the drift theoty based on plate tectonics and ocean floor spreading.

3.1. The Drifting of Continents

In 1912, Alfred Wagener aired his convictions, that the interlocking similarities of the western coasts of Africa and the eastern coast of South America made it imperative that the two seemingly separate continents were once a single entity of the great Pangaea. During the 1950's, a team of scientists in Britain observed curious changes of magnetic polarity in rock samples. Similar rock samples with reversed paleomagnetism were also discovered in many other areas including in the Deccan plateau, Japan, etc. Application of the radioactive dating for age detemination of these rocks revealed startling and interesting results: thats, magnetic polarity might have changed locations from

Silurian - somewhere in the central USA. to the present position: that, some lands as in Britain must have twisted from their original position; and that, some lands must have drifted long distances, such as India, to their present locations.

There is therefor therefore some to prove that the lands have indeed drifted but, how much and from where?, remains yet to be a subject of hot debate. There is, yet, the role of the mid-oceanic ridges and the fold mountains to be encountered in the context of the drift.

3.1.1. The old concept of the drifting of the continents

Wagener, as a pioneer, was very much limited to data available during the time he exposed his idea of the continental drift and was compelled often to make some daring expeditions in search of truth

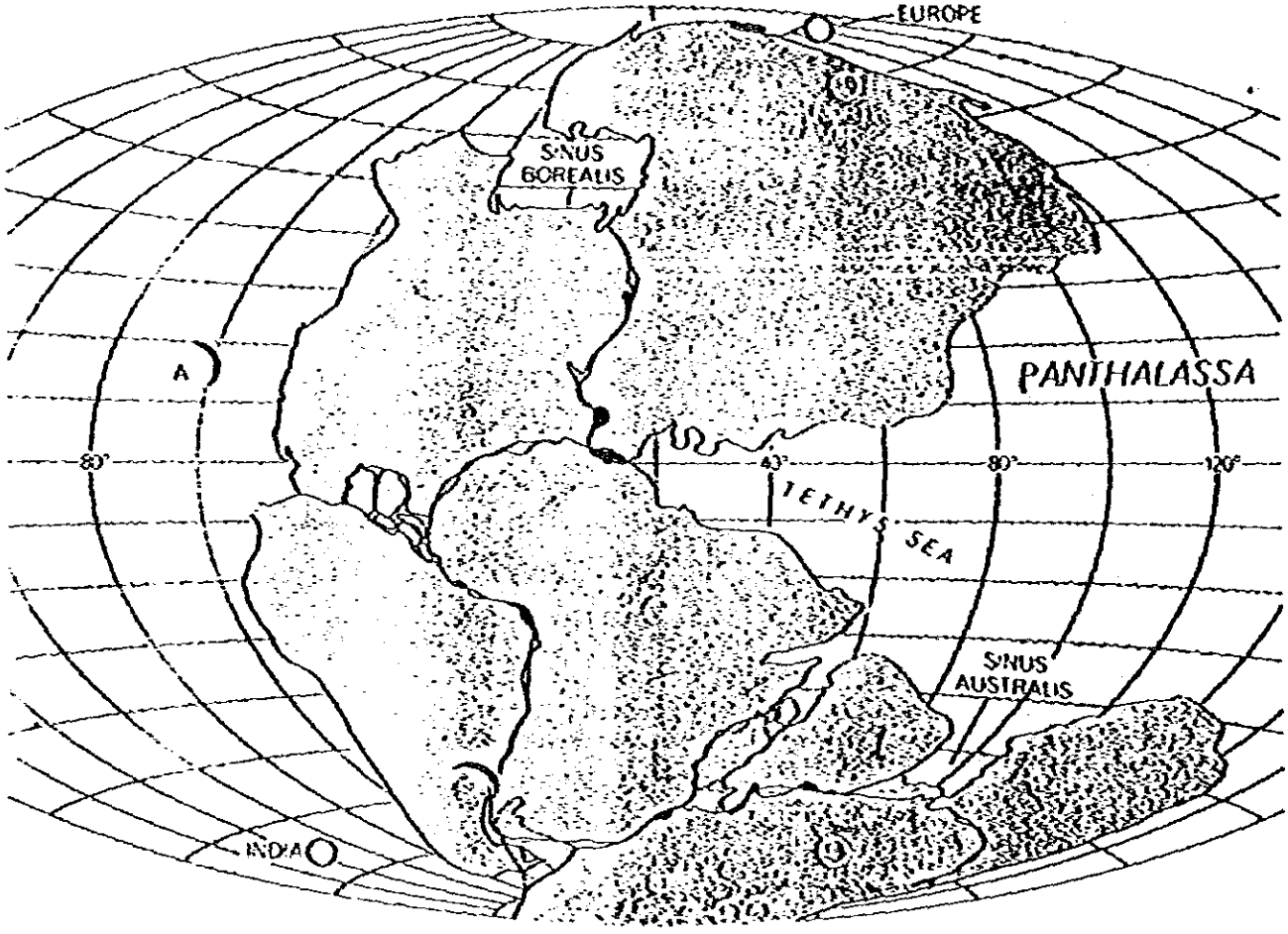

Fig. 3 UNIVERSAL LAND MASS PANGAEA

which eventually costed him his life. Arguments in favour of the drift of the South American continent from Africa had been raised with respect to the resemblances of the continental formations as seen in the Guiana highlands of South America and the upper Guinea of the west Africa. Also contested are the Brazilian highlands of South America with the Angolan plateau of west Africa. The dominant rocks in these regions are said to be Pre-Cambrian, composed of the granites, gneiss, quartzites amphibolites, etc.; typical of the basement system. Also recorded in this area are the sequence of the Paleozoic, Mesozoic, and the Tertiary type of rocks of the corresponding ages.

During the Perno-Carboniferous period, tropical vegetation represented by the Glossoteris fossil plants, was abundant especially in the southern parts of South America, Africa, India and Australia; brewing a belief therefore, that the lands afore mentioned were actually united at the before this period as postulated in the Pangaea concept (Fig. 3).

3.1.2. Modern concept of the drifting of the continents

Modern concept of the drift takes into account the great contribution of the mid-oceanic ridges has had over the mechanism of the continental drift. It is unfortunate that during Wagener's time very little was known about them; for, oceanography was still an infant science.

3.1.2.1. Concept of oceans and seas

Since the First and Second World Wars, the development of the oceanic equipments including the submarines, ships, soner equipment, seismic equipment, etc. has accelerated the study of the oceans and oceanic surface.

Water has been to exist on the surface of the earth for quite a long time even before Cambrian, i.e., the beginning of life on earth, for, the first living organism to exist on earth is said to have lived in the water. The transgression and regression of marine water on land during the different periods of the existance of the earth's crust, led to the concepts of the chronological periods of the Archaic, Protorozoic, Cambrian, Ordovician, Silurian, Devonian,